

โครงสร้าง สมบัติ และการจำลองโมเลกุลของการปรับสภาพพื้นผิว
โพลีเมอร์ชนิดใหม่ และพอลิโอฟีนโคพอลิเมอร์



วิทยานิพนธ์นี้เป็นส่วนหนึ่งของการศึกษาตามหลักสูตรปริญญาวิทยาศาสตรดุษฎีบัณฑิต
สาขาวิชาเคมี
มหาวิทยาลัยเทคโนโลยีสุรนารี
ปีการศึกษา 2555

**STRUCTURES, PROPERTIES AND MOLECULAR SIMULATION
OF SURFACE MODIFICATION OF NATURAL SILK FIBER
AND SOME POLYOLEFIN COPOLYMERS**

Suranaree University of Technology has approved this thesis submitted in partial fulfillment of the requirements for the Degree of Doctor of Philosophy.

Thesis Examining Committee

(Assoc. Prof. Dr. Jatuporn Wittayakun)

Chairperson

(Asst. Prof. Dr. Visit Vao-soongnern)

Member (Thesis Advisor)

(Prof. Dr. Kritsana Sagarik)

Member

(Assoc. Prof. Dr. Vinich Promarak)

Member

(Asst. Prof. Dr. Chaiwat Rakskulpiwat)

Member

(Prof. Dr. Sukit Limpijumnong)

Vice Rector for Academic Affairs

(Assoc. Prof. Dr. Prapun Manyum)

Dean of Institute of Science

ธนีสตรา พินิจมนตรี : โครงสร้าง สมบัติ และการจำลองโมเลกุลของการปรับสภาพพื้นผิว
ใหม่ธรรมชาติและพอลิโอเลฟินโคพอลิเมอร์ (STRUCTURES, PROPERTIES AND
MOLECULAR SIMULATION OF SURFACE MODIFICATION OF NATURAL SILK
AND SOME POLYOLEFIN COPOLYMERS) อาจารย์ที่ปรึกษา : ผู้ช่วยศาสตราจารย์
ดร.วิสิทธิ์ แวสูงเนิน, 196 หน้า.

งานวิจัยนี้เป็นการศึกษาโคพอลิเมอร์ในระดับโมเลกุลทั้งพอลิเมอร์แบบธรรมชาติและพอลิ
เมอร์สังเคราะห์ ชั้นแรก คือ การศึกษาโดยใช้เส้นใยไหมเป็นตัวแทนพอลิเมอร์แบบธรรมชาติ ซึ่งได้
เลือกวิธีการปรับสภาพพื้นผิวมาใช้ในการปรับปรุงสมบัติของไหมธรรมชาติโดยการกราฟท์พอลิ
เมอร์ลงบนเส้นใยไหมด้วยกระบวนการโคพอลิเมโรไลเซชันและวิธีการปั่นเส้นใยไหมด้วยเทคนิคอิ
เล็กโตรสปินนิง ซึ่งสำหรับวิธีที่หนึ่ง พบว่าการกราฟท์ด้วยเมทาไครเลทและไดเมทาไครเลท ให้
ผลผลิตและประสิทธิภาพของเส้นไหมดีขึ้น และมีค่าสูงกว่าการกราฟท์ด้วยเมทาไคราไมด์ (MAA)
การกราฟท์ด้วยเมทาไคราไมด์และไดเมทาไครเลท ยังทำให้เส้นไหมที่ได้มีความนุ่มเมื่อสัมผัสด้วย
มือ ยกเว้นการกราฟท์ด้วยไดไฮดรอกซีเอทิลเมทาไครเลท (HEMA) ที่เส้นใยมีความแข็งมากขึ้น
เส้นไหมที่ผ่านกระบวนการกราฟท์ด้วยมอนอเมอร์ประเภทไดเมทาไครเลทสามารถทนความร้อน
ได้สูงขึ้น ส่วนวิธีที่สอง พบว่าสารละลายไหมมีความหนืดเพิ่มมากขึ้น เมื่อความเข้มข้นสูงขึ้นและ
เส้นใยที่ได้จะเปลี่ยนจากเส้นใยที่มีเม็ดเกาะที่พื้นผิวจะค่อย ๆ กลายเป็นเส้นใยที่มีลักษณะผิวเรียบ
มากขึ้น เมื่อเพิ่มความต่างศักย์ จะทำให้ได้เส้นใยที่มีขนาดเล็กลงเมื่อระยะห่างระหว่างขั้ว
เพิ่มขึ้น เส้นใยเหล่านี้จะมีการเชื่อมต่อกันมากขึ้นเมื่อมีการเติม 1-แอมิล-3-เมทิลอิมิดาโซลเลียม
คลอไรด์ (AmimCl) ลงไปในสารละลายไหม และจะพบว่าพื้นผิวเส้นใยไหมจะมีลักษณะเรียบมาก
ขึ้นเมื่อปริมาณของ AmimCl ลดลง พร้อมกับเพิ่มความต่างศักย์ขณะทำการปั่นเส้นใย เพื่อทำความเข้าใจ
เกี่ยวกับพื้นฐานขององค์ประกอบทางเคมีของโคพอลิเมอร์ ไอโซแทคติกพอลิโพรพิลีน (iPP)
อแทคติกพอลิโพรพิลีน (aPP) และ ซินดีโอแทคติกพอลิโพรพิลีน (sPP) จึงใช้ศึกษาสมบัติเชิงโครง
รูปและเชิงพลวัตการจำลองแบบโมเลกุลด้วยความพิวเตอร์เทคนิคมอนติคาร์โล ซึ่งพบว่า iPP
เคลื่อนที่ได้เร็ว aPP และ sPP สำหรับสารผสมพอลิโพรพิลีนที่มีแทคติกซิตี้ต่างกัน พบว่า iPP และ
aPP เคลื่อนที่ช้าลง ในขณะที่ sPP เคลื่อนที่เร็วขึ้น ซึ่งอันตรกิริยาภายในสายโซ่มีผลสูงกว่าอันตร
กิริยาระหว่างโมเลกุลสำหรับ iPP และ aPP แต่ให้ผลตรงข้ามกับระบบ sPP การศึกษาพฤติกรรมเชิง
พลวัตของ aPP พบว่า สายโซ่ที่มีมอนอเมอร์ต่างชนิดอยู่ติดกันจะเคลื่อนที่ได้เร็วกว่า aPP ที่มีมอนอ
เมอร์ชนิดเดียวกันอยู่ต่อกันในสายโซ่นั้น ซึ่งพบว่าผลของอันตรกิริยาภายในโมเลกุลสูงกว่าผลของ
อันตรกิริยาระหว่างสายโซ่เมื่อ P_{nn} เข้าใกล้ 0 และให้ผลตรงข้ามกับกรณีที่ P_{nn} เข้าใกล้ 1 การกราฟท์

พอลิเอทิลีน (PE) ใช้เป็นแบบจำลองสำหรับการกราฟท์พอลิเมอร์ลงบนเส้นไหม การกราฟท์ PE ลงบนพื้นผิวที่มีอันตรกิริยา จะทำให้สายโซ่จะยืดออกมากขึ้นเมื่อความหนาแน่นและจำนวนของพอลิเอทิลีนที่ใช้กราฟท์มากขึ้น การเพิ่มอุณหภูมิ จะทำให้สายโซ่ที่อยู่ด้านนอกยืดออกมากขึ้นและมีความหนาแน่นลดลง สำหรับระบบที่มีสายโซ่สองค่าผสมกัน พอลิเมอร์สายโซ่ยาวที่อยู่ชั้นนอกจะถูกยืดออกไปมากขึ้น ในขณะที่สายโซ่สั้นจะถูกบีบอัดเข้ามาด้านใน อิทธิพลของอันตรกิริยาระหว่างพื้นผิวกับพอลิเมอร์ที่มีผลต่อการยืดออกของพอลิเมอร์ สามารถเรียงลำดับ ดังนี้ แรงคู่คว $>$ อันตรกิริยาเป็นกลาง $>$ แรงผลักร ส่วนการศึกษาเส้นใยนาโน โดยใช้เอทิลีนโพรพิลีนโคพอลิเมอร์แบบสุ่มจะใช้เป็นแบบจำลองเพิ่มเติมจากโคพอลิเมอร์แบบสลับที่พบในเส้นใยไหม พบว่าสมบัติของเส้นใยนาโนจะขึ้นกับอัตราส่วนของมอนอเมอร์ในระบบนั้น เมื่ออัตราส่วนของเอทิลีนเพิ่มขึ้น ความหนาแน่นโดยรวมของเส้นใยนาโนจะเพิ่มขึ้นเมื่ออยู่ใกล้กับแกนของเส้นใยและจะลดลงตั้งแต่ช่วงกลางไปจนถึงพื้นผิวของเส้นใย ในขณะที่พอลิเมอร์ส่วนปลายจะเกิดการแยกกัน สำหรับขนาดโมเลกุลและการจัดเรียงตัวของเส้นใยนาโนจะมีการลดลงและมีการเปลี่ยนทิศทางการจัดเรียงเมื่ออยู่ใกล้พื้นผิวมากขึ้น



TANISSARA PINIJMONTREE : STRUCTURES, PROPERTIES AND
MOLECULAR SIMULATION OF SURFACE MODIFICATION OF
NATURAL SILK AND SOME POLYOLEFIN COPOLYMERS.
THESIS ADVISOR : ASST. PROF. VISIT VAO-SOONGNERN, Ph.D.
196 PP.

COPOLYMER/GRAFT COPOLYMER/SILK NANOFIBER/ELECTROSPINNING/

The main subject of this dissertation is to study copolymer at the molecular level for both natural and synthetic copolymer. First, silk fiber is studied as the representative model for natural copolymer. Surface modification is applied to improve physical properties of silk fiber by grafted copolymerization and electrospinning technique. For the first approach, the yield and efficiency of grafted silk are increased with methacrylates- and dimethacrylates-grafted silk than those of MAA-grafted system. Methacrylic-grafted silk is hydrophilic and soft to hand except for HEMA-grafted silk which is stiffer. Thermal stability of dimethacrylates-grafted silk is increased. For the second approach, the silk solution viscosity is increased with increased concentration and the beaded-nanofibers are also slightly changed to smoother nanofibers. At high applied voltage, smaller nanofibers are formed when the spinning distance is increased. These fibers are changed to connected-fibers when ionic liquid *i.e.* AmimCl is added to the silk solution and the nanofiber surface becomes smoother when the amount of AmimCl is decreased with higher applied voltage. To understand the fundamental physics of stereochemical copolymer, *i*PP, *s*PP and *a*PP are used to study their structural and dynamic properties via Monte Carlo

Simulation. It is found that *i*PP diffuses faster than *a*PP and *s*PP, respectively. For the PP/PP mixtures with different chain tacticity, *i*PP and *a*PP diffuse slower, while *s*PP diffuses significantly faster as compared to the unmixed system. The effect of intrachain contribution is greater than interchain effect for *i*PP and *a*PP, in contrast to the case of *s*PP. For dynamic behavior of *a*PP melts, the mixed stereochemical sequence diffuses faster than that of the long consecutive diad of the same sequence. The effect of intrachain contribution is greater than that of interchain effect at P_m near 0.0 and the opposite behavior is found at P_m near 1.0. Next, the model of PE brushes is employed as the conceptual model for grafted silks. The PE chains grafted on an interacting hard wall are more stretched in the outer layer when the grafting density and chain length are increased. Increasing temperature led to more chain stretching at the outer region with decreased brush density. For bidisperse brushes, the long chains in the outer region are more stretched while the shorter ones are compressed in the inner layer. The influent of an interacting surface on brush structure can be ordered as: repulsive > neutral > attractive wall system. In addition, poly(ethylene-*ran-atactic* propylene) is used as the conceptual random copolymer model in addition to an alternating copolymer such as natural silk. The properties of this random copolymer nanofiber depend on the PE/PP monomer ratio. When an ethylene fraction is increased, the total density is increased near the fiber axis and then decreased at the middle region toward the free surface where end beads are more abundant segregation. Molecular size and orientation are reduced and directionally changed near the surface.

School of Chemistry

Student's Signature _____

Academic Year 2012

Advisor's Signature _____

ACKNOWLEDGEMENTS

I am grateful to Asst. Prof. Dr. Visit Vao-soongnern, my supervisor, for his guidance towards the completion of this work. I am deeply grateful to Assoc. Prof. Dr. Jatuporn Wittayakun, Prof. Dr. Kritsana Sagarik, Assoc. Prof. Dr. Vinich Promarak, and Asst. Prof. Dr. Chaiwat Raksakulpiwat for serving in my thesis examination committee. I am especially grateful to Prof. Dr. Kiyohito Koyama and Assoc. Prof. Dr. Masataga Sugimoto for their support and very useful discussion on research work.

I would like to thank all Laboratory members who I spend time with almost all day for useful discussion in work, life, hobbies, and good time at Suranaree University of Technology, SUT. My special thanks go to all members in Sugimoto-Koyama Laboratory, Yamagata University, whom I have shared research experience with and for a very good time there and also useful discussion in everything. My thanks go to my old best friends for our good friendship more than ten years and their cheerful on every day.

Lastly, I would like to thank my beloved family and relatives, who are my motivation, for their love, understandings, helps, encouragement and the part of financial support during my education.

Tanissara Pinijmontree

CONTENTS

	Page
ABSTRACT IN THAI.....	I
ABSTRACT IN ENGLISH	III
ACKNOWLEDGEMENTS.....	V
CONTENTS.....	VI
LIST OF TABLES.....	XIV
LIST OF FIGURES	XVII
LIST OF ABBREVIATIONS.....	XXVI
CHAPTER	
I INTRODUCTION.....	1
1.1 Significance of the study.....	1
1.2 Scope and limitations	5
1.3 Research objectives.....	5
1.4 Expected outcome	6
1.5 References.....	6
II LITERATURE REVIEW.....	8
2.1 Graft copolymer of silk fibers.....	8
2.2 Regenerated silk fibroin (RSF) nanofiber by electrospinning	9
2.3 Monte Carlo (MC) simulation of polypropylene (PP) with different tacticity.....	13

CONTENTS (Continued)

	Page
2.4 MC simulation of polyethylene (PE) brush as a model of grafted silk	14
2.5 MC simulation of poly(ethylene- <i>co-atactic</i> propylene) copolymer	16
2.6 MC simulation of polymer system.....	18
2.6.1 MC simulation of polymeric materials on a high coordination lattice.....	19
2.6.2 Coarse graining of polymer model.....	19
2.6.3 Short-range intramolecular interaction of PE and PP chain.....	23
2.6.4 Long-range intermolecular interaction of polymer model on <i>2nnd</i> lattice	25
2.6.5 Moves.....	28
2.6.6 Polymer simulation procedure on <i>2nnd</i> lattice.....	29
2.7 References.....	29
 III GRAFTED-COPOLYMER OF <i>BOMBYX MORI</i> SILK FIBERS WITH METHACRYLIC MONOMERS: CONVENTIONAL PROCESS AND MICROWAVE IRRADIATION METHOD.....	 36
3.1 Abstract	37
3.2 Introduction.....	39
3.3 Experimental	43
3.3.1 Materials.....	43

CONTENTS (Continued)

	Page
3.3.2 Degumming process	43
3.3.3 Grafting process	44
3.4 Characterization	45
3.4.1 Weight gain and grafting efficiency	45
3.4.2 Water retention value (WRV)	45
3.4.3 ATR-FITR	46
3.4.4 Thermal analysis	46
3.4.5 X-ray diffraction (XRD).....	46
3.4.6 Scanning electron microscopy (SEM).....	47
3.5 Results and discussion	47
3.5.1 Textile properties.....	47
3.5.1.1 Weight gain and grafting efficiency.....	47
3.5.1.2 Water retention value (WRV)	48
3.5.2 ATR-FITR.....	50
3.5.3 X-ray diffraction.....	53
3.5.4 Thermal properties	55
3.5.5 SEM.....	58
3.6 Conclusions.....	61
3.7 References.....	62

CONTENTS (Continued)

	Page
IV THE EFFECT OF ADDING IONIC LIQUID ON SPINNABILITY AND CHARACTERISTICS OF REGENERATED <i>BOMBYX MORI</i> SILK FIBROIN NANOFIBER BY ELECTROSPINNING	66
4.1 Abstract	66
4.2 Introduction	67
4.3 Experimental	71
4.3.1 Materials	71
4.3.2 Dissolving process.....	71
4.3.3 Electrospinning process.....	72
4.4 Characterization	73
4.4.1 Rheology and viscosity of silk fibroin solution	73
4.4.2 Surface morphology of fiber and average diameter size of fibers	73
4.5 Results and discussion	73
4.5.1 Effect of RSF concentration and needle diameter on fiber mats	74
4.5.2 The effect of an electric field on nanofiber mats.....	79
4.5.3 The effect of ionic liquid on nanofiber electrospinnability	82
4.5.3.1 The effect of BmimCl on electrospinnability.....	82
4.5.3.2 The effect of adding AmimCl on electrospinnability.....	83

CONTENTS (Continued)

	Page
4.6 Conclusions	91
4.7 References	91
V STRUCTURAL AND DYNAMIC PROPERTIES OF PP/PP BLENDS WITH DIFFERENT CHAIN TACTICITY: MONTE CARLO SIMULATION.....	94
5.1 Abstract	94
5.2 Introduction	95
5.3 Model and method	97
5.4 Results and discussion	98
5.4.1 Neat PP melts	98
5.4.2 PP/PP binary mixture	101
5.4.2.1 <i>i</i> PP chains in PP/PP binary mixtures	103
5.4.2.2 <i>a</i> PP chains in PP/PP binary mixtures	106
5.4.2.3 <i>s</i> PP chains in PP/PP binary mixtures	108
5.5 Conclusions	111
5.6 References	112
VI EFFECT OF STEREOCHEMICAL SEQUENCE ON STRUCTURAL AND DYNAMIC PROPERTIES OF <i>ATACTIC</i> POLYPROPYLENE MELTS.....	116
6.1 Abstract	116

CONTENTS (Continued)

	Page
6.2 Introduction.....	117
6.3 Computational method.....	119
6.4 Results and discussion	119
6.4.1 <i>Atactic</i> polypropylene at $P_m = 0.25$	119
6.4.2 <i>Atactic</i> polypropylene at $P_m = 0.50$	124
6.4.3 <i>Atactic</i> polypropylene at $P_m = 0.75$	127
6.5 Conclusions	130
6.6 References.....	131
VII MONTE CARLO SIMULATION OF POLYETHYLENE END	
GRAFTED ON AN INTERACTING SOLID SUBSTRATE	134
7.1 Abstract.....	134
7.2 Introduction.....	135
7.3 Model and method	139
7.4 Results and discussion	140
7.4.1 Monodisperse polyethylene melt brushes	140
7.4.1.1 Local melt density	140
7.4.1.2 Conformational properties.....	142
7.4.1.3 End bead distributions.....	144
7.4.1.4 Orientation of bond	146
7.4.2 Temperature effect on monodisperse polyethylene brush.....	148

CONTENTS (Continued)

	Page
7.4.2.1 Local melt density	148
7.4.2.2 Conformational properties.....	151
7.4.2.3 End bead distributions	153
7.4.2.4 Orientation of bond	153
7.4.3 Bidisperse polyethylene grafted on interacting wall.....	155
7.4.3.1 Local melt density	155
7.4.3.2 Conformational properties.....	157
7.4.3.3 End bead distributions	160
7.4.3.4 Orientation of bond	162
7.5 Conclusions	163
7.6 References	164
VIII THE STUDY OF POLY(ETHYLENE-<i>CO</i>-<i>ATACTIC</i>	
PROPYLENE) COPOLYMER NANOFIBER BY LATTICE	
MONTE CARLO SIMULATION	
167	
8.1 Abstract	167
8.2 Introduction.....	168
8.3 Model and method	172
8.3.1 System description	172
8.3.2 System construction	173
8.3.2.1 Bulk system.....	173

CONTENTS (Continued)

	Page
8.3.2.2 Nanofibers formation	173
8.4 Results and discussion	175
8.4.1 Density profile	175
8.4.1.1 Radial density profile	175
8.4.1.2 Bead distribution and segregation of chain ends.....	175
8.4.2 Bond orientation	178
8.4.3 Chain properties	181
8.4.3.1 Molecular orientation	181
8.4.3.2 Molecular size	181
8.4.3.3 Chain shape	183
8.4.3.4 Principal moment of radius of gyration.....	183
8.5 Conclusions	186
8.6 References	187
IX CONCLUSION	191
CURRICULUM VITAE	196

LIST OF TABLES

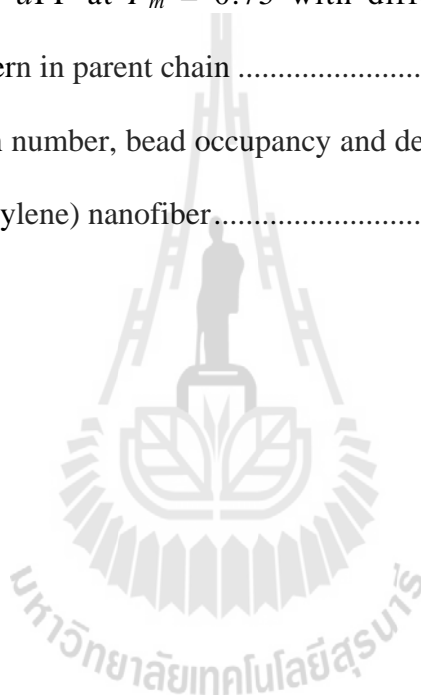
Table	Page
3.1	Experimental conditions for graft copolymerization 45
3.2	Thermal analysis data for conventional method: weight loss for ungrafted and grafted silk fibers at heating rate 10 °C/min 59
3.3	Thermal analysis data for microwave irradiation method: weight loss for grafted silk fibers at heating rate 10 °C/min 59
4.1	Summary of electrospinning of silk fibroin at various conditions..... 70
4.2	Processing parameters of the electrospinning RSF dissolved in formic acid..... 75
4.3	Morphology of electrospun RSF nanofibers at concentration of 13-18 %w/v in formic acid 78
4.4	The morphology and average size diameter of electrospun RSF nanofibers at concentrations of 10-16% w/v in formic acid. 78
4.5	Processing parameters for electrospinning of various RSF concentration and electric field..... 80
4.6	The morphology and average size diameter of RSF nanofibers at concentrations 14%w/v in formic acid at EF from 0.67-4.28 kV/cm..... 80
4.7	Processing parameters of the electrospinning RSF in mixed-solvent..... 84
4.8	The morphology and average size diameter of electrospun RSF fiber at concentration 14 %w/v in formic acid (1) 86

LIST OF TABLES (Continued)

Table	Page
4.9	The morphology and average size diameter of electrospun RSF fiber at concentration 14 % w/v in formic acid (2) 87
4.10	The morphology of electrospun RSF nanofibers at concentration 14 % w/v in FA/AmimCl system (1) 89
4.11	The morphology of electrospun RSF nanofibers at concentration 14% w/v in FA/AmimCl system (2) 90
5.1	Number of chains for PP pure melts and binary mixtures (50% w) 98
5.2	Mean square radius of gyration, $\langle R_g^2 \rangle^{1/2}$ (Å), characteristic ratio, $\langle r^2 \rangle_0/nl^2$ and diffusion coefficient, D (Å ² /MCS) of polypropylene pure melts 101
5.3	Relative value of mean square radius of gyration, characteristic ratio and diffusion coefficient of the chains in PP binary mixtures (50% w) 106
6.1	Repeating sequences, mean square radius of gyration, characteristic ratio, and relative intermolecular PCFs in the third shell and diffusion coefficient of <i>a</i> PP at $P_m = 0.25$ with different stereochemical sequences pattern in parent chain 123
6.2	Repeating sequences, mean square radius of gyration, characteristic ratio, and relative intermolecular PCFs in the third shell and diffusion coefficient of <i>a</i> PP at $P_m = 0.50$ with different stereochemical sequences pattern in parent chain 126

LIST OF TABLES (Continued)

Table		Page
6.3	Repeating sequences, mean square radius of gyration, characteristic ratio and relative intermolecular PCFs in the third shell and diffusion coefficient of <i>a</i> PP at $P_m = 0.75$ with different stereochemical sequences pattern in parent chain	128
8.1	Box size, chain number, bead occupancy and density of poly(ethylene- <i>co-atactic</i> propylene) nanofiber	174



LIST OF SYMBOLS AND ABBREVIATIONS

$^{\circ}\text{C}$	=	degree Celcius
o.w.f.	=	on weight fiber
%RH	=	relative humidity percentage
E	=	potential energy
\AA	=	angstroms
E_{σ}, E_{ω}	=	the first-, second-order short-range interaction energies
t, g^{+}, g^{-}	=	trans, gauche plus, gauche minus
kJ/mol	=	kilo joule per mol
K	=	Kelvin
ε	=	depth of the potential well
σ	=	zero point of Lennard-Jones potential
k_B	=	Boltzmann constant ($\sim 1.38 \times 10^{-23} \text{ J K}^{-1}$)
%w/v	=	weight by volume percentage
cm^{-1}	=	wavenumber (per centimeter)
kDa	=	kilo Dalton

CHAPTER I

INTRODUCTION

1.1 Significance of the study

Polymers are macromolecules built up by linking large numbers of monomer together by polymerization reaction. Homopolymer is made from only one type of monomer. Applications of such materials are limited by some of properties, such as their melting point and stiffness, are unsuitable to be used in some advanced application. These limitations can be overcome by both physical- and chemical treatments. For example, an addition of nucleating agent to reduce the average size of the spherulites, blending with a variety of polymers and by copolymerization with other polymers (Chen *et al.*, 2009), offer the opportunity to obtain innovative materials of which their properties can be suitably modulated depending on all composition and microstructural characteristics of copolymers (Bartczak and Pracella, 2006) that make them available for many advanced applications. In this respect, Copolymer can be made from two or more different types of monomers joined in the same polymer chain. Two monomers can be made to a copolymer in many different patterns such as an alternating copolymer, random copolymer, block copolymer and grafted copolymer.

As natural copolymer, *Bombyx mori* (*B. mori*) silk can be classified as an alternating copolymer of glycine (Gly) and alanine (Ala) with some minor component of other amino acid. Silk is an excellent fibers conventionally used for making yarn,

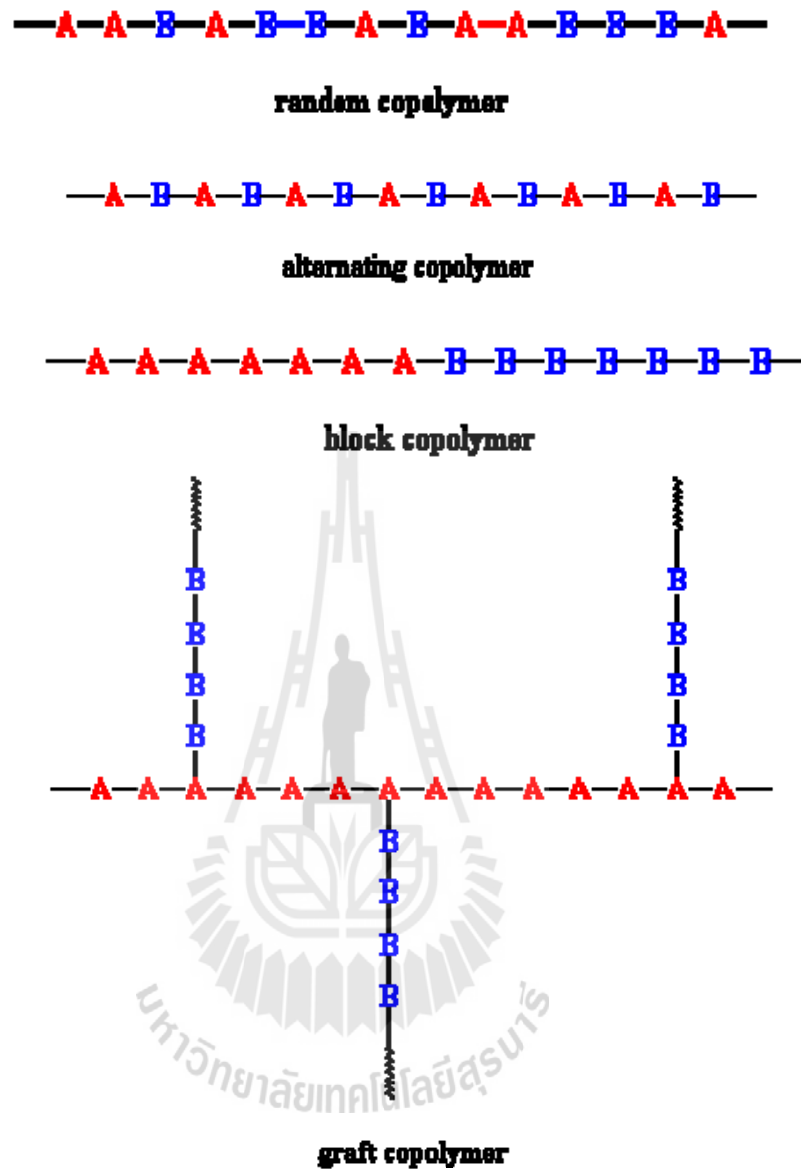


Figure 1.1 Schematic of typical copolymer.

cloth or even the decorative articles in textile manufacturing due to its outstanding attractions, including strength, dyeability, luster and moisture absorption, which distinguish them from other fibers. However, it lacks some important characteristic of fiber in textile uses, such as dimensional stability, abrasion resistance, and color fastness. In addition, it has been known that the structure or monomer sequence of

polypeptide chain, poly(Ala-*alt*-Gly), in silk could not be altered or changed. So, to improve the value of silk fibers for various applications, surface modification is utilized to enhance the property of silk fibers. Graft copolymerization has long been used to modify physical and chemical properties of silk fibers and it depend not only depend on the extent of grafting but also on the characteristics of the functional group carried out by the monomer (Bhattacharya, 2004; Prachayawarakorn and Kyratsamee, 2006). Moreover, besides textile uses, there is a high potentially interesting biomaterials with various applications, such as tissue-engineering scaffolds, wound dressings and drug delivery systems (Zeng, 2003; Sill and von Recum, 2008), good biocompatibility, biodegradability, and minimal inflammatory reaction and excellent mechanical properties (Altman *et al.*, 2003). Those applications have an advantage from the high surface area of such materials. Accordingly, the electrospinning technique is applied to generate silk nanofibers to reduce the size and increase the surface area of natural silk fiber which are of considerable interest for various applications.

One of the simplest structures polymer used to study in this work is polyolefin copolymers of ethylene and propylene. There are many published information about copolymer of ethylene-propylene, including strength, toughness and degradation properties (Koh *et al.*, 2005; Suárez *et al.*, 2010). Poly(ethylene-*co*-propylene) copolymer (EP copolymer) have tremendous potential in various applications as their macroscopic properties can vary from elastomeric to plastic depending on the volume fraction of ethane and propane.

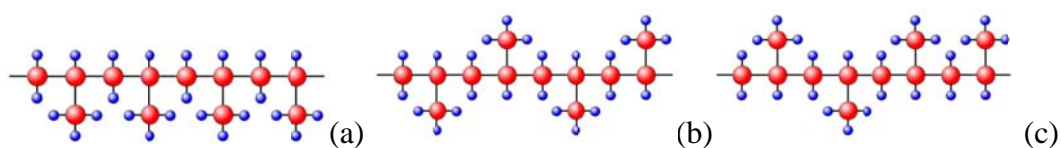


Figure 1.2 Structure of polypropylene (a) *iPP*, (b) *sPP* and (c) *aPP*.

An interesting concept of copolymer can also be illustrated for stereoisomers in polymer chain. Stereoisomerism arise from an orientation of the side chain group in the polymer chain, where *meso* (*m*) and *racemo* (*r*) diad are designated as consecutive monomer pairs with either the same *m* or opposite *r* configuration. *Isotactic* chains are resulted from an addition monomer in which its side chain has all *meso* diad. If polymer chains have *racemo* diad, it is called as *syndiotactic* chain. Different from these two cases, *atactic* chains do not have any consistent placement of the side chain groups (Busico and Cipullo, 2001). For example, tacticity of PP chain affects many properties such as thermal properties, crystallization and diffusion of chain. *aPP* is an amorphous rubbery materials, it has an irregular structure which exhibits poor strength, high tackiness.

On the other hand, *iPP* is a semi-crystalline polymer with high degree of crystallinity, high melting point (160-180°C), high temperature toughness but low of transparency level and heat resistance. In contrast, *sPP* has an excellent toughness and elastic properties but low crystallinity, modulus, yield stress, crystallization temperature, melting point (138-160°C), and reduced flow ability. These properties become an important factor to limit commercial utilization in comparison with *iPP*.

1.2 Scope and limitations

1.2.1 Grafted silk: The silk fibers would be degummed and then grafted copolymerization by both conventional method and microwave irradiation technique.

1.2.2 Silk nanofiber: The electrospun regenerated silk fibroin nanofibers would be prepared using formic acid, and Ionic liquid as solvent and co-solvent, respectively.

1.2.3 Conceptual studied by computer simulation: Lattice Monte Carlo (MC) Simulation would be applied to all computer simulation works to study structural and dynamic properties of copolymer model: (1) PP melts: PP/PP blend with different tacticity and its melts with different stereochemical sequences, (2) PE brush: the model of grafted copolymer onto the silk surface (mono- and bidispersed PE brush on both inert and interacting surface including the temperature effect), and (3) EP copolymer nanofiber: A model of copolymer nanofiber using poly(ethylene-*co*-propylene) random copolymer as a model.

1.3 Research objectives

1.3.1 To investigate the correlation between structures and properties of silk surface modification via grafted-copolymerization and electrospinning.

1.3.2 To apply computational simulation technique to gain more understanding of copolymer model: including copolymer blend, grafted polymer surface and interface, and random copolymer nanofiber.

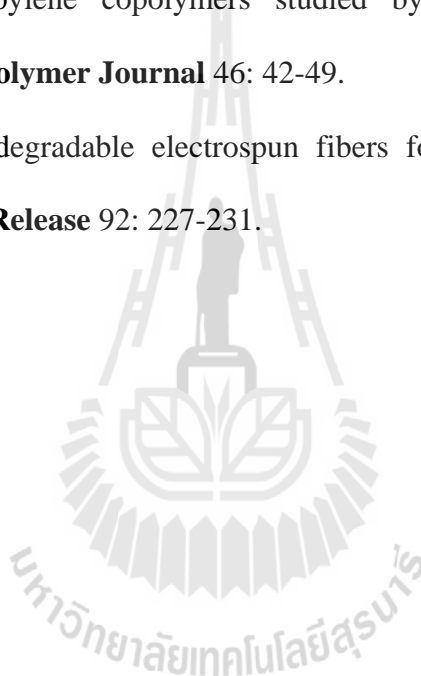
1.4 Expected outcome

Understand at the molecular level for the correlation between structure and properties of modified- and regenerated silk fiber and copolymer model via molecular modeling study.

1.5 References

- Altman, G.H., Diaz, F., Jakuba, C., Calabro, T., Horan, R.L., Chen, J., Lu, H., Richmond, J. and Kaplan, D.L. (2003). Silk-based biomaterials. **Biomaterials** 24: 401-416.
- Bartczak, Z. and Pracella, M. (2006). Blends of propylene-ran-ethylene and propylene-ran-(1-butene) copolymers: Crystal superstructure and mechanical properties. **European Polymer Journal** 42: 1819-1829.
- Bhattacharya, A. (2004). Grafting: a versatile means to modify polymers techniques, factors and applications. **Progress in Polymer Science** 29: 767-814.
- Busico, V. and Cipullo, R. (2001). Microstructure of polypropylene. **Progress in Polymer Science** 26: 443-533.
- Chen, X.H., Ma, G.Q., Li, J.Q., Jiang, S.C., Yuan, X.B. and Sheng, J. (2009). Study on morphology evolution and fractal character of the miscible blend between isotactic polypropylene and copolymer of ethylene and propylene. **Polymer** 50: 3347-3360.
- Koh, H.N., Yong, W.S., Hideto, H., Satoshi, T. and Minoru, T. (2005). Morphology and mechanical properties in the binary blends of isotactic polypropylene and novel propylene-co-olefin random copolymers with isotactic propylene sequence 1. Ethylene–propylene copolymers. **Polymer** 46: 965-975.

- Prachayawarakorn, J. and Kryratsamee, W. (2006). Dyeing properties of *bombyx mori* silks grafted with methyl methacrylate and methacrylamide. **Journal of Applied Polymer Science** 100: 1169-1175.
- Sill, T.J. and von Recum, H.A. (2008). Electrospinning: applications in drug delivery and tissue engineering. **Biomaterials** 29: 1989-2006.
- Suárez, I., Caballero, M.J. and Coto, B. (2010). Composition effects on ethylene/propylene copolymers studied by GPC-MALS and GPC-IR. **European Polymer Journal** 46: 42-49.
- Zeng, J. (2003). Biodegradable electrospun fibers for drug delivery. **Journal of Controlled Release** 92: 227-231.



CHAPTER II

LITERATURE REVIEW

2.1 Graft copolymer of silk fibers

Graft copolymer is a polymer which different types of monomers are covalently bonded together. For grafted-silk fiber, grafting process usually occurs in the amorphous region of silk fiber which is owing to steric and chemical reasons, such as reagent diffusion, availability of reactive groups, *etc.* The physical and chemical properties of the grafted silks are depended on both the extent of grafting and the characteristics of the functional group carried out by those monomers (Prachayawarakorn and Kryratsamee, 2006). Many works on silk grafting various vinyl monomers are found that this monomer can improve the properties of silk fibers after grafted with such monomers, such as thermal stability, wrinkle recovery, increased hygroscopicity and dyeing affinity. Methacrylamide (MAA) is a widely used vinyl monomer because of its lower cost, higher water solubility, relatively lower toxicity. It also gives grafted silk product with soft hand, crease recovery and increase hygroscopicity. Most of various methacrylates and dimethacrylates monomer have graft yield higher than MAA and have hydrophilic properties that lead to more comfortable during the usage of silk fabric, except 2-hydroxyethyl-methacrylate (HEMA) which exhibits stiffer fiber than other monomers (Freddi *et al.*, 1996).

In addition, silk fibers which were grafted with HEMA or methyl methacrylate (MMA) were studied and it found that the HEMA-grafted silk has a higher moisture

regain and better acid and alkaline resistances than the degummed silk (Prachayawarakorn and Boonsawat, 2007). Moreover, silk fibers which were grafted with methacrylic monomers were also investigated. It was found that most of these monomers have a grafted yield higher than that of MAA and better properties including soft handle and good dyeing behavior. Differential Scanning Calorimeter (DSC) and Thermogravimetric Analysis (TGA) analysis of these fibers also indicate a moderate increased thermal stability after grafting (Ferrero *et al.*, 2007).

Furthermore, microwave irradiation was used to grafted-copolymerize onto silk fiber surface. It was found that the weight gain of *Bombyx mori* silk with HEMA significantly increased when the initial monomer concentration was raised to 400% on weight fiber (o.w.f). The tensile properties of silk fibers grafted with MAA and HEMA remained unchanged. The surface morphology of fibers treated with graft-copolymerized with vinyl monomers was almost unaffected, with an exception for HEMA-grafted fibers, which had a presence of homopolymer deposited on the silk surface when the weight gain exceeding 20% (Tsukada *et al.*, 2005).

2.2 Regenerated silk fibroin (RSF) nanofiber by electrospinning

Electrospinning is an attractive method to produce fibers with diameters ranging from micrometers down to tens of nanometers. The electrospun regenerated silk fibers, with high specific surface area, high porosity and good biocompatibility, have extensive applications in the field of biomaterials, such as wound dressing, scaffolds for tissue engineering and drug delivery. Previously, *Bombyx mori* silk has been electrospun to produce fibers from 98% formic acid solution with various silk concentrations. The results showed that pH and concentration had a remarkable

influence on the properties of RSF solutions. With an increase in silk concentration and a decrease in pH, the rheological behavior of RSF solutions exhibited a transition from Newtonian to non-Newtonian fluid. At the same time, lowering pH could induce gel formation and decrease the electrospinnable concentration of RSF aqueous solutions. With a decrease in both pH and silk concentration, the morphology of the electrospun silk fibers changed from the belt-like shape to a uniform cylinder. The average diameter of electrospun silk fibers was smaller than that of natural silk fiber which were reported in the range of 10-20 μm (Wang *et al.*, 2006). It was also decreased with decreasing concentration and pH (Ayutsede *et al.*, 2005; Ki *et al.*, 2007; Zhu *et al.*, 2007). Moreover, the structure and morphology of the fibers were strongly influenced by the solution concentration and the processing voltage, such as spinning velocity, elongation rate, and draw ratio. It has been suggested that high draw ratio was not the only factor in the transformation of SF from random-coil (Zhu *et al.*, 2008) and α -helix conformations to a β -sheet conformation (Zainuddin *et al.*, 2008).

In addition, the behavior of the aged RSF solutions has also been investigated. Upon ageing, turbidity was developed in solution and the viscosity was continuously decreased prior to a drastic increased near the gelation time. Shear thinning with anomalous short recovery within a certain range of low shear rates occurred in both fresh and aged solution. While the solution behaved as pseudo-plastic materials. The chain conformation in aged solution adopted all secondary configurations with β -strand being the predominant (Zainuddin *et al.*, 2008)

Multiple methods have been utilized to prepare electrospinning dopes with silk fibroin dissolved in formic acid or water. All of these spin dopes require a time-

consuming more than 1 week. Moreover, the molecular weight of silk slightly decreased in dialysis step. Compared to the limited number of solvents available today, ionic liquids have taken the spotlight as the green and designer solvent, with many combinations that offer an unprecedented versatility and tenability (Phillips *et al.*, 2004). Ionic liquids (IL) have been used to successfully dissolve other biological macromolecules such as cellulose by 1-butyl-3-methylimidazolium chloride (BmimCl). It can be used to prepare cellulose solutions up to 25 %w/w (Swatloski *et al.*, 2002; Wu *et al.*, 2004). The success of using BmimCl has been attributed to the ability of chloride anion to disrupt the hydrogen bonding present between the cellulose chains. The ability of ionic liquids to disrupt hydrogen bonding makes it an attractive solvent for silk fibroin. Hence, ionic liquids BmimCl, 1-butyl-2, 3-dimethylimidazolium chloride (DmbimCl) and 1-ethyl-3-methylimidazolium chloride (EmimCl) have been used to dissolve silk fibroin. It was found that when the radical of IL increased, whereas anion was similar, the maximum concentration of silk fibroin are decreased (Phillips *et al.*, 2004).

As a spin dope, ionic liquids exhibit several advantages over the aforementioned spin dopes, such as negligible volatility and ease of solvent recovery. All of spinning techniques for these solutions utilized a methanol coagulation bath to remove the spinning solvent and induce crystallization in the fibers. 10 %w/w silkworm cocoon silk was prepared by heating the solution at 95°C and stirred in EmimCl while it was exposed to an ambient air with 20 %RH. The spin dope was placed into the syringe with an inside diameter of 0.26 mm and an overall length of 23 mm while hot, and the air was removed. The spinning was performed by extruding the spin dope into a coagulation bath with several types of solvents. The extruded fiber swelled to a

diameter of about 1 mm before entering the coagulation bath. It has been found that only the fibers from the methanol bath could be handled and formed clear, solid fibers. The diameters of the fibers were 250 and 150 nm. The as-spun fiber did not show significant crystallite alignment, while the fibers which were drawn appear to show crystallite alignment along the fiber axis. Methanol is known to induce β -sheet formation in silkworm silk and was also able to dissolve EmimCl. Therefore, the methanol treatment may be primarily responsible for initial crystallinity in fibers. (Phillips *et al.*, 2005; Phillips *et al.*, 2007)

Viscosity became an important issue with ionic liquid solution when silk content was increased. To be useful as a spin dope, the solution must flow and must have a high enough silk fibroin concentration to allow the molecules to interact with hydrogen bonding during the spinning process. A desirable other low viscosity ionic liquids can be lead to lower solution viscosity. More recently, a novel IL, AmimCl, was synthesized and was used to carry out homogeneous esterification of cellulose (Wu *et al.*, 2004; Zhang *et al.*, 2005) and silk fibroin (Wang *et al.*, 2012). It was also indicated that AmimCl was a good solvent for silk fibroin up to 15 %w/w. AmimCl exhibits a stronger solvation capability for RSF molecules, due to its lower melting point. Interestingly, if sealed at room temperature, that solution can be stored for more than 1.5 years without any apparent instability effects. Flow curves of the solution with low concentration showed lower shear thinning, followed by Newtonian flow in the subsequent shear rate range, which was similar to that of pure AmimCl solution. As the concentration increased, the region of lower shear thinning became less evident and found pseudo-plastic flow, which were the Newtonian region. Moreover,

the zero shear viscosity, η_0 , showed a power-law dependence on concentration and the critical concentration, C^* , was identified as about 5 %w/w (Wang *et al.*, 2012).

2.3 Monte Carlo (MC) simulation of polypropylene (PP) with different tacticity

The tacticity of PP affects many properties such as the thermal properties, diffusion and crystallization (Chen *et al.*, 2007). It was known that in the melts state, *isotactic* polypropylene (*i*PP) diffuses faster than *syndiotactic* polypropylene (*s*PP) but the maximum rate was found for the diffusion of *syndiotactic* polypropylene (*a*PP) (Antoniadis *et al.*, 1999) at an intermediate stereochemical composition. It has been found that *m* and *r* sequences in *a*PP chain diffuse faster than that in *i*PP and *s*PP chain (Waheed *et al.*, 2007).

A small difference in the covalent structure of the polymer chains was subject to strong change in qualitative appearance of the phase diagram (Krishnamoorti *et al.*, 1996). The mixing behavior of polymeric hydrocarbon melts to minor structure change was illustrated by various experimental and theoretical investigation of conventional polyolefin (Thomann *et al.*, 1996; Akten and Mattice, 2001). However, most of polymer blends are heterogeneous on mesoscale and often leads to macroscopic phase separation, due to the micro-phase separation between polymers, though macroscopically homogeneous.

It is well known that the micro-phase separation structure of polymer blend is controlled by its compositions (Leung *et al.*, 2009). PP melt provides very interesting example on the sensitivity of the mixing of hydrocarbon polymers. A two component melts of *a*PP and *i*PP are miscible (Lohse, 1986), but immiscibility was observed

when slightly replaced either *a*PP or *i*PP with *s*PP chain (Thomann *et al.*, 1996). The mobility of *i*PP and *s*PP has also been studied and found that both *i*PP and *s*PP had similar average mobilities. But individual beads of each chain can be departed strongly from an average. Every bead in *i*PP melt can move in the short time. In case of *s*PP melt, a few beads could not move during the longer time. In *s*PP/*i*PP melts system, when the *s*PP was more strongly diluted by *i*PP, all beads of *s*PP had the mean-square displacement higher than that in pure *s*PP melts. The mobility analysis of individual beads in *s*PP chains in blended system expressed slow mobility of *s*PP when its environment changes from *i*PP to *s*PP (Clancy *et al.*, 2000).

2.4 MC simulation of polyethylene (PE) brush as a model of grafted silk

Grafted polymers or polymer brush have been studied in various applications of polymer science and technology, such as surface modification, lubrication, adhesion, colloidal stability, biocompatibility and biotechnology (Eisenriegler, 1982).

The most successful theoretical method to analyze the grafted polymer is the Self-Consistent mean-Field (SCF) theory which gives a valid mean-field description at high grafting density system (Birshtein *et al.*, 1990). It has been found a parabolic form for the density profile supported by MC simulation of ideal chains in case of non-adsorption surface (Skvortsov *et al.*, 1988). In addition, it usually deformed and stretched out in the perpendicular direction to form a brush at the surface, if there was no adsorption between solid surface and polymer chains (Milner, 1991). Moreover, the depletion layer was found at the region near the grafting surface while the free ends of the chains are not excluded from region near the grafting surface and

exhibited the universal behavior in good agreement with the prediction of SCF theory. Moreover, the region close to the substrate was fully occupied by segment belonging to grafted chains. As higher grafting density, free chains are progressively expelled from the surface region and the local melt density in the region which is closest to the interface illustrated systematically higher than that in the bulk, exhibited distinct local maxima due to polymer adsorption.

However in reality, it is unavoidable the polydispersity feature on the polymer brush structure. It has been found the completely change of the density profile from the uniform distribution polymers (Chakrabarti and Toral, 1990), the longer chain ends were localized at the brush edge (Descas *et al.*, 2006) when the difference in molecular weight between the two chains was small, and the segment density profiles of two symmetrical brushes compresses together. Moreover, the inner structure was formed by a mixture of long and short chains, and the top region was composed only of the segment of longer chains. The width of the transition zone did not depend on the brush height. In addition, There was a compression close to the grafting interface for short chains, whereas longer chains have a characteristic flower-like distribution (Lai and Zhulina, 1992).

For grafted polymer on an interacting flat surface (Chakrabarti *et al.*, 1992), both attractive and repulsive interactions. It has been found that the layer thickness of polymer grafted on attractive interacting surface was depended on the total strength of the interaction potential without any dependence on the particular shape of the potential well. On the other hand, for repulsive interactions, the exclusion zone was found from which the free chain ends were excluded as predicted by SCF calculation. It also had to be noted that $z = 0$ played an important role to govern the structure of

the polymer brush (Ball *et al.*, 1991). Moreover, there was a previous study on the effect of an interaction between the solid wall and PE thin film (Jang and Mattice, 1999). The results showed a significant density increase near the solid wall with the strongest interaction, giving rise to the contraction of film thickness, which was in accordance with experimental observation. In addition, the presence of the solid wall reduced an interaction and the interfacial width relative to the free-standing film and the extent of this reduction had a tendency to grow with the strength of an interaction and lowering temperature. The population of chain end groups was significantly depressed near the attractive solid wall.

2.5 MC simulation of poly(ethylene-*co-atactic* propylene) copolymer

Poly(ethylene-*co-atactic* propylene) copolymer, EP copolymer has been studied in a wide range of application in the past decade. It became an important class of thermoplastic elastomers with excellent physical properties. Two commercially classes of EP elastic copolymer were ethylene-based and propylene-based copolymer.

EP copolymers with ethylene content lower than 60 %w/w are essentially amorphous (Bassi *et al.*, 1970). The non-crystalline of EP copolymer can be used to improve transparency, relative softness, sealing temperature, and impact strength, glass-transition temperature of elastic materials. The copolymers with 6-18 %w/w ethylene content are inherently elastic with an elongation at break ratio larger than 1000% (Pegoraro *et al.*, 2000). The EP copolymer with dominant propylene moiety and *i*PP has been also studied (Mighri *et al.*, 2001) to develop the technological opportunity of these materials in fibers form. It indicated that an insertion of the propylene moiety led to a pseudo hexagonal crystalline structure at high-propylene

content and the disorder in the crystalline phase of ethylene sequence gradually increase (de Ballesteros *et al.*, 1996). Moreover, the presence of ethylene units also reduced the melting point and crystallinity by introducing irregularities into the main polymeric chain (Blom *et al.*, 1998). The reasons of the crystallization rate decreased in EP copolymer may be caused by a reduction of PP nucleation and the diffusion rate was slow down during crystallization (Li *et al.*, 1997).

It has been known that the ethylene crystals can be formed in the ethylene-based copolymer and propylene crystals were formed in the propylene-based crystals. Such crystals were associated with the melting point and their corresponding structure was changed upon deformation. Two types of the categorized morphology of ethylene-based copolymers crystallization were fringed-micellar, and both fringed-micellar and lamellar crystalline morphologies (Minick *et al.*, 1995).

The effect of nanofiber size on properties of PE nanofibers have been recently investigated by MIT group (Curgul *et al.*, 2007). The results were found that the mass density at the center of all fibers was constant and comparable to that of the bulk polymer. The surface layer thickness for all fibers slightly increased with fiber size and the chains at the surface were more confined compared to the chains at the center of the nanofiber. Moreover, the structural and dynamic properties of PE nanofiber were also studied (Vao-soongnern *et al.*, 2000). The density profiles were hyperbolic tangent with end beads being more abundant than middle beads at the surface. The orientation preferred at the surface on the scale of individual bonds and the whole chains. The local and global equilibrium properties have been distinguishable when fibers were different in their thickness.

2.6 MC simulation of polymer system

MC method is a stochastic strategy that is relied on probabilities which gathers samplest in a random method. The simulation uses random numbers for making decision for enhance step during a run. In terms of molecular mechanics, MC simulation provides another way to explore a conformational space. This simulation can find a conformational state in a stochastic way by generating random numbers. For example, a given potential like Eq. 2.1, the simulation involves a successive energy evaluation to make a decision for acceptance of a move attempt which is chosen randomly. The decision is accomplished by Metropolis algorithm (Metropolis *et al.*, 1953) in the most cases, which has the criteria as express in Eq. 2.2.

$$V_{total} = \underbrace{V(r)_{bond} + V(\theta)_{angle} + V(\phi)_{torsion} + V(\chi)_{out-of-plane}}_{V_{bonded}} + \underbrace{V(r)_{vdw} + V(r)_{elec}}_{V_{non-bonded}} \quad (2.1)$$

$$\Delta E = V(r)_{new} - V(r)_{old} \leq 0 \text{ accepted}$$

$$\Delta E = V(r)_{new} - V(r)_{old} > 0 \text{ AND } \exp(-\Delta E / kT) \geq rand(0,1) \text{ accepted} \quad (2.2)$$

$$\Delta E = V(r)_{new} - V(r)_{old} > 0 \text{ AND } \exp(-\Delta E / kT) < rand(0,1) \text{ rejected}$$

To consider the new state, if it is in a lower energy state, then, it will replace the previous state. If it is in a higher energy state, the energy difference between two states will be used to make a decision. MC simulation allows a system to move to higher energy state. The probability to overcome the higher energy barrier depends on the energy difference between the new and the current conformation. By such method, the ensemble averaged properties are calculated. One of the efforts to increasing the computational efficiency of MC simulation is to run the simulation on a suitable

lattice, which reduces the floating number calculation. Another way to gain speed in the MC simulation is to use an efficient move algorithm that allows the faster relaxation. With such that way, many polymer beads can move at a single move attempt. The computational time of the lattice simulation based on MC method is proportional to the power of 1 to 2 depending on the quality of the potential energy function.

2.6.1 MC simulation of polymeric materials on a high coordination lattice

There is considerable interest in an application of Monte Carlo algorithm to determine the properties of large molecules. The approach was used for small flexible molecules and could be extended to large molecular weight materials such as polymers. However, the practice of changing randomly the torsional angle leads to a high rejection rate. Even a relatively small change in the torsional angle in the middle of large flexible molecule results in a large translational displacement of the terminal atoms. Therefore, there is a high probability of molecular overlap resulting in the rejection of the move. The limitation of the small flexible molecule approach is determining Euler angles or using quaternion ions for each atom of a large molecule requires considerable computational effort.

2.6.2 Coarse graining of polymer model

Often the energy state of a molecule can be described by a sum of energetic contributions of internal coordinates and non-bonded interactions. The bond stretching and angle bending are very strong effect due to the large force constants. They just slightly change with time and stay at the most probable bond length and

bond angle. Since computational efficiency is indispensable for a polymer simulation, those terms are neglected in most cases. Accordingly, a property of a polymer chain is not dependent on the remaining energy terms, torsional energy and non-bonded energy. Furthermore, if a polymer chain is not perturbed by the existence of others, the importance of the long-range interaction is diminished. In that case, the partition function of a single chain can be expressed by only torsional partition function or conformational partition function, then the average of a property, $\langle A \rangle$, can be written as Eq. 2.3-2.4. The continuous torsional states can be grouped to have several discrete states. This assumption is reasonable because the discrete torsional states are separated by an activation barrier. These torsional states are called Rotational Isomeric State (RIS), the conformational partition function can be rewritten as the summation over the discrete conformational space as express in Eq. 2.5.

$$Z = \int \dots \int_{\phi_1 \phi_n} \exp\left(-\frac{E_{\phi_1 \dots \phi_n}}{kT}\right) d\phi_1 \dots d\phi_n \quad (2.3)$$

$$\langle A \rangle = Z^{-1} \int \dots \int_{\phi_1 \phi_n} \exp\left(-\frac{E_{\phi_1 \dots \phi_n}}{kT}\right) A(\phi_1 \dots \phi_n) d\phi_1 \dots d\phi_n \quad (2.4)$$

$$Z = \sum_{\phi_1} \dots \sum_{\phi_n} \exp\left(-\frac{E_{\phi_1 \dots \phi_n}}{kT}\right) \quad (2.5)$$

The RIS model (Mattice and Suter, 1994) is a coarse grained polymer model, which only considers the discrete rotational isomeric states with other internal coordinates frozen. Schematically, the mapping from a realistic polymer chain to a RIS chain is illustrated in Figure 2.1. Figure 2.2 shows the structure of the high

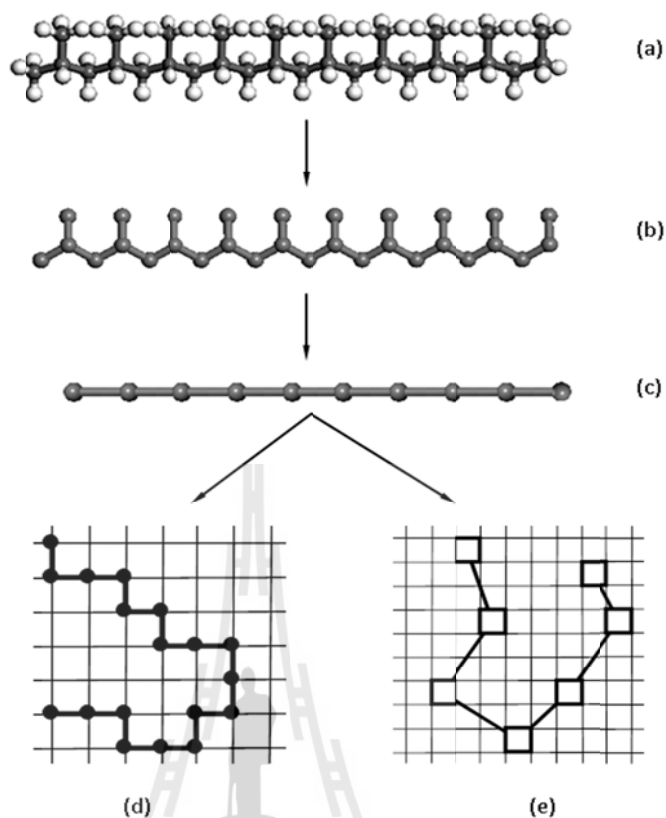


Figure 2.1 Schematic representations of different models of PP chains. (a) Fully atomistic model, (b) united atom model, (c) high coordination lattice model, (d) simple cubic lattice model, (e) bond fluctuation model, (d) and (e) are the representations in two dimensions.

coordination lattice and the twelve coordination sites around a central bead. This coarse-grained lattice provides a better computational efficiency due to the reduction in the number of particles and in the number of conformational states, which facilitates its application to the fairly large polymeric systems. A further coarse-grained lattice from the RIS model can be obtained by discarding every second site from the tetrahedral lattice. The coarse graining generates a slanted cubic cell whose length is 2.5 \AA in a, b, and c directions, and the angles between any two unit vectors

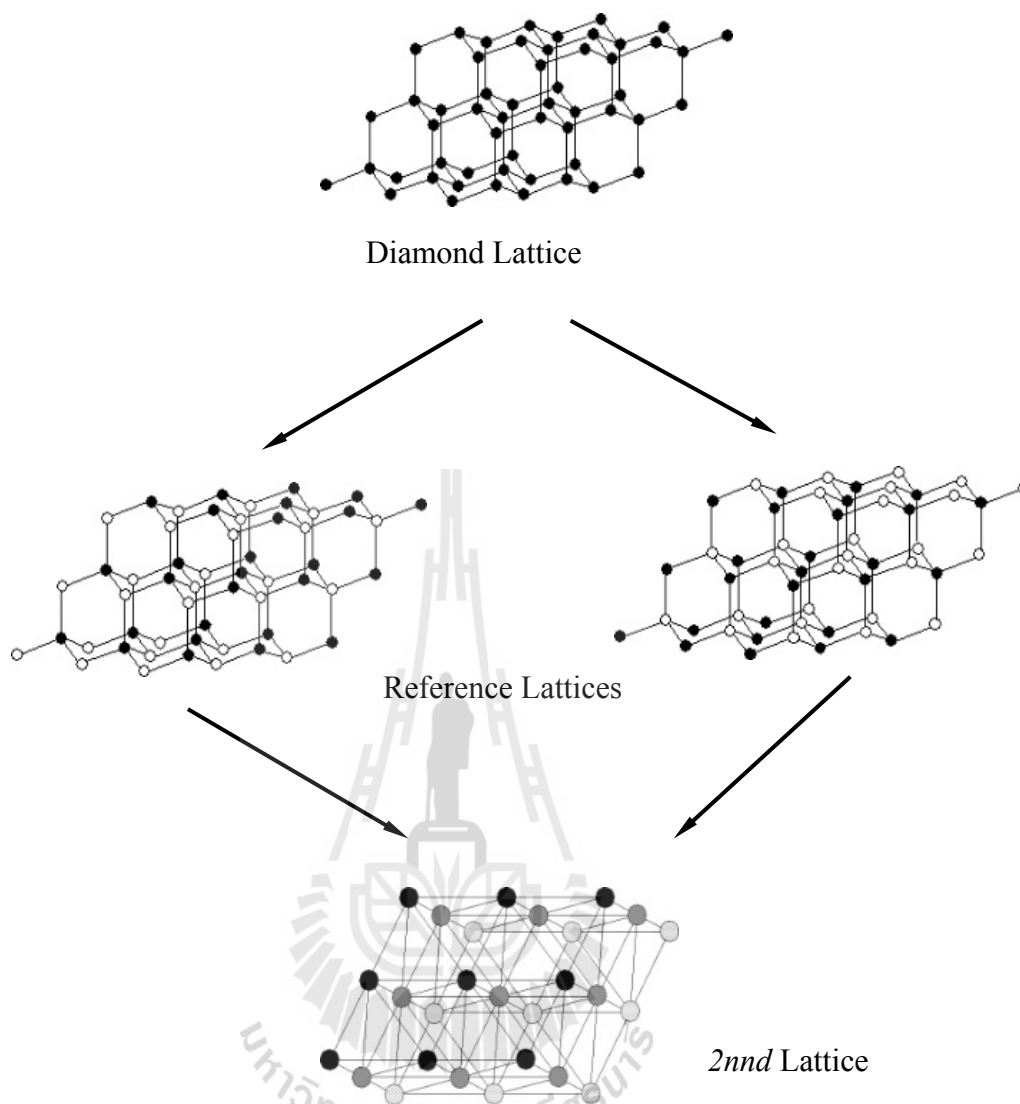


Figure 2.2 Construction of *2ndnd* lattice from a diamond lattice.

are 60° . The modification produces a coordination number of 12 (or $10i^2 + 2$ sites in shell i), which is higher than that of the tetrahedral lattice. The high coordination number provides a flexibility to define a rotational state in the lattice. The new lattice is identical to the closest packing of uniform hard spheres and is named as the “second nearest neighbor diamond (*2ndnd*) lattice”. Each occupied site in this model represents an ether ethylene ($-\text{CH}_2-\text{CH}_2-$) or propylene ($-\text{CH}_2-\text{CH}-\text{CH}_3-$) group.

2.6.3 Short-range intramolecular interaction of PE and PP chain

A Hamiltonian consisting of two parts (short- and long-range interactions) is introduced into the simulation on the 2nd lattice. The short-range interactions come from the local intramolecular contribution of the chain conformation, which is based on the RIS models to describe the nature of bead polymer chains. A RIS model for PE is defined by the following statistical weight matrix.

$$\mathbf{U} = \begin{bmatrix} 1 & \sigma & \sigma \\ 1 & \sigma & \sigma\omega \\ 1 & \sigma\omega & \sigma \end{bmatrix} \quad (2.6)$$

The unperturbed PE has the values E_σ, E_ω of 2.1, 8.4 kJ/mol, respectively.

$$\sigma = \exp(-E_\sigma / RT) \quad (2.7)$$

$$\omega = \exp(-E_\omega / RT) \quad (2.8)$$

The rows and columns of the matrix are the conformation state of $(i-1)^{\text{th}}$ bond and i^{th} bond, respectively. The orders of indexing are t, g^+ and g^- . The detailed description of the statistical weight matrix for coarse-grained PE bonds was discussed and summarized in textbook which written by Mattice and Suter.

In the case of PP, the specific RIS model is described the values for the short-range energies of E_η, E_τ and E_ω with 0.29, 3.9 and 8.0 kJ/mol, respectively (Suter *et al.*, 1975). Due to PP have different stereochemical sequences, *isotactic*, *syndiotactic* and *atactic*, it could be represented by the statistical weight matrix of

diad, such as m and r diad. Different situations have the following statistical weight matrixes as expressed in Eq. 2.9 and 2.10. During the simulations, the statistical weight matrixes are applied to calculate the partition function in the discretized form which express in Eq. 2.11. Then the bond probability of a specific state, η , at bond i could be expressed by Eq. 2.12.

$$U_d = \begin{bmatrix} \eta & 1 & \tau \\ \eta & 1 & \tau\omega \\ \eta & \omega & \tau \end{bmatrix}, U_l = \begin{bmatrix} \eta & \tau & 1 \\ \eta & \tau & \omega \\ \eta & \tau\omega & 1 \end{bmatrix}, U_{dd} = \begin{bmatrix} \eta\omega & \tau\omega & 1 \\ \eta & \tau\omega & \omega \\ \eta\omega & \tau\omega^2 & \omega \end{bmatrix},$$

$$U_{dl} = \begin{bmatrix} \eta & \omega & \tau\omega \\ \eta\omega & 1 & \tau\omega \\ \eta\omega & \omega & \tau\omega^2 \end{bmatrix}, U_{ld} = \begin{bmatrix} \eta & \tau\omega & \omega \\ \eta\omega & \tau\omega^2 & \omega \\ \eta\omega & \tau\omega & 1 \end{bmatrix} \quad (2.9)$$

$$U_{ll} = \begin{bmatrix} \eta\omega & 1 & \tau\omega \\ \eta\omega & \omega & \tau\omega^2 \\ \eta & \omega & \tau\omega \end{bmatrix} \quad (2.10)$$

$$Z = \prod_i U_i \quad (2.11)$$

$$p_{\eta;i} = \frac{Z_{\eta;i}}{Z} = \frac{U_1 U_2 \cdots U_{i-1} U'_{\eta;i} U_{i+1} \cdots U_n}{Z} \quad (2.12)$$

$$p_{\xi\eta;i} = \frac{Z_{\xi\eta;i}}{Z} = \frac{U_1 U_2 \cdots U_{i-1} U'_{\xi\eta;i} U_{i+1} \cdots U_n}{Z} \quad (2.13)$$

$$q_{\xi\eta;i} = \frac{p_{\xi\eta;i}}{p_{\xi;i-1}} \quad (2.14)$$

$$p_{\text{short}} = \frac{p_{\text{new}}}{p_{\text{old}}} = \frac{q_{\alpha\beta^*;i-1}^- q_{\beta^*\gamma^*;i-1}^+ q_{\gamma^*\delta^*;i}^- q_{\delta^*\epsilon^*;i}^+ q_{\epsilon^*\eta^*;i+1}^- q_{\eta^*\xi^*;i+1}^+ q_{\xi^*\lambda^*;i+2}^-}{q_{\alpha\beta^*;i-1}^- q_{\beta\gamma^*;i-1}^+ q_{\gamma\delta^*;i}^- q_{\delta\epsilon^*;i}^+ q_{\epsilon\eta^*;i+1}^- q_{\eta\xi^*;i+1}^+ q_{\xi\lambda^*;i+2}^-} \quad (2.15)$$

$$\Delta E_{\text{short}} = -RT \ln p_{\text{short}} \quad (2.16)$$

Similarly, the probability of two neighbor bonds, which have different states, for example, bond $i-1$ in ξ state and bond i in η state, can be written as Eq. 2.13. The conditional probability $q_{\xi\eta,i}$, which is defined that bond i is in η state given the bond $i-1$ is in ξ state, has the following expression by Eq. 2.14. During the simulation, the bond states change before and after moves. The probability of the move can be calculated by the conditional probability of C–C bonds by the Eq. 2.15. Here, the asterisk denotes the new state. The difference of short-range interactions before and after move can be obtained by a logarithm expression.

2.6.4 Long-range intermolecular interaction of polymer model on $2nnd$ lattice

The long-range interaction includes the intermolecular interaction and long-range intramolecular interaction, which can be obtained by modification of the classic technique for description of the second virial coefficient, B_2 , of a non-ideal ethane (for PE) or propane (for PP) gas using the Mayer function, f , and the Lennard-Jones (LJ) potential energy function.

The long-range interaction is non-bonded interaction. On the $2nnd$ lattice, the parameters for this interaction may be equal to parameters representing the interaction between one monomer at the origin and the other in the specified $2nnd$ lattice site. A spherically symmetric potential is acting between two monomers. According to the imperfect gas theory, the B_2 can be written as Eq. 2.17 where $\beta = 1/kT$ and k is the Boltzmann constant. The f replaces the integral in Eq. 2.17. On the $2nnd$ lattice, B_2 is written in a discretized form by separating the integral into the sub-integrals for each lattice cell and regrouping them for each neighbor which are

expressed in Eq. 2.18. The volume element $\int_{\text{cell}} d\mathbf{r}$ is the volume V_c of one lattice cell of the 2nd lattice. The cell averaged Mayer function, $\langle f \rangle$, is introduced in Eq. 2.19. In the calculation of $\langle f \rangle$, the center of the one monomer is allowed to be anywhere in the given lattice cell if the other one is fixed in the origin. Therefore Eq. 2.18 could be rewritten as Eq. 2.20. Here, z_i is the coordination number of the i^{th} shell with the form of $10i^2 + 2$. The overall average Mayer function is the arithmetic mean of $\langle f \rangle$.

$$B_2 = \frac{1}{2} \int \{ \exp[-\beta u(r)] - 1 \} d\mathbf{r} = \frac{1}{2} \int f d\mathbf{r} \quad (2.17)$$

$$B_2 = -\frac{1}{2} \left[-\int d\mathbf{r} + \sum_{1\text{st}} \int_{\text{cell}} f d\mathbf{r} + \sum_{2\text{nd}} \int_{\text{cell}} f d\mathbf{r} + \sum_{3\text{rd}} \int_{\text{cell}} f d\mathbf{r} + \dots \right] \\ = \frac{V_c}{2} \left[1 - \sum_{1\text{st}} \langle f \rangle_{1\text{st}} - \sum_{2\text{nd}} \langle f \rangle_{2\text{nd}} - \sum_{3\text{rd}} \langle f \rangle_{3\text{rd}} - \dots \right] \quad (2.18)$$

$$\langle f \rangle = \int_{\text{cell}} f d\mathbf{r} / \int_{\text{cell}} d\mathbf{r} \quad (2.19)$$

$$B_2 = \frac{V_c}{2} \left[1 - z_1 \bar{f}_{1\text{st}} - z_2 \bar{f}_{2\text{nd}} - z_3 \bar{f}_{3\text{rd}} - \dots \right] \quad (2.20)$$

$$\exp(-\beta u_i) - 1 = \bar{f}_{i\text{th}} \quad (2.21)$$

$$u = \begin{cases} \infty & r < 2.5 \text{ \AA} \\ u_{\text{LJ}} = 4\epsilon \left[\left(\frac{\sigma}{r} \right)^{12} - \left(\frac{\sigma}{r} \right)^6 \right] & r \geq 2.5 \text{ \AA} \end{cases} \quad (2.22)$$

Finally the effective interaction parameter, u_i , representing the i^{th} neighbor is defined as Eq. 2.21 which only one interaction parameter is applied to a given shell. In this simulation, the LJ potential energy function with hard core is used to ensure the volume exclusion as shown in Eq. 2.22.

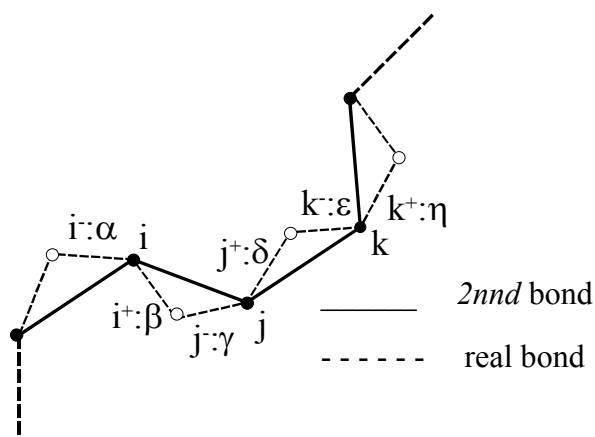


Figure 2.3 Schematic of representation a subchain on the $2nd$ lattice and the corresponding detailed backbone chain on the underlying diamond lattice.

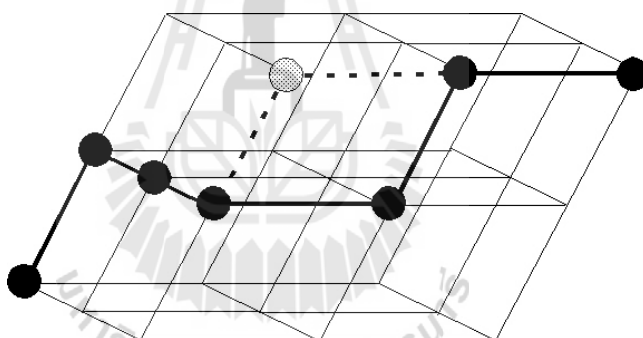


Figure 2.4 Schematic of representation for single bead move on $2nd$ lattice.

The parameters used in the simulations were the values from the experiments. For PE, the LJ parameters employed $\epsilon = 185$ K, $\sigma = 0.55$ nm and interaction energies between first (u_1), second (u_2) and third (u_3) neighboring shells were 16.214, 0.731 and -0.623 kJ/mol at 473 K, respectively. In case of PP, the input LJ potential used $\sigma = 0.512$ nm and $\epsilon/k_B = 237$ K, which reproduced the experimental density of the melt at 473 K (Cho and Mattice, 1997).

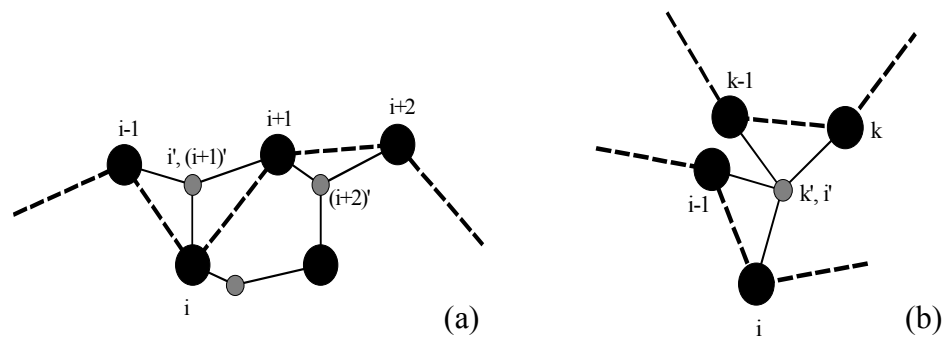


Figure 2.5 Schematic of representation for two kinds of unphysical collapses; (a) intramolecular collapse, and (a) intermolecular collapse. i' and $i+1'$ in (a), k' and i' in (b) occupy the same lattice site after reverse-mapping.

2.6.5 Moves

For every Monte Carlo Step (MCS), a single bead and pivot moves are performed. Every bead is tried once, on average, both in single bead moves and pivot moves, respectively. Therefore every bead is attempted twice, on average, within one MCS. Moves to cause double occupy and collapses are prohibited and the Metropolis rule with the following formalism is applied to determine whether the move is made or not.

$$P = \begin{cases} \exp(-\Delta E / RT) & \Delta E > 0 \\ 1 & \Delta E \leq 0 \end{cases} \quad (2.23)$$

ΔE is the energy difference between the new and old conformation, which includes the short- and long-range interactions. R is the universal gas constant and T is the absolute temperature. In case of $\Delta E \leq 0$, the move is accessed. Otherwise, a random number is generated to determine whether the move is successful or not.

2.6.6 Polymer simulation procedure on 2nd Lattice

The procedure of polymer simulation is listed as the following steps. First, set desired chains in the lattice with the experimental density and then select beads for the attempt of moves. After obtain new configuration according to the rule of moves, the excluded volume effect was checked to remove double occupancy of lattice site. Similarly, bond reverse and unphysical collapse were also checked and calculated short- and long-range interactions. Next, apply Metropolis rule to determine whether the move is made or not and record the chain configurations every set interval of MCS. Finally, the configuration was analyzed to obtain static or dynamic properties.

2.7 References

- Akten, E.D. and Mattice, W.L. (2001). Monte Carlo Simulation of Head-to-Head, Tail-to-Tail Polypropylene and Its Mixing with Polyethylene in the Melt. **Macromolecules** 34: 3389-3395.
- Antoniadis, S.J., Samara, C.T. and Theodorou, D.N. (1999). Effect of Tacticity on the Molecular Dynamics of Polypropylene Melts. **Macromolecules** 32: 8635-8644.
- Ayutsede, J., Gandhi, M., Sukigara, S., Micklus, M., Chen, H.-E. and Ko, F. (2005). Regeneration of Bombyx mori silk by electrospinning. Part 3: characterization of electrospun nonwoven mat. **Polymer** 46: 1625-1634.
- Ball, R.C., Marko, J.F., Milner, S.T. and Witten, T.A. (1991). Polymers grafted to a convex surface. **Macromolecules** 24: 693-703.

- Bassi, I.W., Corradini, P., Fagherazzi, G. and Valvassori, A. (1970). Crystallization of high ethylene EPDM terpolymers in the stretched state. **European Polymer Journal** 6: 709-718.
- Birshtein, T.M., Liatskaya, Y.V. and Zhulina, E.B. (1990). Theory of supermolecular structures of polydisperse block copolymers: 1. Planar layers of grafted chains. **Polymer** 31: 2185-2196.
- Blom, H.P., Teh, J.W., Bremner, T. and Rudin, A. (1998). Isothermal and non-isothermal crystallization of PP: effect of annealing and of the addition of HDPE. **Polymer** 39: 4011-4022.
- Chakrabarti, A., Nelson, P. and Toral, R. (1992). Structure of polymer chains end-grafted on an interacting surface. **Physical Review A** 46: 4930-4934.
- Chakrabarti, A. and Toral, R. (1990). Density profile of terminally anchored polymer chains: a Monte Carlo study. **Macromolecules** 23: 2016-2021.
- Chen, X., Ozisik, R., Kumar, S.K. and Choi, P. (2007). Influence of stereoerrors on the formation of helices during early stage crystallization of isotactic polypropylene. **Journal of Polymer Science Part B: Polymer Physics** 45: 3349-3360.
- Cho, J. and Mattice, W.L. (1997). Estimation of Long-Range Interaction in Coarse-Grained Rotational Isomeric State Polyethylene Chains on a High Coordination Lattice. **Macromolecules** 30: 637-644.
- Clancy, T.C., Pütz, M., Weinhold, J.D., Curro, J.G. and Mattice, W.L. (2000). Mixing of Isotactic and Syndiotactic Polypropylenes in the Melt. **Macromolecules** 33: 9452-9463.

- Curgul, S., Van Vliet, K.J. and Rutledge, G.C. (2007). Molecular Dynamics Simulation of Size-Dependent Structural and Thermal Properties of Polymer Nanofibers. **Macromolecules** 40: 8483-8489.
- de Ballesteros, O.R., Auriemma, F., Guerra, G. and Corradini, P. (1996). Molecular organization in the pseudo-hexagonal crystalline phase of ethylene-propylene copolymers. **Macromolecules** 29: 7141-7148.
- Descas, R., Sommer, J.-U. and Blumen, A. (2006). Concentration and saturation effects of tethered polymer chains on adsorbing surfaces. **The Journal of Chemical Physics** 125: 214702.
- Eisenriegler, E. (1982). Adsorption of polymer chains at surfaces: Scaling and Monte Carlo analyses. **The Journal of Chemical Physics** 77: 6296-6307.
- Ferrero, F., Periolatto, M. and Luraschi, M. (2007). Silk grafting with methacrylic monomers: process optimization and comparison. **Journal of Applied Polymer Science** 103: 4039-4046.
- Freddi, G., Massafra, M.R., Beretta, S., Shibata, S., Gotoh, Y., Yasui, H. and Tsukada, M. (1996). Structure and properties of *bombyx mori* silk fibers grafted with methacrylamide (MAA) and 2-hydroxyethyl methacrylate (HEMA). **Journal of Applied Polymer Science** 60: 1867-1876.
- Jang, J.H. and Mattice, W.L. (1999). The effect of solid wall interaction on an amorphous polyethylene thin film, using a Monte Carlo simulation on a high coordination lattice. **Polymer** 40: 4685-4694.
- Ki, C.S., Kim, J.W., Hyun, J.H., Lee, K.H., Hattori, M., Rah, D.K. and Park, Y.H. (2007). Electrospun three-dimensional silk fibroin nanofibrous scaffold. **Journal of Applied Polymer Science** 106: 3922-3928.

- Krishnamoorti, R., Graessley, W.W., Dee, G.T., Walsh, D.J., Fetters, L.J. and Lohse, D.J. (1996). Pure Component Properties and Mixing Behavior in Polyolefin Blends. **Macromolecules** 29: 367-376.
- Lai, P.Y. and Zhulina, E.B. (1992). Structure of a bidisperse polymer brush: Monte Carlo simulation and self-consistent field results. **Macromolecules** 25: 5201-5207.
- Leung, B.O., Hitchcock, A.P., Brash, J.L., Scholl, A. and Doran, A. (2009). Phase Segregation in Polystyrene-Polylactide Blends. **Macromolecules** 42: 6.
- Li, L., Chen, L., Bruin, P. and Winnik, M.A. (1997). Morphology evolution and location of ethylene-propylene copolymer in annealed polyethylene/polypropylene blends. **Journal of Polymer Science Part B: Polymer Physics** 35: 979-991.
- Lohse, D.J. (1986). The melt compatibility of blends of polypropylene and ethylene-propylene copolymers. **Polymer Engineering & Science** 26: 1500-1509.
- Mattice, W.L. and Suter, U.W. (1994). **Conformational theory of large molecules: The rotational isomeric state model in macromolecular systems**. Wiley, New York.
- Metropolis, N., Rosenbluth, A.W., Rosenbluth, M.N., Teller, A.H. and Teller, E. (1953). Equation of State Calculations by Fast Computing Machines. **The Journal of Chemical Physics** 21: 1087-1092.
- Mighri, F., Huneault, M.A., Aji, A., Ko, G.H. and Watanabe, F. (2001). Rheology of EPR/PP blends. **Journal of Applied Polymer Science** 82: 2113-2127.
- Milner, S.T. (1991). Polymer brushes. **Science** 251: 905-914.

- Minick, J., Moet, A., Hiltner, A., Baer, E. and Chum, S.P. (1995). Crystallization of very low density copolymers of ethylene with α -olefins. **Journal of Applied Polymer Science** 58: 1371-1384.
- Pegoraro, M., Severini, F., Di Landro, L., Braglia, R. and Kolarik, J. (2000). Structure and morphology of a novel ethylene-propylene copolymer and its blends with poly(propylene). **Macromolecular Materials and Engineering** 280-281: 14-19.
- Phillips, D.M., Drummy, L.F., Conrady, D.G., Fox, D.M., Naik, R.R., Stone, M.O., Trulove, P.C., De Long, H.C. and Mantz, R.A. (2004). Dissolution and regeneration of *bombyx mori* silk fibroin using ionic liquids. **Journal of the American Chemical Society** 126: 14350-14351.
- Phillips, D.M., Drummy, L.F., Naik, R.R., De Long, H.C., Fox, D.M., Trulove, P.C. and Mantz, R.A. (2005). Regenerated silk fiber wet spinning from an ionic liquid solution. **Journal of Materials Chemistry** 15: 4206-4208.
- Phillips, D.M., Mantz, R.A., Trulove, P.C. and DeLong, H.C. (2007). Regeneration of ilk and silk-like fibers from ionic liquid spin dopes. United States of America, the United States of America as represented by the Secretary of the Air Force, Washington, DC (US): 4.
- Prachayawarakorn, J. and Boonsawat, K. (2007). Physical, chemical, and dyeing properties of *bombyx mori* silks grafted by 2-hydroxyethyl methacrylate and methyl methacrylate. **Journal of Applied Polymer Science** 106: 1526-1534.
- Prachayawarakorn, J. and Kryratsamee, W. (2006). Dyeing properties of *bombyx mori* silks grafted with methyl methacrylate and methacrylamide. **Journal of Applied Polymer Science** 100: 1169-1175.

- Skvortsov, A.M., Pavlushkov, I.V., Gorbunov, A.A., Zhulina, Y.B., Borisov, O.V. and Pryamitsyn, V.A. (1988). Structure of densely grafted polymeric monolayers. **Polymer Science U.S.S.R.** 30: 1706-1715.
- Suter, U.W., Pucci, S. and Pino, P. (1975). Epimerization of 2,4,6,8-tetramethylnonane and 2,4,6,8,10-pentamethylundecane, low molecular weight model compounds of polypropylene. **Journal of the American Chemical Society** 97: 1018-1023.
- Swatloski, R.P., Spear, S.K., Holbrey, J.D. and Rogers, R.D. (2002). Dissolution of Cellulose with Ionic Liquids. **Journal of the American Chemical Society** 124: 4974-4975.
- Thomann, R., Kressler, J., Rudolf, B. and Mülhaupt, R. (1996). Morphology and phase behaviour of blends of syndiotactic and isotactic polypropylene: 2. Differential scanning calorimetry, light transmission measurements, and PVT measurements. **Polymer** 37: 2635-2640.
- Thomann, R., Kressler, J., Setz, S., Wang, C. and Mülhaupt, R. (1996). Morphology and phase behaviour of blends of syndiotactic and isotactic polypropylene: 1. X-ray scattering, light microscopy, atomic force microscopy, and scanning electron microscopy. **Polymer** 37: 2627-2634.
- Tsukada, M., Islam, S., Arai, T., Boschi, A. and Freddi, G. (2005). Microwave Irradiation Technique to Enhance protein Fiber Properties. **AUTEX Research Journal** 5: 40-48.
- Vao-soongnern, V., Doruker, P. and Mattice, W.L. (2000). Simulation of an amorphous polyethylene nanofiber on a high coordination lattice. **Macromolecular Theory and Simulations** 9: 1-13.

- Waheed, N., Mattice, W.L. and von Meerwall, E.D. (2007). Enhanced Diffusion at Intermediate Stereochemical Composition in Polypropylene by Dynamical Monte Carlo. **Macromolecules** 40: 1504-1511.
- Wang, H., Shao, H. and Hu, X. (2006). Structure of silk fibroin fibers made by an electrospinning process from a silk fibroin aqueous solution. **Journal of Applied Polymer Science** 101: 961-968.
- Wang, Q., Yang, Y., Chen, X. and Shao, Z. (2012). Investigation of Rheological Properties and Conformation of Silk Fibroin in the Solution of AmimCl. **Biomacromolecules** 13: 1875-1881.
- Wu, J., Zhang, J., Zhang, H., He, J., Ren, Q. and Guo, M. (2004). Homogeneous Acetylation of Cellulose in a New Ionic Liquid. **Biomacromolecules** 5: 266-268.
- Zainuddin, Le, T.T., Park, Y., Chirila, T.V., Halley, P.J. and Whittaker, A.K. (2008). The behavior of aged regenerated Bombyx mori silk fibroin solutions studied by ¹H NMR and rheology. **Biomaterials** 29: 4268-4274.
- Zhang, H., Wu, J., Zhang, J. and He, J. (2005). 1-Allyl-3-methylimidazolium Chloride Room Temperature Ionic Liquid: A New and Powerful Nonderivatizing Solvent for Cellulose. **Macromolecules** 38: 8272-8277.
- Zhu, J., Shao, H. and Hu, X. (2007). Morphology and structure of electrospun mats from regenerated silk fibroin aqueous solutions with adjusting pH. **International Journal of Biological Macromolecules** 41: 469-474.
- Zhu, J., Zhang, Y., Shao, H. and Hu, X. (2008). Electrospinning and rheology of regenerated Bombyx mori silk fibroin aqueous solutions: The effects of pH and concentration. **Polymer** 49: 2880-2885.

CHAPTER III

GRAFTED-COPOLYMER OF *BOMBYX MORI* SILK

FIBERS WITH METHACRYLIC MONOMERS:

CONVENTIONAL PROCESS AND MICROWAVE

IRRADIATION METHOD

3.1 Abstract

Silk fiber surface was modified by graft copolymerization with various methacrylic monomers using both conventional chemical reaction process and microwave irradiation method. Textile properties of grafted silk fibers were examined. The yield and efficiency of grafting increased when add-on monomer was increased. Silk grafted with methacrylates and dimethacrylates gave graft yields higher than that of methacrylamide (MAA) in the same operating condition. However, silk fibers which were grafted with MAA and dimethacrylates had relative more hydrophilic properties and softer to hand touch while 2-hydroxyethyl-methacrylate-grafted (HEMA-grafted) silk was stiffer fibers. Attenuated total reflectance-fourier transform infrared spectroscopy (ATR-FTIR) analysis was utilized to confirm the molecular functionality of grafted silk in the structural pattern of silk fibroin in addition to grafted copolymers. There was no change in X-ray diffraction peak confirmed that the silk fiber structure was not affected by the graft-copolymerization reaction with selected vinyl monomers. Differential scanning calorimeter (DSC) analysis was also

performed to evaluate the influence of grafted copolymer on the thermal behavior of grafted silk fibers. Thermal stability of grafted silk was also examined by thermogravimetric analysis (TGA) to confirm DSC results. An increase of thermal stability for grafted silk samples weighted with dimethacrylates was observed. The surface morphology of grafted silk fibers was seen as the deposition of polymer on the surface of silk fibers and its amount was increased with increased monomer adding on grafting copolymerization.

3.2 Introduction

For natural copolymer such as silk which was produced by *Bombrx mori* silkworm, it has long been known as the “queen of fibers” for over thousands of years. It is a high quality and performance fiber with outstanding properties and can be used as excellent materials, distinguish them from other natural and synthetic fibers. These characteristics, as well as their chemical properties and good biocompatibility, had made silk an attractive materials not only for textile but also for non-textile applications. Silk protein had been used in various fields; for example, biomedical and electrical application, tissue-engineered scaffolds, wound dressings and drug delivery systems (Zeng, 2003). Silk was a good biocompatibility, biodegradability, minimal inflammatory reaction and excellent mechanical properties as well (Altman *et al.*, 2003).

Silk fiber contains a fibrous protein termed “fibroin” in the fiber core and connected together by glue-like proteins termed “sericin”. The fibroin protein is highly

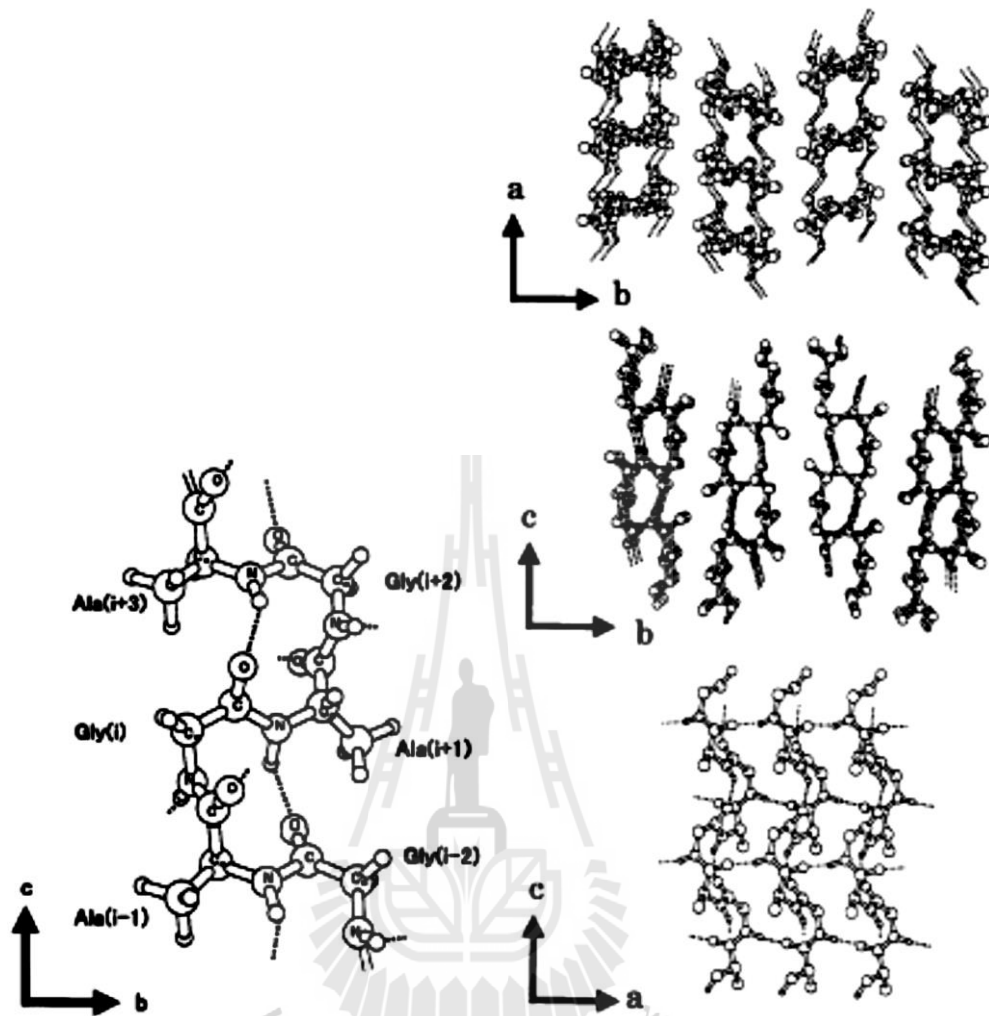


Figure 3.1 Repeated β -turn model of silk I proposed by Asakura *et al.*

(Asakura *et al.*, 2001)

insoluble protein and contains 90% of amino acid such as alanine, glycine, serine which leads to β -pleated sheet formation in the fibers. The silk fibroin structure is organized as an alternating copolyptide with a high content of a small side chain of amino acids, which is composed of 45.9% glycine, 30.3% alanine, 12.1% serine, 5.3% tyrosine, 1.8% valine, and only 4.7% of others 15 amino acid types. The structure of two fibroin forms has been reported as silk I and silk II. Silk I form, as well as the

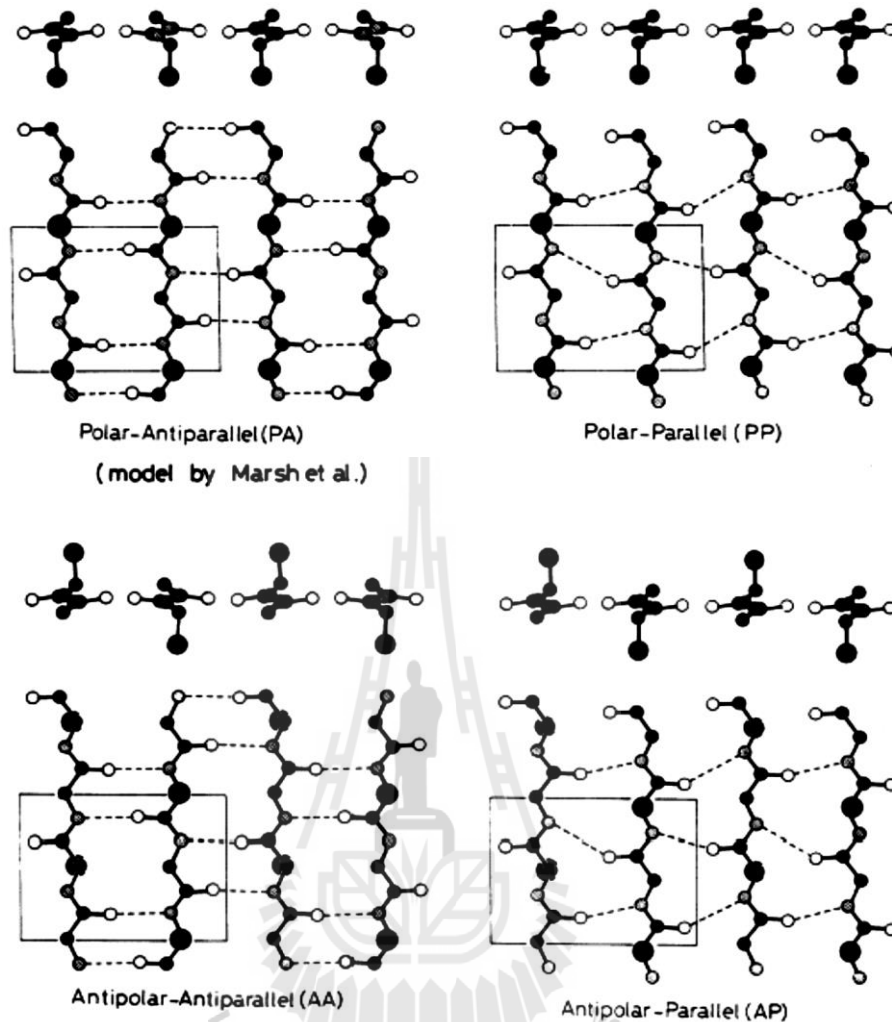


Figure 3.2 Models of molecular conformations of silk II (Takahashi *et al.*, 1999)

random-coil form. It is meta-stable and easily converts to the more stable form under mild conditions which are known as an anti-parallel β -sheet structure in silk II. Moreover, silk fibroin could adopt with silk I structure with alternating copolyptide, $(\text{Ala-Gly})_n$ (Taddei and Monti, 2005; Gus'kova *et al.*, 2008).

Silk fiber is facing some tough competition from the synthetic fibers that have many useful properties such as thermal stability, chemical resistance, washable, *etc.* So, silk fiber must be developed to improve its value. However, the structure or monomer sequence of polypeptide chain in silk could not be altered or changed. If

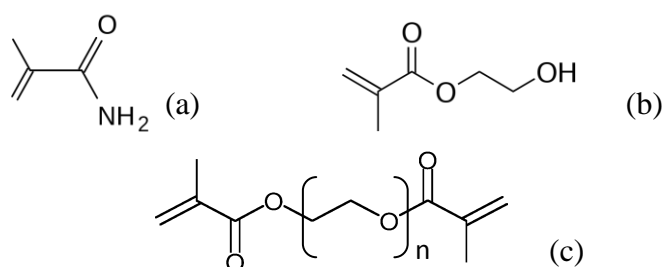


Figure 3.3 Structure of various types of monomer; (a) MAA, (b) methacrylate monomer, HEMA and (c) dimethacrylate monomer, where $n = 1$ for EGDMA, $n = 2$ for EGDMA-2, $n = 3$ for TEGDMA and $n \sim 550$ for PEG550DMA.

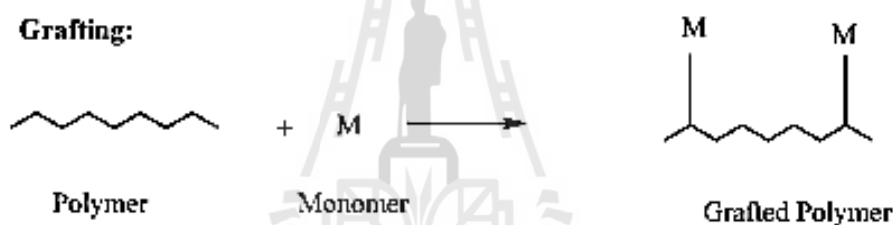
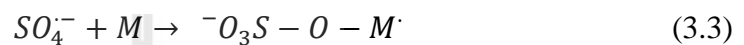
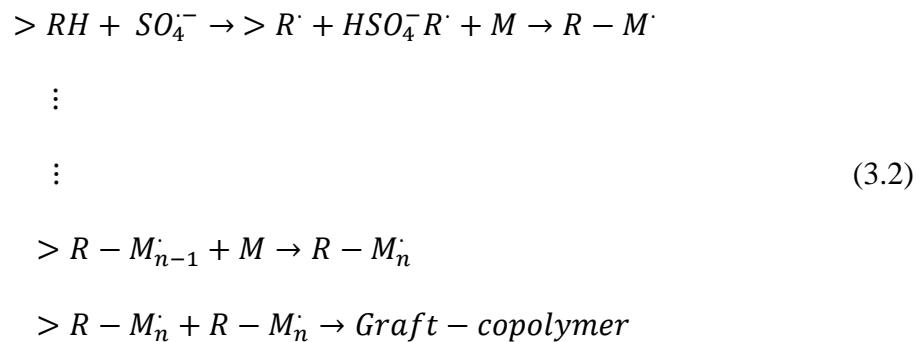


Figure 3.4 Schematic of graft copolymerization reaction.

one needs to improve application properties of silk copolymer, one therefore has to modify at the silk surface. One interesting method is to directly graft copolymerize some selected monomers onto the silk surface where monomers are covalently bonded with the silk surface (Bhattacharya, 2004). The physical and chemical properties of the grafted silks are depended not only on the extent of grafting but also on the characteristics of the functional group carried out by the monomer (Prachayawarakorn and Kryratsamee, 2006). Grafting occurs in the amorphous region of the silk fiber owing to steric and chemical reasons: reagent diffusion, availability of reactive groups, *etc.* Many works on silk grafting have been developed

using various vinyl monomers *i.e.* MAA (Freddi *et al.*, 1996), methacrylonitrile (Tsukada *et al.*, 1993) and several methacrylates: HEMA (Prachyawarakorn and Boonsawat, 2007), ethoxyethyl-methacrylate (Tsukada *et al.*, 1992), and dimethacrylates: polyethylene glycol dimethacrylate (PEGDMA), diethylene glycol dimethacrylate (EGDMA-2) (Chen *et al.*, 2006), ethyleneglycol-dimethacrylate (EGDMA), triethyleneglycol-dimethacrylate (TEGDMA) (Ferrero *et al.*, 2008) to improve properties of silk fiber such as thermal stability, wrinkle recovery, increased hygroscopicity and dyeing affinity. MAA is a widely used vinyl monomer because of its lower cost, higher water solubility, relatively lower toxicity. It also gives the final product with soft hand, crease recovery and increase hygroscopicity. Most of various methacrylate and dimethacrylate monomers show grafted yield higher than MAA and have hydrophilic properties that lead to more comfortable during the wearing of silk fabric, except HEMA which exhibits stiffer product than others (Ferrero *et al.*, 2007). Moreover, grafted silk fiber has an increased thermal stability and chemical resistance. Preparation of graft copolymerization includes chemical, radiation, photochemical, plasma-induced techniques and enzymatic grafting (Bhattacharya, 2004). Redox reaction is the conventional technique to produce free radicals from the initiators and has been used in graft copolymerization as schematically presented in chemical reaction (3.1) – (3.3) (Tsukada *et al.*, 1998), where $>RH$, R' , and M represent silk, primary silk macroradical, and monomer, respectively.





Reaction 3.1 and 3.3 describe the primary radical formation, and the initial state of monomer homopolymerization. Reaction 3.2 shows the steps of graft copolymerization. Free radicals could be formed using an initiator that interacts with the reactive sites on silk fibroin backbones, formed a macroradical, mostly of carboxyl, amine, and hydroxyl side group of various amino acid residues. There was also emphasized the role of glycine residues as the site for grafting on silk, the -NH moieties of the peptide bond. The silk macroradicals were reacted with the monomer, led to the propagation of a grafted polymer chain. Homopolymer can be formed as well, by interaction of the initiating free radicals with the monomer. The coexistence of both grafted chains and homopolymer within silk fiber matrix cannot be excluded.

It has been known that such grafting process has large energy consumption. In recent years, microwave irradiation as the non-contact heating techniques is emerging as an efficient tool for the chemical and physical activities of the grafting process (Mahmoodi *et al.*, 2010). In the case of a free-radical mechanism, various initiator systems, such as peroxide, ammonium persulfate and redox systems have been applied to generate free radical (Misra *et al.*, 1982).

In this work, the silk surface modification by graft copolymerization was studied to improve the properties in textile application and focused mainly on the improvement of thermal property for grafted silk fiber. The grafted copolymerization was prepared by both conventional and microwave irradiation method. MAA, HEMA, EGDMA, Diethyleneglycol-dimethacrylate (EGDMA-2), TEGDMA and PEGDMA were utilized as monomer for graft-copolymerization. Characterizations of modified silk fibers were carried out by various techniques to obtain structure and properties of grafted silk fibers.

3.3 Experimental

3.3.1 Materials

Raw silk fibers (*B. mori*) were obtained from local silk plant in Nakhon Ratchasima province, Thailand. MAA and EGDMA were supplied by Fluka analytical. EGDMA-2, TEGDMA and HEMA were supplied by Aldrich Chemistry. PEG550DMA was supplied by Aldrich. Ammonium persulfate (APS) which was used as radical initiator and formic acid was supplied by QRec. Terginol NP-10 which was used as non-ionic surfactant was supplied by Sigma and Sodium carbonate (Na_2CO_3) was supplied by Sigma-Aldrich. All chemical are used without further treatment.

3.3.2 Degumming process

Raw silk fibers were immersed in an aqueous solution containing 0.05 %w/v Na_2CO_3 (Prachayawarakorn and Boonsawat, 2007) with 1:30 of the material-to-liquor and then heat to 90°C for 30 min and repeated 2 times. Then, fibers were washed with hot distilled water several times and then washed with room

temperature distilled water to remove sericin from fibers. The sample was dried in hot air oven at 60°C for 24 h and kept in desiccators over silica gel.

3.3.3 Grafting process

For the conventional reaction, the degummed silk fibers were soaked in grafting solution in sealed test tube for 1 h at room temperature. The grafting solution contains 3 % o.w.f. of initiator (APS), 40-70 % o.w.f. of methacrylic monomer. Non-ionic surfactant (Terginol NP-10) at concentration of 1.0 g/L for TEGDMA, PEGDMA and 0.2 g/L for others monomer were used. The pH of system was adjusted by adding small amount of 99 % formic acid. The material-to-liquor was 1:60.

The experimental conditions were presented in Table. 3.1. Then, the sealed test tubes were heated up from room temperature to 80°C in shaking water bath and kept constant for 1 h. At the end of reaction, all samples were soaked at 80°C for 30 min in 0.2-1.0 g/L terginol NP-10 solution as same concentration as grafting process. The sample was taken off and washed with terginol NP-10 solution at 80°C for 3 times and 10 min each to remove any unreacted monomer and oligomer, and then thoroughly rinse with distilled water at room temperature for several times to remove surfactant (Ferrero *et al.*, 2008) . Finally, the samples were dried in hot air oven at 105°C for 2 h and cooled to room temperature in a desiccator for 10 h before characterization.

For microwave technique, degummed silk fibers were immersed in grafting solution for 5 min at room temperature in sealed container and was irradiated in microwave oven with power 450 watt for 10 min and repeated 3 times. Then, all samples were washed by distilled water in microwave oven with the same power and

Table 3.1 Experimental conditions for graft copolymerization.

Chemical	% (o.w.f.)*
Initiator (APS)	4
Monomer	40, 50, 60, 70
Formic Acid	~ 0.40-0.45 ml, pH~3

* % (o.w.f.) = % on weight fiber

time as grafting process. At the end of reaction, the procedure was done as same as the conventional system.

3.4 Characterization

3.4.1 Weight gain and graft yield

The weight gain of grafted silk fibers, which is the add-on of polymer was calculated using Eq. 3.4 and the fraction of the total polymer that was grafted onto silk fiber was also calculated by Eq. 3.5, where $w_{grafted}$ is the weight of grafted silk, $w_{original}$ is the weight of original silk, and $w_{monomer}$ is the weight of monomer introduced into the grafting solution.

$$\text{Weight gain (\%)} = \frac{w_{grafted} - w_{original}}{w_{original}} \times 100 \quad (3.4)$$

$$\text{Graft yield (\%)} = \frac{w_{grafted} - w_{original}}{w_{monomer}} \times 100 \quad (3.5)$$

3.4.2 Water retention value (WRV) use to represent water absorption ability of grafted silk fiber which were examined by following the literature method (Ojah and Dolui, 2006). Samples were immersed in distilled water for 2 h. Then the fibers

were taken out from the water. The excess water was removed by applying porous filter paper. The weight of fibers were recorded (wet weight) and then dried in a vacuum oven at 40°C for 10 h. water absorption measurement was calculated as follow:

$$\text{WRV (\%)} = \frac{W_{\text{wet}} - W_{\text{dry}}}{W_{\text{dry}}} \times 100 \quad (3.6)$$

3.4.3 ATR-FITR (Attenuated Total Reflectance-Fourier Transform Infrared Spectrophotometer Perkin Elmer model Spectrum GX, ATR-FTIR) was applied to determine the conformational structure of grafted fiber. FTIR spectra were gathered by utilizing an ATR-FTIR cell on FTIR spectrometer. The measurements were taken in the range of 4000-600 cm^{-1} at a resolution of 4 cm^{-1} with 128 scans.

3.4.4 Thermal analysis (DSC Q2000 and TGA Q50 TA instrument) was employed to study thermal property of grafted fiber. DSC and TGA thermograms were recorded in the temperature range of 50-400°C and from 50°C to 800°C, respectively, at heating rate of 10°C /min under nitrogen atmosphere.

3.4.5 X-ray diffraction (XRD) was used to determine the change in molecular crystallinity of grafted fiber. XRD patterns were obtained by utilizing X-ray diffractometer. Ni-filtered Cu-K_α (1.54 Å) radiation was used at 40 kV and 20 mA. All samples were scanned between 10° - 40° of 2θ with the speed 0.5°/min.

3.4.6 Scanning Electron microscopy (SEM) was employed to observe the macroscopic morphology and surface texture of grafted silk fiber. The surface morphology of the samples was determined with scanning electron microscope. All samples were kept in vacuum for 24 h before used and then were coated with gold in a sputtering coater for 10 minutes. The morphology was observed with operation at accelerating voltage of 15 kV. Acceleration voltage was 15 kV. The current probe was used at 9 and working distance were 15 mm.

3.5 Results and discussion

3.5.1 Textile properties

3.5.1.1 Weight gain and graft yield

The comparison between different methacrylic monomers, at the same conditions is reported. Figure 3.5 presents the weight gain and graft yield of grafted silk fiber at various concentration of monomer. Both factors are increased with increasing monomer content for both grafting methods. The silk fibers which were grafted by microwave irradiation have slightly lower weight gain and graft yield than those by convention method for most monomers, except for HEMA, which shows a dramatically decrease in comparison with grafting by conventional method. It is seen that grafted silk fibers gives high weight gain when they were grafted with methacrylate, HEMA, and dimethacrylate (EGDMA, TEGDMA, PEGDMA, and EGDMA-2) monomers. MAA grafting seems to be less useful for weighting comparison with other monomers. This may be attributed from the distribution of reagents in grafting solution. Grafting by conventional method was done in shaking

bath which all reagents always move during the reaction. While grafting with microwave irradiation, the reagents could not move during the reaction.

3.5.1.2 Water retention value (WRV)

Comfortable during wearing of silk fabrics is very important for fabric application. It is indirectly determined via the ability to absorb moisture of the fabric. However, the weight gain shows an effect on the water absorption of grafted fibers which are displayed in Figure 3.6. Grafted silk fibers show various values of water absorption with various weight gain of grafted silk. It is found the difference of water absorption on grafted silk fiber. The ability of grafted silk to absorb and bind water is closely related to the hydrophobic/hydrophilic balance of the silk/polymer combination. Although the grafted polymer is thought to form separate domains within the silk matrix, filling the void space available in the amorphous regions and limiting chemical and physical interactions with silk fibroin chains to boundary contacts, its relative contribution to the total amount of absorbed water may become significant. For example, dimethacrylate monomers, such as EGDMA-2 show an increase of water retention value with increasing weight gain. This result confirms that EGDMA-2-grafted can enhance the moisture absorption of silk fibers more effectively and also improve the comfort of silk fabric greatly (Chen *et al.*, 2006). In contrast, for acrylamide monomer, MAA, P(MAA) is hydrophilic in nature (Tsukada *et al.*, 2001), as demonstrated by the positive slope of the curve slightly increase with increasing weight gain. This leads to less comfortable of MAA-grafted silk in comparison to EGDMA-2, and it results in a hand touching which is quite similar to ungrafted silk fiber but more smoother. However, silk fibers were treated with

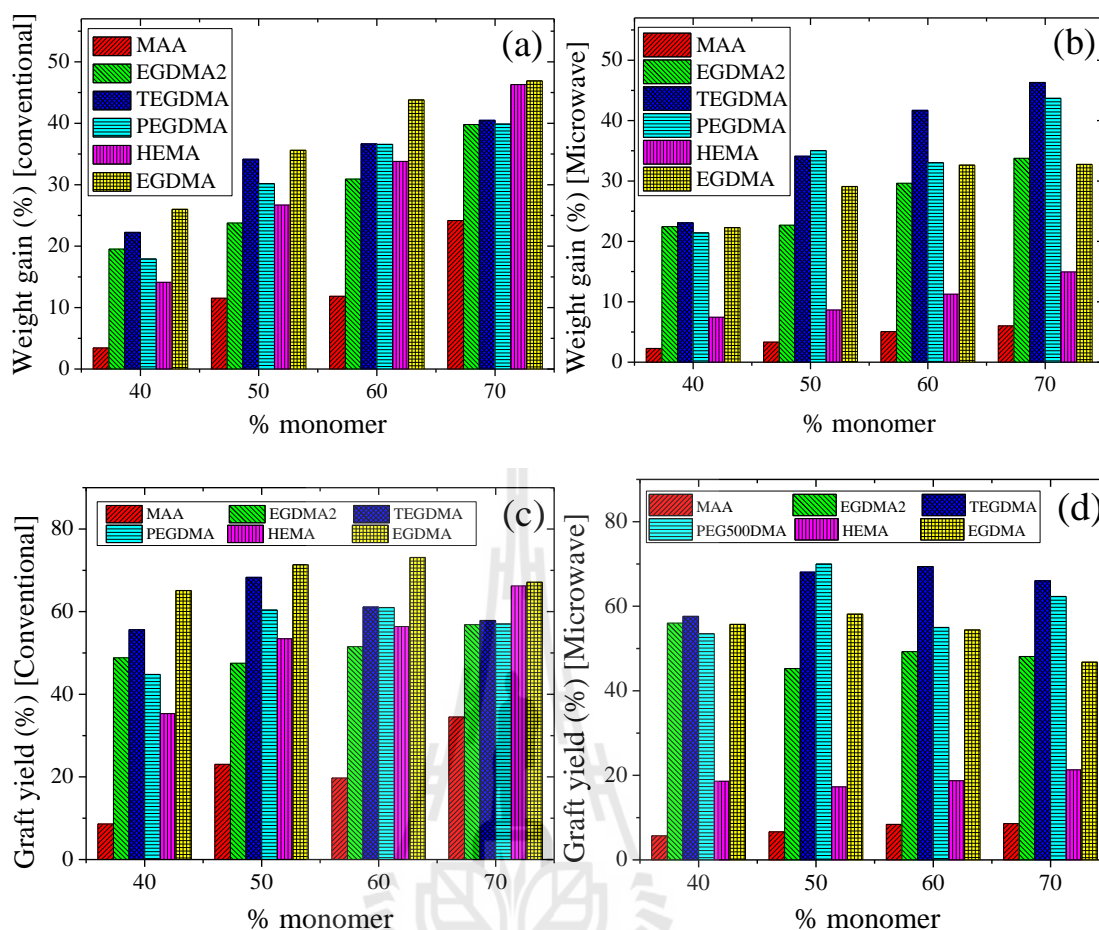


Figure 3.5 Weight gains for silk fiber grafted with various methacrylic monomers; (a) conventional method and (b) microwave irradiation, and graft yield for silk fiber grafted with various methacrylic monomers; (c) conventional method and (d) microwave irradiation.

dimethacrylate *i.e.*, EGDMA, TEGDMA, PEGDMA, and EGDMA-2, gave softer hand fibers, whereas fibers of HEMA-grafted were stiffer than others. It had been reported previously (Tsukada *et al.*, 1993; Prachayawarakorn and Boonsawat, 2007) that due to the hydrophilic characteristics of poly(HEMA), water retention value of the HEMA-grafted silk is slightly increased and as expected, a greater weight gain. This result in slightly higher water absorption (Tsukada *et al.*, 2001).

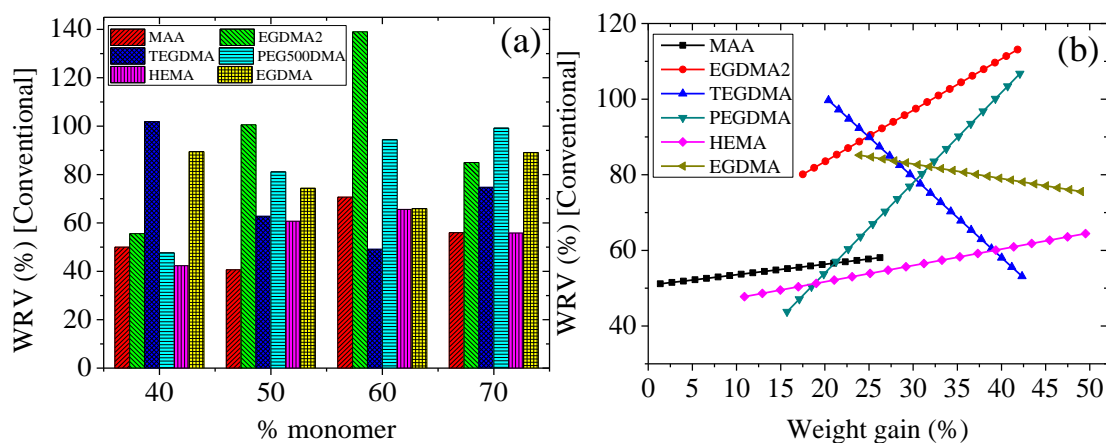


Figure 3.6 (a) Water retention values and (b) tendency of water retention values against weight gain for grafted silk fiber with various methacrylic monomers.

3.5.2 ATR-FITR

The successful grafting process can be confirmed by FTIR characterization which grafted silk should show the characteristic absorption bands of fibroin with β -sheet structure of crystalline regions. The typical absorption bands of silk fibroin which overlapped are observed at: (1) 1630 cm^{-1} which is attributed to C=O stretching of amide I, (2) N-H stretching of amide II at 1520 cm^{-1} , 1265 cm^{-1} of amide III, and its intensity is increased by increasing the polymer add-on (Ferrero *et al.*, 2008). Moreover, there is a CH_2 stretching deformation of $-\text{CH}_2=\text{CH}-$ at 2926 cm^{-1} (Ojah and Dolui, 2007) and the stretching deformation of N-H bond in β -sheet structure at 3411 , and 3295 cm^{-1} (Prachayawarakorn and Kryratsamee, 2006).

Figure 3.7-3.9 demonstrate the ATR-FTIR spectrum of methacrylic monomers, degummed silk and immersed silk fiber, and grafted-silk with such monomers by both conventional method and microwave irradiation method,

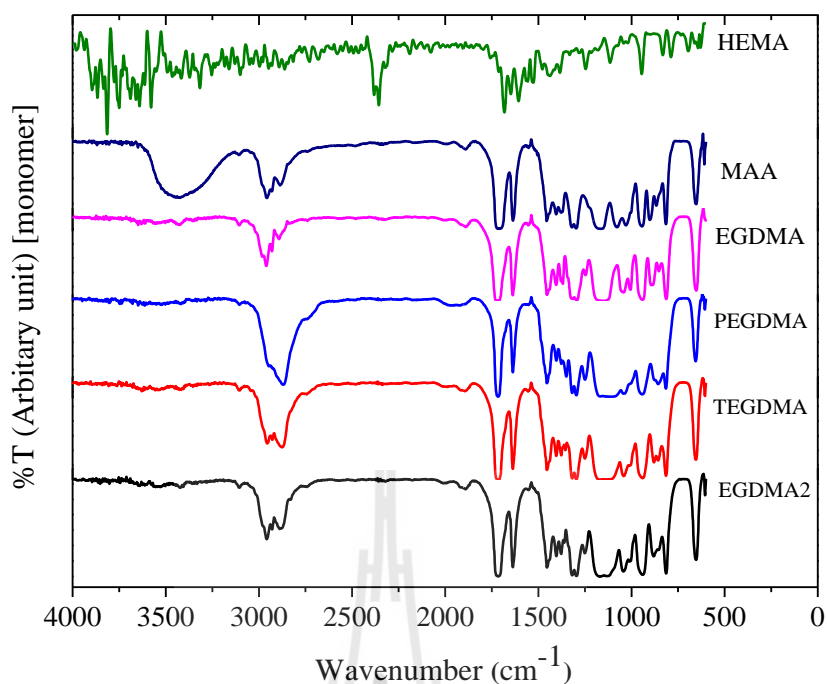


Figure 3.7 ATR-FTIR spectra of methacrylic monomers.

respectively. There was no difference between an immersed silk fiber and the controlled silk fiber or ungrafted silk fiber which shows in Figure 3.8. It can be confirmed an assumption that there is no any significant difference with respect to the controlled silk for all monomer types. The spectra of MAA-grafted silk are reported in Figure 3.9 which show weak additional bands at 1516 cm^{-1} and 1636 cm^{-1} which are attributed to C-O stretching and N-H bending in primary amide poly(MAA) (Ferrero *et al.*, 2007), respectively. Stronger monomer features are found in the spectra of grafted silk with increasing add-on polymer. HEMA-grafted silk exhibits minor shoulders at 1724 cm^{-1} and 1262 cm^{-1} of C=O stretching in the ester group of poly(HEMA) in addition to the absorption bands of ungrafted fiber (Prachayawarakorn and Boonsawat, 2007).

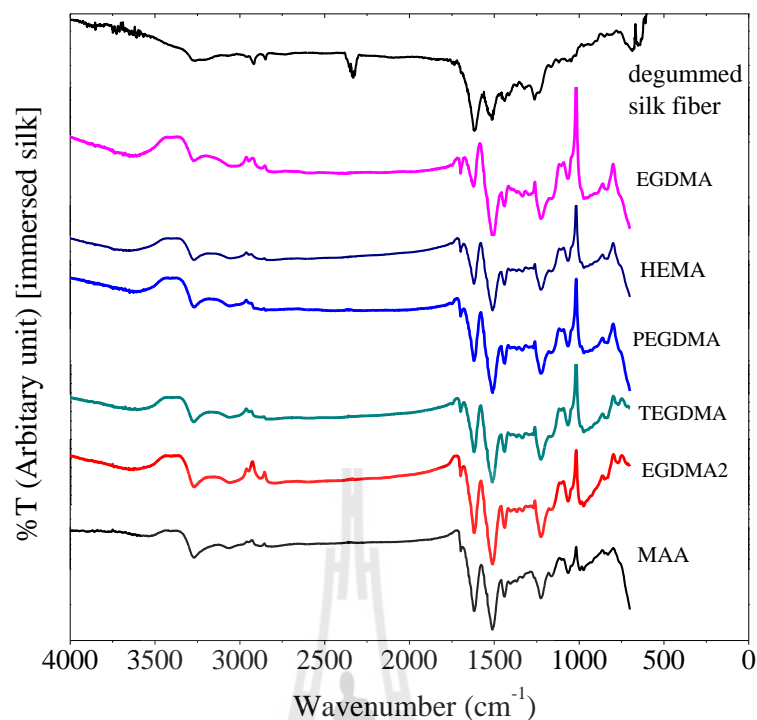


Figure 3.8 ATR-FTIR spectra of degummed silk fiber and silk fiber which are immersed in grafting solution with various methacrylic monomers.

FTIR analysis of grafted silk confirms that the structural pattern of fibroin was not substantially modified, but in the spectra of silk weighted with dimethacrylates the overlap of strong bands occur because the monomer could mask some minor features related to crystallinity and orientation of fibroin. The spectrum of grafted silk with EGDMA give a peak at 1730 cm^{-1} of C=O stretching of the ester group from methacrylic acid (Ferrero *et al.*, 2007). This is justified since for EGDMA, the ether group is lacking. Silk grafted with TEGDMA and PEGDMA show a strong peak at about 1110 cm^{-1} , which is attributable to PEG aliphatic ether absorption. Moreover, the spectra also show an absorption band at 1730 cm^{-1} which is attributed to C=O stretching of the ester group derived from methacrylic acid (Ferrero *et al.*, 2007).

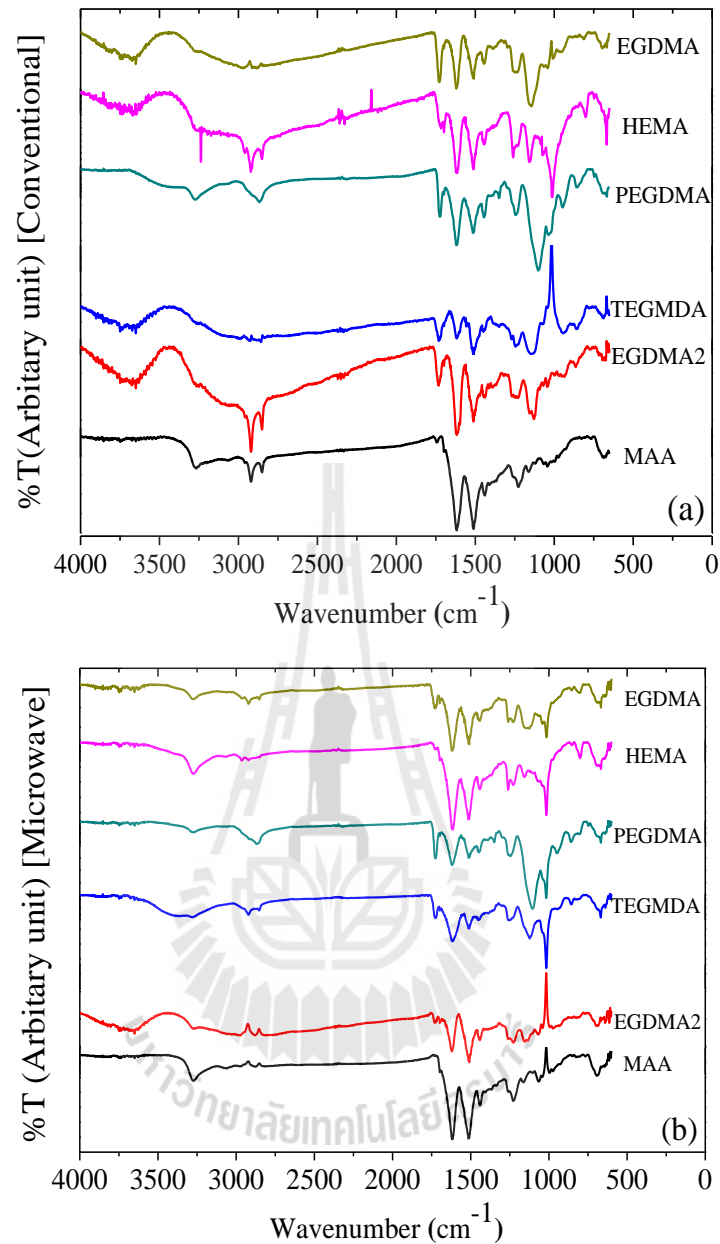


Figure 3.9 ATR-FTIR spectra of grafted silk fiber with various methacrylic monomers; (a) conventional method and (b) microwave irradiation.

3.5.3 X-ray diffraction

Figure 3.10 shows the X-ray diffractograms of silk fibers and grafted silk fibers with various monomers by both copolymerization methods. The peak at $2\theta \approx 20.5^\circ$ is the characteristic of the β -sheet crystals of silk fibroin which is indicated that

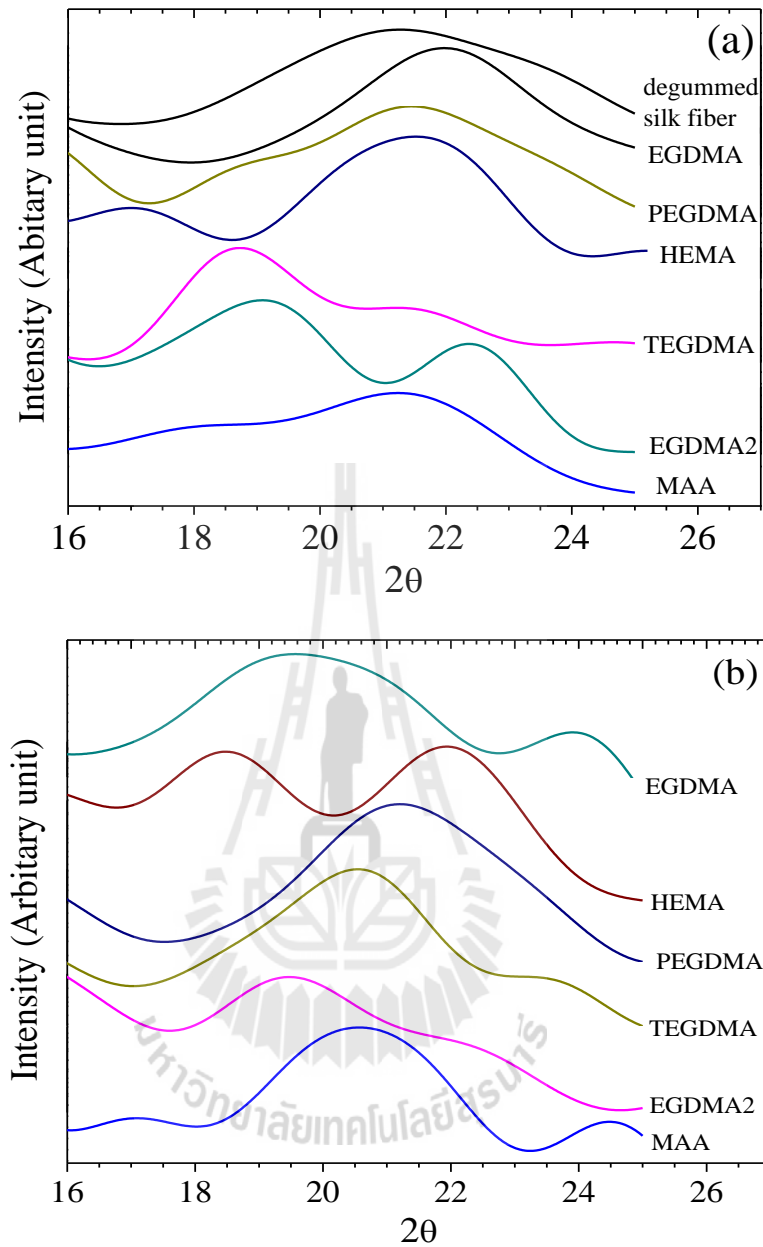


Figure 3.10 XRD patterns obtained by grafting of various methacrylic monomers onto silk fiber; (a) conventional method and (b) microwave irradiation.

there is also a different type of crystalline structure, which does not appear in the original silk fiber. The control sample exhibits a major x-ray diffraction peak which is slightly shifted forward from 21.5° corresponding to the crystalline spacing of 4.39 \AA (Tsukada *et al.*, 1993). It is the characteristic of silk fibers with high molecular

orientation. The position and intensity of the main x-ray diffraction peak do not change regardless of different monomer types as shown in Figure 3.10. These accumulated data are consistent with those reported for silk fibers grafted with other vinyl monomers, demonstrating that the crystalline structure with oriented p' crystals is not affected by the graft-copolymerization reaction occurring inside the fiber (Tsukada *et al.*, 1993).

3.5.4 Thermal properties

Samples of silk obtained by various grafting tests were subjected to DSC measurement. Figure 3.11 shows DSC thermograms of ungrafted- and grafted silk fiber. The ungrafted silk fibers show a single endothermic peak at $\sim 312^\circ\text{C}$ which is attributed to the thermal decomposition of silk fibroin with oriented β -configuration (Tsukada *et al.*, 1993). Some DSC thermograms of silk fiber grafted with various methacrylic monomers are different in weight gains by both conventional and microwave irradiation method. The shifting of decomposition temperature (T_d) indicates that thermal stability of grafted silk fibers is enhanced (Ojah and Dolui, 2006). The DSC curves of MAA-grafted silk fibers has two distinct peaks indicating incompatible of poly(MAA) and silk fibroin in the grafted fiber. It exhibits the endothermic peak at around 260°C owing to thermal decomposition of poly(MAA) and at 315°C is attributed to the thermal decomposition of silk fibroin with an oriented β -configuration (Ferrero *et al.*, 2008).

TGA curves with the weight retention in the range $100\text{-}800^\circ\text{C}$ for ungrafted silk and grafted silk fiber via both conventional and microwave irradiation method are displayed in Figure 3.12. There are two distinct steps of weight loss which

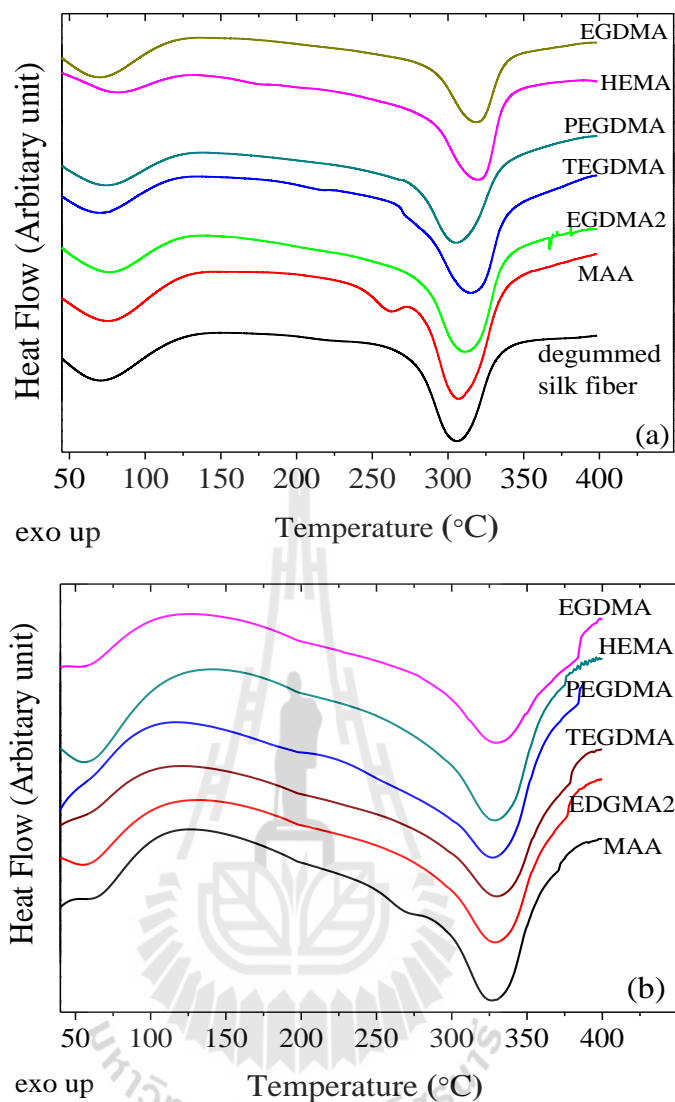


Figure 3.11 DSC thermograms of degummed silk and grafted-silk fibers with various methacrylic monomers; (a) conventional method and (b) microwave irradiation.

is attributed to the moisture content in fiber about 50°C and follows by the beginning of thermal degradation of the fibroin about 280°C (Tsukada *et al.*, 1993), respectively.

The initial decomposition temperature for the ungrafted fiber is about 310°C, whereas it shows two peaks for the MAA-grafted fibers. However the derivative curves found in MAA-grafted silk which are the major signals at higher

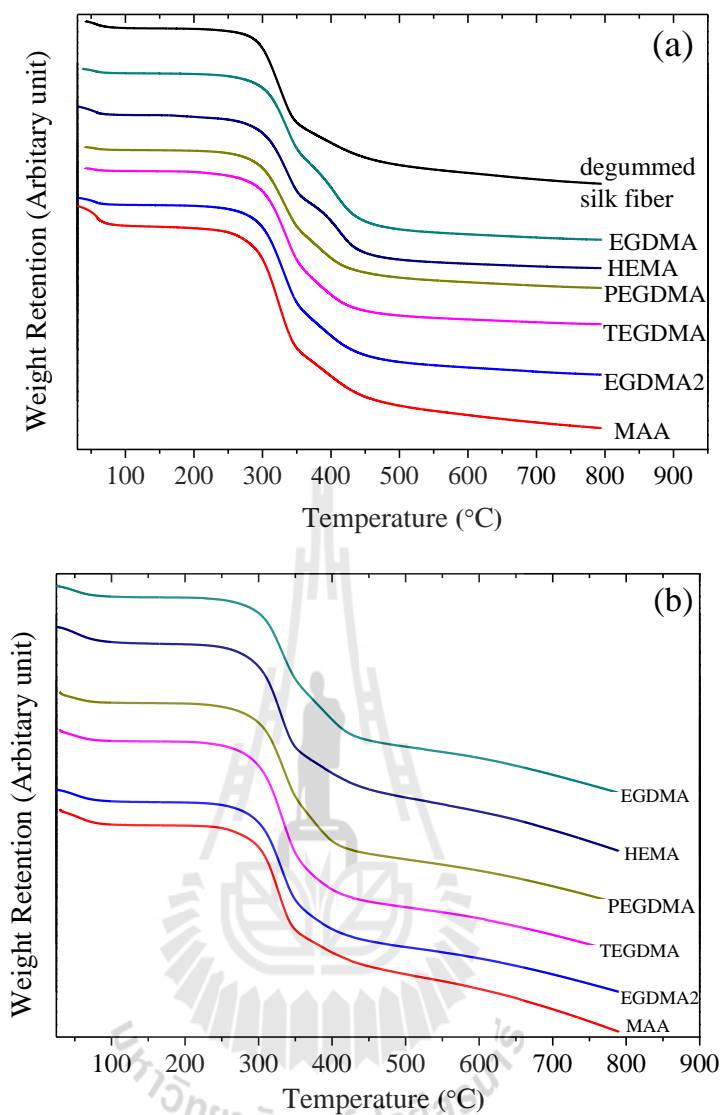


Figure 3.12 Thermogravimetric (TGA) curves of degummed silk and silk fiber grafted with various methacrylic monomers; (a) conventional method and (b) microwave irradiation.

temperature is similar to that observed in the untreated sample. The smaller peak at lower temperature is attributed to the degradation of poly(MAA) due to thermal degradation of the fiber. Unlike MAA-grafted silk, DSC analyses of the fibers weighted with the other methacrylic monomers show only the endothermic peak of

fibroin decomposition, confirming that grafted silk fiber are compatible and have more enhance thermal stability.

TGA curves display only one inflection point in the range of 200-400°C, but the thermal stability is differently affected by the monomer type, as illustrated in Table 3.2 for conventional process and in Table 3.3 for microwave irradiation method. A similar trend is observed in other values of the weight loss of the fibers.

In terms of weight loss, the ungrafted fibers showed a 10% weight loss at 370°C and grafted silk fiber are expressed higher thermal stability comparing with the ungrafted fiber. While, only MAA-grafted shows lower temperature at 268°C without substantial modification of the thermal stability possibly due to incompatibility of monomer and silk fiber.

For the case of HEMA and dimethacrylate monomers, the peak of the derivative curve was shifted to higher temperature than the untreated fiber, showing a moderate increase of thermal stability. However the degradation process seems to be faster for all grafted samples, as shown by 50% weight retention values about 350°C. However, microwave irradiation method also shows a similar trend for thermal stability of the grafted silk fiber and any weight loss temperature is quite similar.

3.5.5 SEM

The appeal of silk consists primarily in its smooth and shiny surface, whose modification may seriously impair the quality of silk articles. The drawback in grafting process is the surface deposition of homopolymer that occur during the reaction. The surface morphology of raw silk fiber and degummed silk fiber are observed in Figure 3.13 which can be seen that the fibers are smoother after removing

Table 3.2 Thermal analysis data for conventional method: weight loss for ungrafted and grafted silk fibers at heating rate 10°C/min.

Nature of silk fibers	Temperature (°C) at % weight loss			
	5%	10%	15%	50%
Ungrafted	79	272	291	376
MAA-grafted	69	268	293	378
EGDMA2-grafted	226	280	300	349
TEGDMA-grafted	190	278	298	348
PEG550DMA-grafted	230	284	304	359
HEMA-grafted	237	289	306	370
EGDMA-grafted	160	291	310	375

Table 3.3 Thermal analysis data for microwave irradiation method: weight loss for grafted silk fibers at heating rate 10°C/min.

Nature of silk fiber	Temperature (°C) at weight loss			
	5%	10%	15%	50%
MAA-grafted	71	275	300	360
EGDMA2-grafted	80	279	300	352
TEGDMA-grafted	110	279	299	347
PEG550DMA-grafted	160	284	304	359
HEMA-grafted	75	272	298	359
EGDMA-grafted	101	289	309	374

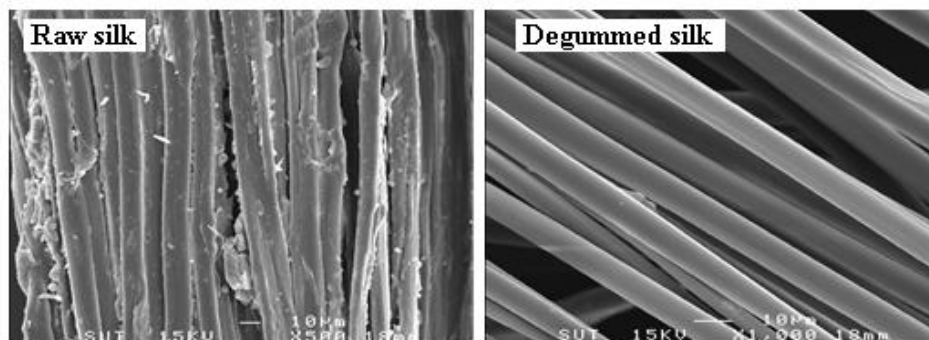


Figure 3.13 The morphology of raw silk fiber and degummed silk fiber.

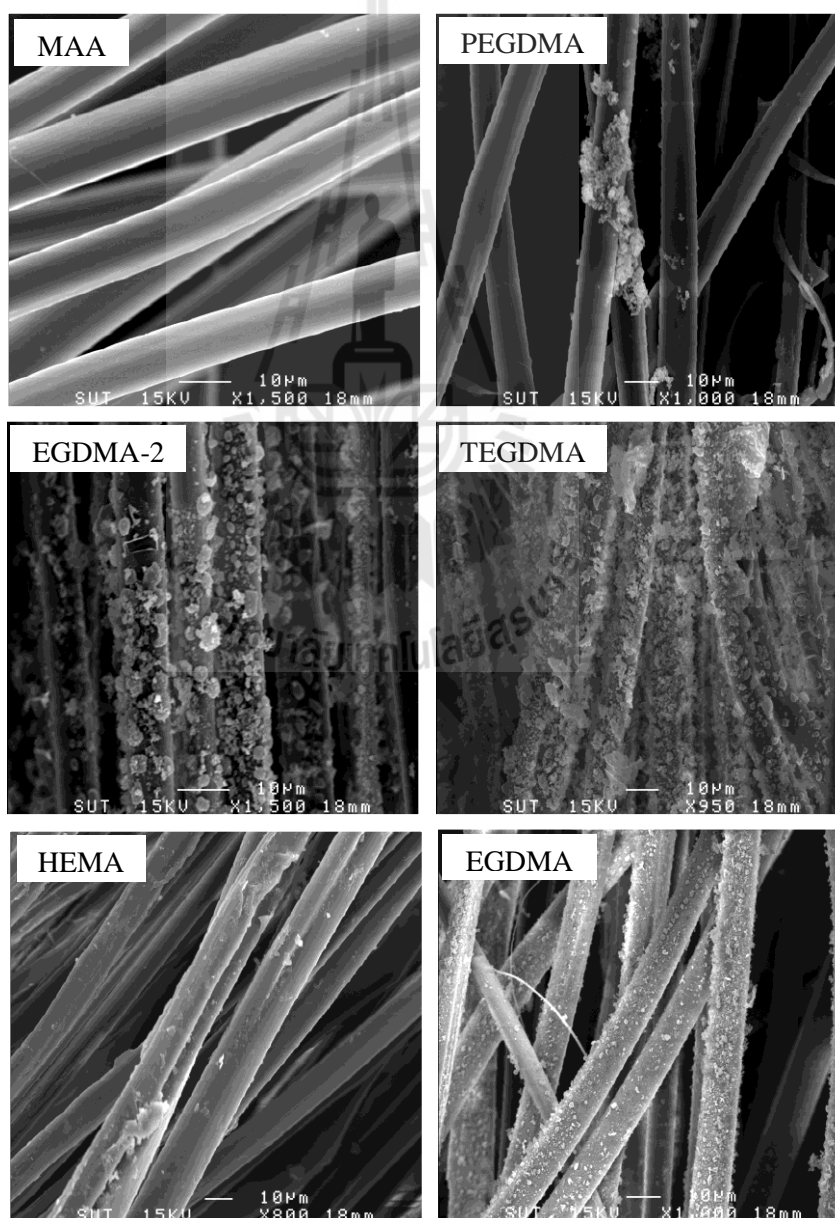


Figure 3.14 The morphology of silk fiber grafted with various methacrylic monomers.

sericin glue-like protein from raw silk fibers. All grafted silk has surface morphology are shown in Figure 3.14. MAA-grafted silk fibers are as smooth as that of untreated silk. The use of dimethacrylate monomers lead to much more morphological differences compared to other samples. Silk grafted with HEMA exhibits only slight traces of surface deposition of a very thin and uneven layer of poly(HEMA). The deposition becomes more frequent and thicker on the surface of silk fibers grafted with increased add-on monomer.

3.6 Conclusions

Silk fibers were grafted with various methacrylic monomers by heating via both conventional process and microwave irradiation. The grafted yield and efficiency were increased with add-on monomer increased. Methacrylates and dimethacrylates grafted onto silk had graft yields higher than MAA in the same operating condition. Silk fibers grafted with MAA and dimethacrylates were hydrophilic properties and gave softer touch to hand while HEMA which was good dyeing behavior were stiffer fibers. The molecular structure of grafted silk was investigated by ATR-FTIR analysis to confirm the structural pattern of fibroin with some peaks in addition to grafted polymer. XRD peak did not change regardless of different monomer types which confirmed that the fiber structure did not affected by the graft-copolymerization reaction with vinyl monomers. DSC analyses of metacrylic-grafted silk were performed to evaluate the influence of grafted monomer on the thermal behavior of grafted silk fibers. Thermal stability of grafted silk was further examined by TGA, which confirmed the results of DSC analyses and showed an increase of thermal stability for samples weighted with dimethacrylates. The surface morphology of

grafted silk fibers was observed that the deposit of polymer on the surface of silk fibers grafted with increase monomer add-on.

3.7 References

- Altman, G.H., Diaz, F., Jakuba, C., Calabro, T., Horan, R.L., Chen, J., Lu, H., Richmond, J. and Kaplan, D.L. (2003). Silk-based biomaterials. **Biomaterials** 24: 401-416.
- Asakura, T., Ashida, J., Yamane, T., Kameda, T., Nakazawa, Y., Ohgo, K. and Komatsu, K. (2001). A repeated β -turn structure in poly(Ala-Gly) as a model for silk I of *bombyx mori* silk fibroin studied with two-dimensional spin-diffusion NMR under off magic angle spinning and rotational echo double resonance. **Journal of Molecular Biology** 306: 291-305.
- Bhattacharya, A. (2004). Grafting: a versatile means to modify polymers techniques, factors and applications. **Progress in Polymer Science** 29: 767-814.
- Chen, G.Q., Guan, J.P., Xing, T.L. and Zhou, X. (2006). Properties of silk fibers modified with diethylene glycol dimethacrylate. **Journal of Applied Polymer Science** 102: 424-428.
- Ferrero, F., Periolatto, M. and Luraschi, M. (2007). Silk grafting with methacrylic monomers: process optimization and comparison. **Journal of Applied Polymer Science** 103: 4039-4046.
- Ferrero, F., Periolatto, M. and Songia, M.B. (2008). Silk grafting with methacrylic and epoxy monomers: thermal process in comparison with ultraviolet curing. **Journal of Applied Polymer Science** 110: 1019-1027.

- Freddi, G., Massafra, M.R., Beretta, S., Shibata, S., Gotoh, Y., Yasui, H. and Tsukada, M. (1996). Structure and properties of *bombyx mori* silk fibers grafted with methacrylamide (MAA) and 2-hydroxyethyl methacrylate (HEMA). **Journal of Applied Polymer Science** 60: 1867-1876.
- Gus'kova, O.A., Khalatur, P.G., Bäuerle, P. and Khokhlov, A.R. (2008). Silk-inspired 'molecular chimeras': atomistic simulation of nanoarchitectures based on thiophene-peptide copolymers. **Chemical Physics Letters** 461: 64-70.
- Mahmoodi, N.M., Moghimi, F., Arami, M. and Mazaheri, F. (2010). Silk degumming using microwave irradiation as an environmentally friendly surface modification method. **Fibers and Polymers** 11: 234-240.
- Misra, S., Nayak, P.L. and Sahu, G. (1982). Grafting vinyl monomers onto silk fibers. XV. Graft copolymerization of methyl methacrylate onto silk using thallium (III) as initiator. **Journal of Applied Polymer Science** 27: 1903-1911.
- Ojah, R. and Dolui, S.K. (2006). Graft copolymerization of methyl methacrylate onto *Bombyx mori* initiated by semiconductor-based photocatalyst. **Bioresource Technology** 97: 1529-1535.
- Ojah, R. and Dolui, S.K. (2007). Graft copolymerization of vinyl monomers onto silk fibers initiated by a semiconductor-based photocatalyst. **Journal of Applied Polymer Science** 105: 2164-2175.
- Prachayawarakorn, J. and Boonsawat, K. (2007). Physical, chemical, and dyeing properties of *bombyx mori* silks grafted by 2-hydroxyethyl methacrylate and methyl methacrylate. **Journal of Applied Polymer Science** 106: 1526-1534.

- Prachayawarakorn, J. and Kryratsamee, W. (2006). Dyeing properties of *bombyx mori* silks grafted with methyl methacrylate and methacrylamide. **Journal of Applied Polymer Science** 100: 1169-1175.
- Taddei, P. and Monti, P. (2005). Vibrational infrared conformational studies of model peptides representing the semicrystalline domains of *bombyx mori* silk fibroin. **Biopolymers** 78: 249-258.
- Takahashi, Y., Gehoh, M. and Yuzuriha, K. (1999). Structure refinement and diffuse streak scattering of silk (*Bombyx mori*). **International Journal of Biological Macromolecules** 24: 127-138.
- Tsukada, M., Arai, T., Freddi, G., Imai, T. and Kasai, N. (2001). Grafting vinyl monomers onto silk (*Bombyx mori*) using different initiators: Properties of grafted silk. **Journal of Applied Polymer Science** 81: 1401-1409.
- Tsukada, M., Freddi, G., Ishiguro, Y. and Shiozaki, H. (1993). Structural analysis of methacrylamide-grafted silk fibers. **Journal of Applied Polymer Science** 50: 1519-1527.
- Tsukada, M., Freddi, G., Matsumura, M., Shiozaki, H. and Kasai, N. (1992). Physical properties and dye ability of silk fibers modified with ethoxy ethylmethacrylate polymer. **Journal of Applied Polymer Science** 44: 799-805.
- Tsukada, M., Freddi, G., Monti, P. and Bertoluzza, A. (1993). Physical properties of silk fibers grafted with a binary mixture of styrene and n-butyl methacrylate. **Journal of Applied Polymer Science** 49: 1565-1571.

- Tsukada, M., Freddi, G., Monti, P., Bertoluzza, A. and Shiozaki, H. (1993). Physical properties of 2-hydroxyethyl methacrylate-grafted silk fibers. **Journal of Applied Polymer Science** 49: 1835-1844.
- Tsukada, M., Freddi, G., Shiozaki, H. and Pusch, N. (1993). Changes in physical properties of methacrylonitrile (MAN)-grafted silk fibers. **Journal of Applied Polymer Science** 49: 593-598.
- Tsukada, M., Imai, T., Freddi, G., Lenka, S. and Kasai, N. (1998). Grafting of vinyl monomers onto silk using redox systems. yellowing of silk. **Journal of Applied Polymer Science** 69: 239-246.
- Tsukada, M., Kasai, N. and Freddi, G. (1993). Structural analysis of methyl methacrylate-grafted silk fibers. **Journal of Applied Polymer Science** 50: 885-890.
- Zeng, J. (2003). Biodegradable electrospun fibers for drug delivery. **Journal of Controlled Release** 92: 227-231.

CHAPTER IV

THE EFFECT OF ADDING IONIC LIQUID ON SPINNABILITY AND CHARACTERISTICS OF REGENERATED *BOMBYX MORI* SILK FIBROIN NANOFIBER BY ELECTROSPINNING

4.1 Abstract

The electrospinning of *Bombyx mori* silk fibroin in formic acid, ionic liquid, and formic acid/ionic liquid mixture were investigated. The concentration of solution, needle diameter and an electric field were the main parameter to study their effect on the regenerated electrospun silk fibroin nanofiber. The rheological behavior of silk fibroin solution exhibited a transition from Newtonian fluid to non-Newtonian and the viscosity of silk fibroin solution is increased with increased silk fibroin concentration. The fiber could not be formed if the concentration was low and molecular weight was not high enough for chain entanglement. There was less beaded-fiber and progressively more smoothed-fiber as the silk solution concentration was increased. The fiber diameter size was changed with changing the electric field, the ratio of an applied voltage and distance between a tip and collector. Using high applied voltage resulted in smaller fiber with increased spinning distance. For a co-solvent system (formic acid/AmimCl), the beaded-fiber was gradually changed to smoothed-fiber with increasing AmimCl concentration. The morphology of silk fibroin was

slightly changed to connected-fiber with increasing AmimCl content and the fiber could not be formed as the concentration of ionic liquids was high enough.

4.2 Introduction

Due to alternating amino sequences in silk fibroin is always at fixed pattern and the chemical structure of poly(Ala-*alt*-Gly) in natural silk fibroin could not be changed. Another possible method to enhance the property of silk apart from grafting with polymer is to increase its surface area of silk fiber using an electrospinning technique to generate nanofiber. Nanofiber is the fiber with a diameter in the range micrometer down to tens of nanometers, depending on the polymer type and processing conditions. These nanofibers are of considerable interest for various kinds of applications, because they have several useful properties such as high specific surface area and high porosity. Possible application area are fiber membranes, wound dressings and scaffolds for tissue engineering (Sill and von Recum, 2008).

Basically, an electrospinning system consists of three major components: (1) a high voltage D.C. power supply, (2) a spinneret (*e.g.* a pipette tip *etc.*) and (3) a grounded collecting plate (a metal screen in usually, plate, or rotating drum) and utilizes a high voltage source to inject charge of a certain polarity into materials in solution or melt state. Then, it is accelerated towards a collector of opposite polarity.

Various parameters have a significant influence on its spinnability such as an applied voltage, tip to collector distance, concentration and viscosity. At high voltage, there have been reported that the fiber diameter was decreased and had a narrow diameter distribution, and the bead formation on the fiber was also decreased (Chen *et al.*, 2006) with rapid evaporation of solvent from the fiber. The fiber diameter was

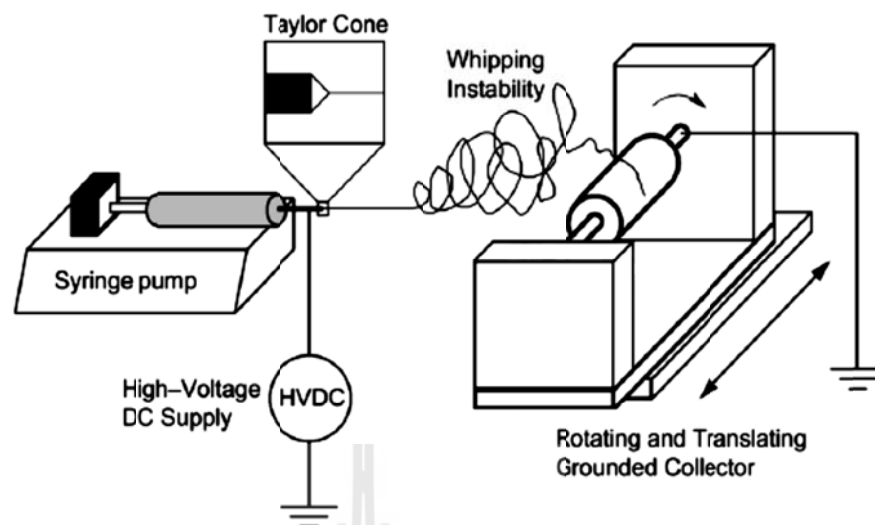


Figure 4.1 Schematic of a typical electrospinning system (Sill and von Recum, 2008).

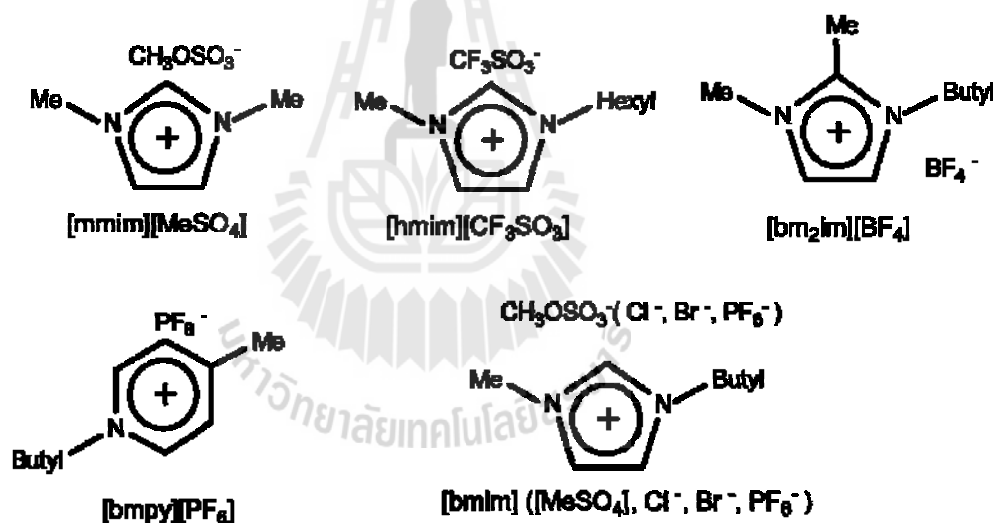


Figure 4.2 The structure and an example of ionic liquid.

also depended on distance between the tip and collector, when the tip to collector distance was increased, the fiber diameter was decreased. By varying the concentration, it results in different solution viscosity which affects the structure and diameter of the fiber. Low concentration or viscosity causes a discontinuous fiber formation. On the other hand, at high concentration or viscosity, there is a difficulty to

inject the solution from the tip to form fiber. High concentration can also cause the bead formation and the fiber diameter to be increased (Ayutsede *et al.*, 2005). Table 4.1 presents some conditions of electrospinning silk fibroin in various preparation conditions.

Generally, silk fibroin can be dissolved in Ajisawa's reagent (Lv *et al.*, 2005), LiBr (Chen *et al.*, 2006) or LiSCN. Then, salt ions can be removed by dialysis method and silk solution can be lyophilized to obtain silk fibroin. The process is time-consuming more than one week. Currently, ionic liquid has been used to successfully dissolve silk fibroin by disruption hydrogen bonding in silk fibroin (Phillips *et al.*, 2005; Sashina *et al.*, 2008). Ionic liquid, such as 1-Butyl-3-methylimidazolium chloride (BmimCl) can be used to dissolve silk fibroin for film casting and spinning (Phillips *et al.*, 2004; Philips *et al.*, 2007) but there is little study of ionic liquid in spinning silk process. In addition, the effect of coagulant after spun can induce β -sheet crystallite formation (Phillips *et al.*, 2005; Philips *et al.*, 2007). More recently, 1-allyl-3-methylimidazolium chloride (AMIMCl) was used to carry out silk fibroin (Wang *et al.*, 2012). It can be classified as good solvent for silk fibroin. The viscosity of ionic liquid solution was increased when its concentration was increased. For an electrospinning technique, the solution must flow and must have a high enough concentration to allow the molecules to hydrogen bond during the process to make long dimension fibers. A desirable other way to get low viscosity solution is to mix with other solvent to make a low viscosity of spinning dopes.

Hence, the binary solvent can be applied by dissolving silk fibroin in the main solvent and then gradually add small amount of cosolvent to make electrospinning solution. In this study, the focus is on the effect of adding an ionic liquid as cosolvent.

Table 4.1 Summary of electrospinning of silk fibroin at various conditions.

Condition (concentration, applied voltage, DTC, needle diameter, pH)	Viscosity	Fiber diameter size	Ref.*
12-15%, 15 kV, 7 cm, 0.495 mm.	250-600 cP	Average 80 nm., range 30-120 nm.,	1
12-18%, 15 kV, 20 cm, 0.7 mm.	-	Range 100-400 nm.	2
9-15%, 10-15 kV, 5, 7, 10 cm, 1 mm.	-	(9%) 8-223 nm., (15%) 12-397 nm.	3
17, 28, 39%, 20, 40 kV, 11 cm, 0.9 mm. pH 7.68	17%- 40 mPas. 28%- 250 mPas. 39%- 3000 mPas.	(17%) small droplets. (28%) 400-800 nm. (39%) 100-900 nm.	4
*natural silk fiber = 10-20 um.			
22-39%, 4 kV/cm, 0.6 mm, pH 4.8-6.9	0.1-5.3 Pas. (Increase with increasing concentration.)	Av 265-893 nm. (Decrease with decreasing concentration and pH.)	5

* 1 (Park *et al.*, 2004), 2 (Ki *et al.*, 2007), 3 (Ayutsede *et al.*, 2005), 4 (Wang *et al.*, 2006), 5 (Zhu *et al.*, 2007).

The small amount of ILs would be added into silk fibroin in formic acid solution little by little. The rheological behavior of some solution is also examined

before electrospinning. The morphology and the diameter size of electrospun fibers would be also investigated.

4.3 Experimental

4.3.1 Materials

Raw silk cocoons (*B. mori*) were obtained from the local silk plant in Nakhon Ratchasima province, Thailand. Raw cocoons were washed with water to remove any impurity from cocoons and cut into small pieces with the dimension of 1×1 cm approximately. Then, they were treated to remove sericin from fibroin by the same degumming process which described in prior Chapter III. Formic acid and methanol were supplied by QRec. Ionic liquid (ILs), BmimCl was provided by Takahashi's Lab, Kyushu University, and AmimCl was also synthesized in that lab. Na₂CO₃ was supplied by Sigma-Aldrich. All chemical are used without further treatment.

4.3.2 Dissolving process

Degummed silk cocoons were dissolved in Ajisawa's reagent at 80°C for 40 minutes until the solution was clear. Then, this solution was filtered to remove solidified silk fibroin and small fibers and followed by dialyzing against water for 3-4 days in cellulose tube with the molecular weight cut off (MWCO) 12-14 kDa to remove salt ions from silk fibroin. The dialysis tubes were soaked in water and were changed every day. After that, pure fibroin solution was lyophilized at -20°C for 24 h to obtain silk fibroin sponge. The sponges were kept in vacuum desiccators filled with silica gel for further use.

The other way to obtain silk fibroin was dried in hot air oven at 60°C. The pure fibroin after removed salt ion were dried in polystyrene dish in hot air oven at 60°C to obtain silk fibroin film. The fibroin was kept in vacuum chamber for electrospinning process. Electrospinning solution was prepared by dissolving silk fibroin sponge or film in the proper solvent. For Formic acid, fibroin was dissolved in 98% formic acid and stirred for 2 h or until the solution was clear and homogeneous. The concentration of silk fibroin solution was varied from 10-18% w/v. BmimCl and AmimCl were also used as solvent for electrospinning process, silk fibroin was dipped into ILs at a certain concentration and then heat in vacuum oven at 120 °C for 2 h. In the case of mixed solvent, the solution was prepared by dissolving silk fibroin in formic acid and gradually added ILs into the solution and stirred until the solution became homogenous.

4.3.3 Electrospinning process

The silk fibroin solution in formic acid was contained in a plastic syringe, which was connected to a metal needle with an inner diameter of 0.2 and 0.6 mm. A high-voltage power supply applied a voltage of 5-30 kV to the collector (flat piece covered with an aluminum foil). The electrospinning process was carried out at room temperature. The collector contained nonwoven fibers were immersed into methanol bath overnight in order to remove solvent from the electrospun fibers. Then, these fibers mats sample were dried in vacuum chamber for 10-20 min to remove methanol and kept in vacuum chamber more than 24 h before characterization.

4.4 Characterization

4.4.1 Rheology and viscosity of silk fibroin solution

The rheological behaviors were measured by Rheometer, Physical MCR301 (Anton Paar). The measurement geometry was the parallel plate with 25 mm diameter under air atmosphere for silk solution in formic acid. For silk solution in Ionic Liquids, geometry of measurement is the cone plate with a diameter of 25 mm under Nitrogen atmosphere. All measurements were carried out with 0.05 mm gap.

4.4.2 Surface morphology of fiber and average diameter size of fibers

The morphology of fiber was characterized by Scanning Electron Microscope: SEM JEOL JSM5310 and 3DSEM (KEYENCE VE9800 Real 3D system). Scanning electron microscope at 20 kV. Beam 6-8 and the working distance of 17-18 cm.

The diameter size of the electrospun fibers were examined by the statistical analysis. An image analysis software (WinRoof) was used to measure the diameter of fiber appeared in SEM image. SEM image was chosen at the same magnification (5000X and 10000X). The diameter size of fibers was calculated to investigate the average value of the silk fibroin fibers which appeared in SEM.

4.5 Results and discussion

There are many important processing parameters that affect the fiber morphology and its diameter of the regenerated SF fibers in electrospinning process, such as solution concentration, voltage, the distance between tip and collection plate

and the solvent type. Concentration of silk fibroin also affects the viscoelasticity of electrospin solution.

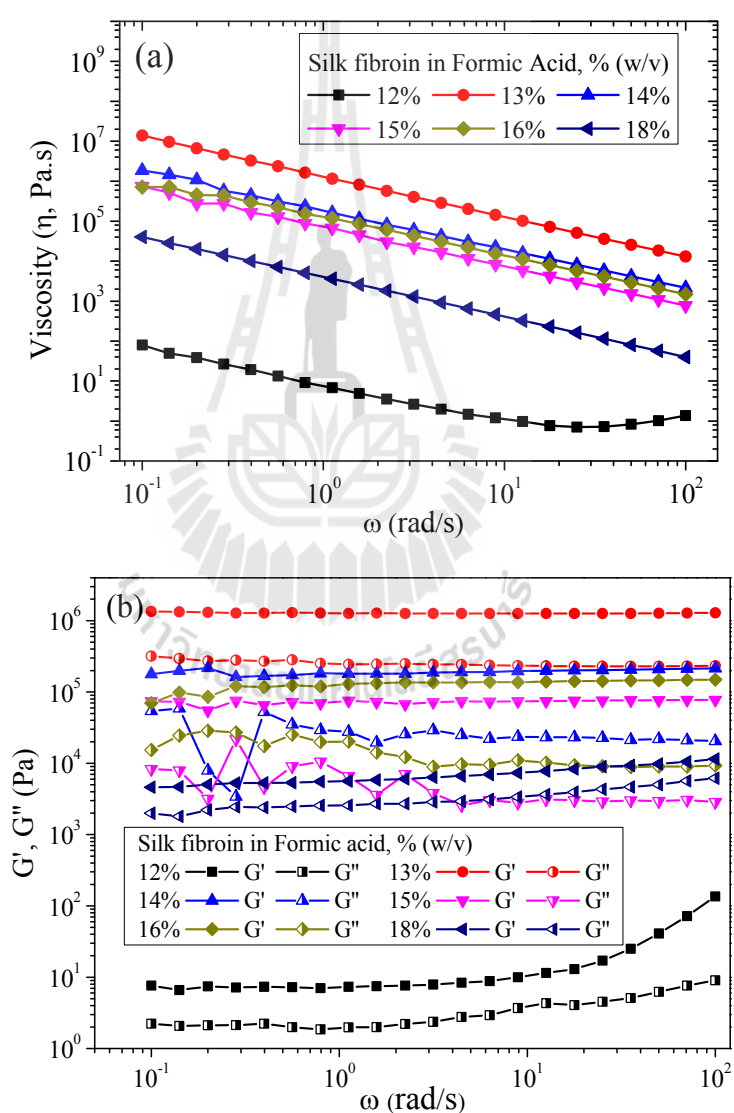
4.5.1 Effect of RSF concentration and needle diameter on fiber mats

Table 4.2 presents the processing parameter for the regenerated silk fibroin electrospinning process, *i.e.*, the range of concentration and needle inner diameter utilized in this experiment. Rheological behavior of solutions is very important for electrospinning. The viscosity and rheological behavior of RSF solutions with different concentrations is shown in Figure 4.3. It has been known that the shear thickening behavior is a stress induced phase separate and crystallization. However, the viscosity of silk fibroin solution is independent of shear rate. It can be observed that the shear thinning behavior at lower shear rate and the viscosity tends to be constant when further increasing the shear rates. This behavior indicates that the solutions are homogeneous and behave as a Newtonian fluid. These show that there are an intermolecular interactions at low shear rate for concentrated RSF solutions and constant viscosity is very helpful for electrospinning.

It is found that the viscosity of the RSF solutions at the concentration lower than 12 %w/v is too diluted. The silk fibroin molecules are in a random coil conformation with little entanglement between them (Wang *et al.*, 2006). So, it cannot be regenerated to fiber. The fiber can be formed at the concentration higher than 13 % w/v when the viscosity is increased by an entanglement from silk fibroin molecules in the electrospin solution to prevent the breakup of the electrically driven jet and to allow the electrostatic stress to further elongate the jet and draw it to fiber. The fluctuation of the viscosity is observed as the concentration dependent. This may be

Table 4.2 Processing parameters of the electrospinning RSF dissolved in formic acid.

	Process I	Process II
Needle inner diameter	0.9 mm	0.2 mm
Electric field	1.20-1.50 kV/cm	0.67-4.29 kV/cm
Concentration	12-18 %w/v	10-16 %w/v

**Figure 4.3** (a) viscosity and (b) rheological behaviors of silk solution in formic acid at various concentrations.

attributed to a difference of silk fibroin molecular weight from different batch in a preparation process. At higher concentration at 18 %w/v, the viscosity of solution is lower than 14 %w/v or 16 %w/v which is attributed to the sample ageing before measurement and the network-structure like conformation are formed during that time. These results suggest that there are intermolecular interactions of these RSF solutions and the constant viscosity or Newtonian fluid behavior is very helpful for electrospinning.

To confirm the behavior of the silk solution, the storage and loss modulus of silk fibroin solution were also investigated. All solutions indicated that there was a network structure like conformation or chain entanglement in solution. For 12 %w/v solution, it behaves as shear thickening at high shear rate in agreement with the viscosity data, while at higher concentration, 18 %w/v, the storage modulus (G') dominated the loss modulus (G'') due to the β -strand was more aligned in the solution and results in a solid-like behavior of such solution.

The morphology of electrospun fiber was observed by SEM technique. Table 4.3 shows the morphology of electrospun fiber of silk solution in formic acid with difference concentration and electric field (process I). The regenerated silk fibroin electrospun fibers were formed with many beaded-fibers at an initial concentration of 13 %w/v. At the same electric field, the electrospun fibers became more cylinder shape and thinner diameter with some beaded-fibers when the solution concentration was increased. This was attributed to lack of molecular entanglement in the solution. However, at high electric field and high concentration, the electrospun fiber became smoother and had less beaded in fibers.

From Table 4.3, the uniform cylindrical fibers with an average diameter of 195 nm could be obtained from an electrospun of the silk solution at concentration of 18 %w/v and the electric field (EF) at 2.0 kV/cm. Whereas, the smallest average fiber size was 166 nm at concentration of 14 %w/v at the same EF. Moreover, the largest average diameter fiber was 437 nm at concentration of 18 %w/v and EF at 1.2 kV/cm.

Moreover, the effect of needle diameter size was also studied with various concentration of silk solution (comparison between process I and II). The condition for the electrospinning process is composed of a difference in (1) an inner diameter of needle, (2) concentration and (3) electric field applied during an experiment which is already presented in Table 4.3. There were also similar results with previous finding as shown in Table 4.3. The silk fibroin fiber at 10 %w/v also has beaded-fibers and it can be seen that the fiber gradually smoother when the concentration is increased. This result is attributed to very low molecular entanglement of silk fibroin resulting that the fiber cannot be formed. At high concentration, there is high enough molecular entanglement to form smoothed and less beaded-fibers.

An inner diameter of a needle is also considered here. It can be observed that the electrospun fiber gave the larger fibers when an inner diameter of needle is larger (process I). At EF 2.00 kV/cm and concentration 16 %w/v, the average diameter of fibers decreased from 210 nm (Table. 4.3) to 148 nm (Table. 4.4). The relationship between concentration and average diameter size of fibers is presented in Figure 4.4 which indicates similar results as previous discussion.

Table 4.3 Morphology of electrospun RSF nanofibers at concentration of 13-18 %w/v in formic acid.

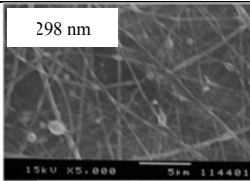
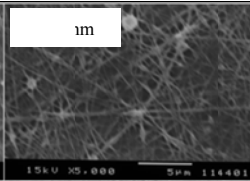
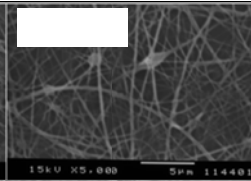
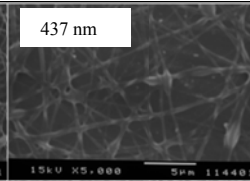
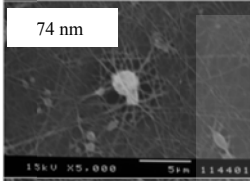
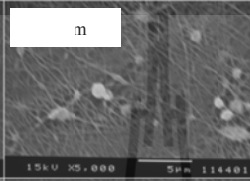
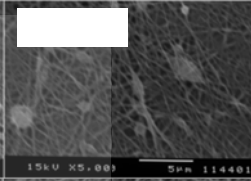
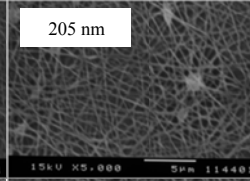
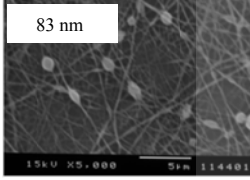
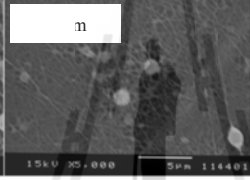
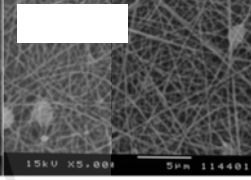
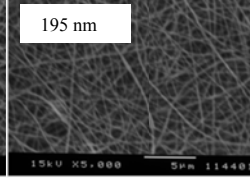
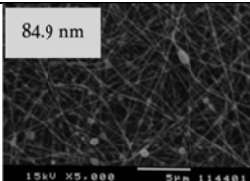
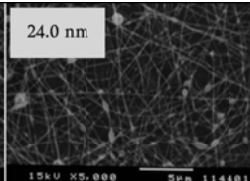
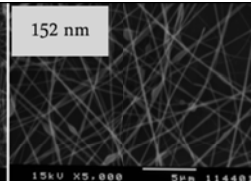
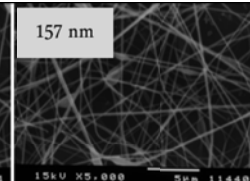
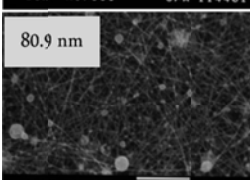
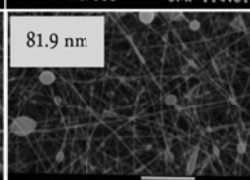
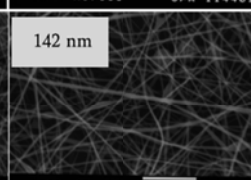
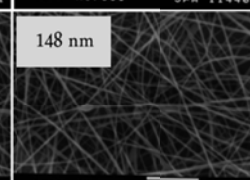
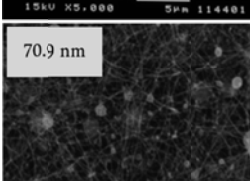
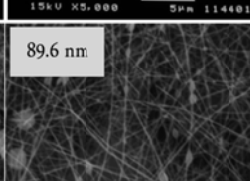
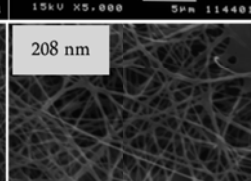
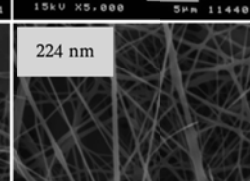
EF, kV/cm	Morphology and average diameter size (nm) at various concentration (%w/v)			
	13	14	16	18
1.2				
1.5				
2.0				

Table 4.4 The morphology and average size diameter of electrospun RSF nanofibers at concentrations of 10-16 %w/v in formic acid.

EF, kV/cm	Morphology and average diameter size (nm) at various concentration (%w/v)			
	10	12	14	16
1.00				
2.00				
3.00				

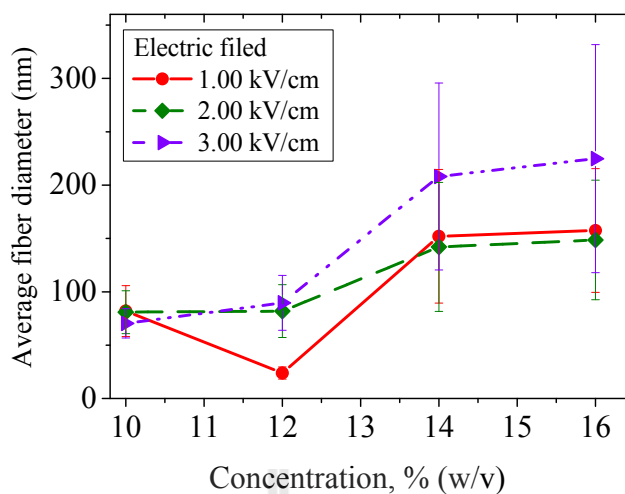


Figure 4.4 The relationship between an average fiber diameter and silk concentrations in formic acid at 10-16%w/v and electric field at 1.00-3.00 kV/cm.

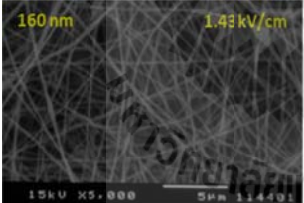
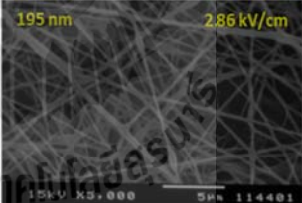
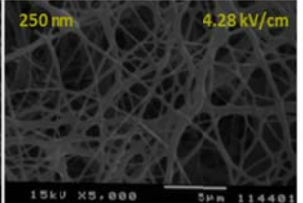
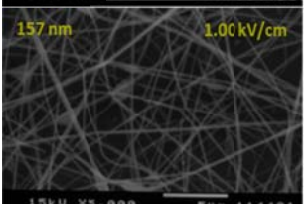
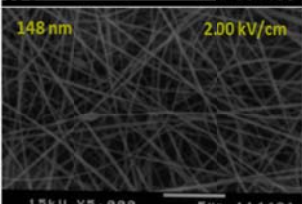
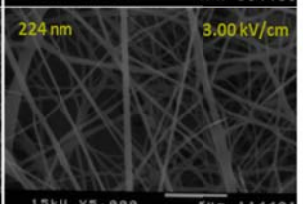
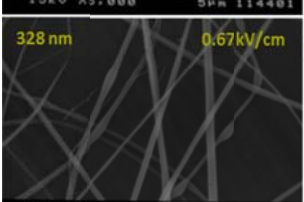
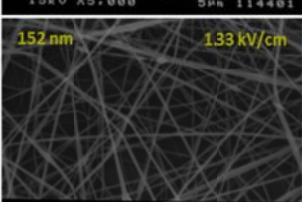
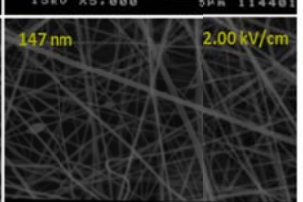
4.5.2 The effect of an electric field on nanofiber mats

Other factor which influenced the electrospinning process was also observed. Processing parameters for electrospinning is shown in Table 4.5 (Process III) to study the effect of an electric field (EF) and the distance between tip and collector (DTC) on the diameter size of electrospun fibers. The morphology and an average size diameter of the electrospun RSF nanofibers at concentration 14 %w/v at various EF are expressed in Table 4.6. Similar trend is also observed for the relationship between an average fiber diameter and the EF which is exhibited in Figure 4.5. For low applied voltage, the fiber diameter was increased with increasing the distance between tip and collector. This was because there was not enough an electric force to pull out the fibroin molecule and this led to coagulation of silk fibroin molecule resulting in thicker fibers when they were deposited on the collector. In contrast, at high applied voltage, the diameter of electrospun fibers became greater

Table 4.5 Processing parameters for electrospinning of various RSF concentration and electric field.

Process III	
Solvent	Formic acid
Needle inner diameter	0.2 mm
Electric field	0.67-4.28 kV/cm
Concentration	10-16 %w/v

Table 4.6 The morphology and average size diameter of RSF nanofibers at concentrations 14 %w/v in formic acid at EF from 0.67-4.28 kV/cm.

DTC (cm)	Applied Voltage (kV)		
	10	20	30
7			
10			
15			

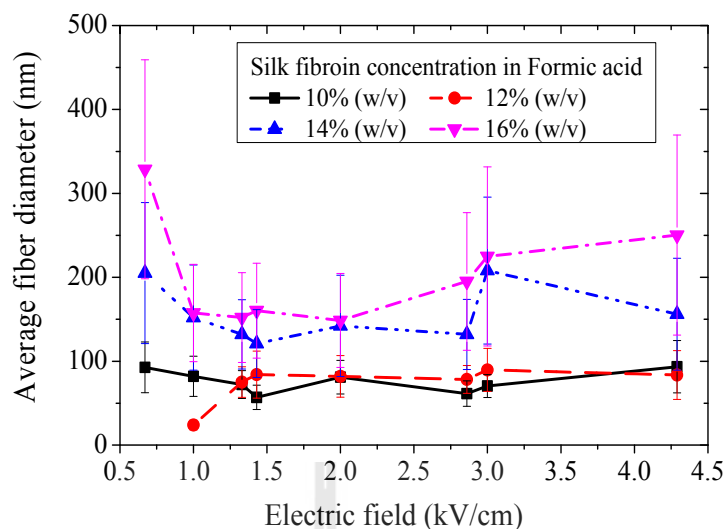


Figure 4.5 The relationship between an average fiber diameter and electric field at concentrations of silk fibroin in formic acid at 10-16 %w/v.

when the collector was placed close to the needle tip. These were attributed from the fibroin molecules which were pulled out and deposited on the collector in very short time. Hence, there was no enough time for the evaporation of solvent and the stretching of fibroin molecule to form a small fiber size.

Moreover, the DTC is one dominant factor on electrospun fibers. At same distance, the fiber diameter was increased with increasing applied voltage and it sometime gave connected-fiber. In contrast, at 15 cm DTC, the fiber diameter was decreased with increasing applied voltage which could be discussed by the same reason as prior effect. Furthermore, at the same EF, the fiber diameter was slightly decreased with higher applied voltage and DTC, but it was insignificant.

4.5.3 The effect of ionic liquids on nanofiber electrospinnability

4.5.3.1 The effect of BmimCl on electrospinnability

For the silk in BmimCl solution, it was found that the viscosity of the solution was increased with increasing concentration of silk fibroin as shown in Figure 4.6. At low concentration, 10-12 %w/v, silk fibroin molecules were random coil conformation with less molecular entanglement. At higher concentration, 14-18 %w/v of silk fibroin was higher viscosity with sufficient molecular entanglements. Hence, the viscosity of silk in BmimCl solution was higher than that in formic acid. The rheological behaviors of these solutions were also investigated, it was found that at concentration 10 %w/v and 12 %w/v, the G'' dominated G' at high shear rate and the crossover point was observed in both solutions which indicate the gelation behavior. For concentration at 18 %w/v, the solution was observed as the network-like structure or there was sufficient chain entanglement of silk fibroin molecules.

Electrospinning of some solution was processed and it was found that silk fibroin solution in BmimCl could not be electrospun (no fibers were formed) which is shown in Figure 4.7. This was caused by too high viscosity and too large surface tension of the solution and it was resulted in gel formation.

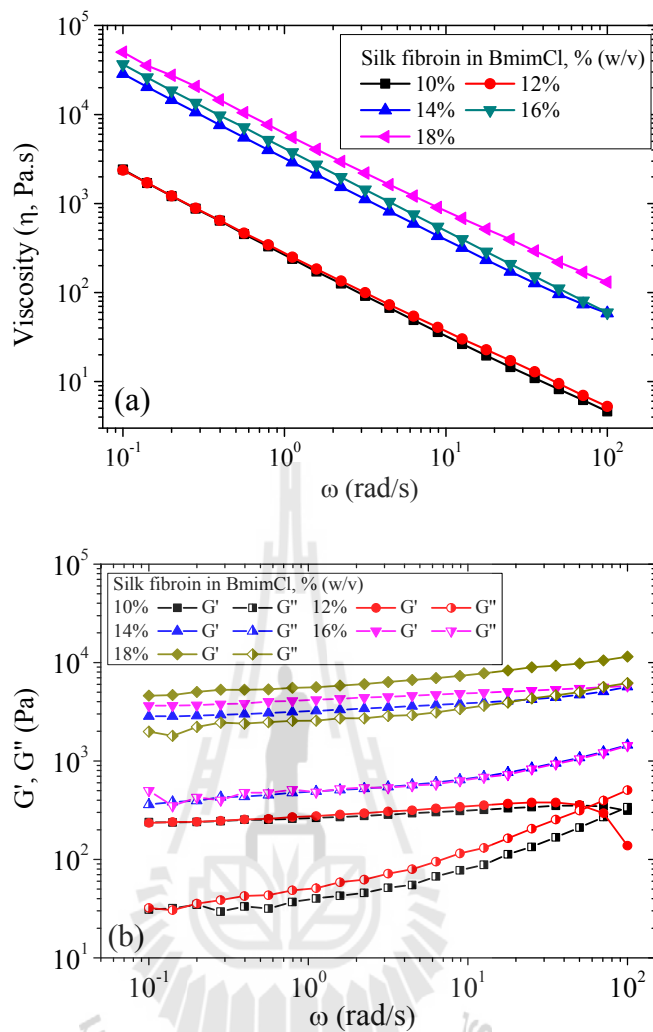


Figure 4.6 (a) viscosity and (b) rheological behaviors of silk fibroin in BmimCl with various concentrations.

4.5.3.2 The effect of adding AmimCl on electrospinnability

First, the silk fibroin in formic acid (Process IV) was studied to optimize the process parameters to compare with the co-solvent system (Process V). Similar results were observed as the previous experiment with some different conditions as displayed in Table 4.7.

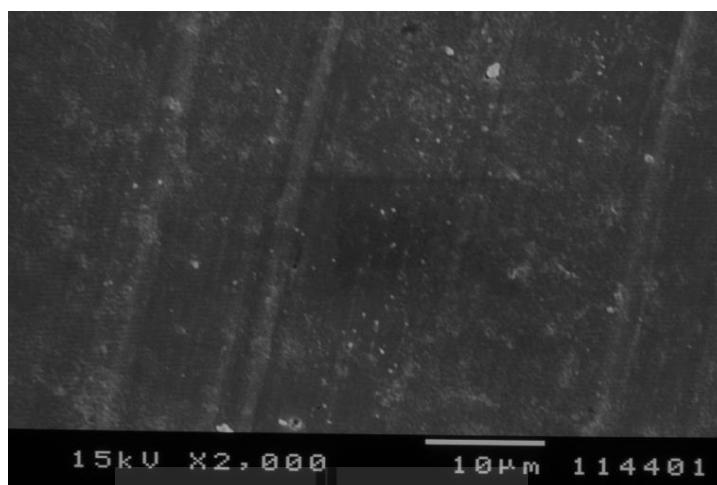


Figure 4.7 The morphology of electrospun silk fibroin in BmimCl solution at concentration of 12 %w/v.

Table 4.7 Processing parameters of the electrospinning RSF in mixed-solvent.

	Process IV	Process V
Solvent	Formic acid	Formic acid/AmimCl
Needle inner diameter	0.2 mm	0.6 mm
Electric field	0.67-4.28 kV/cm	2.00-3.40 kV/cm
AmimCl (%v*)	0	1-4 %v
Concentration	14 %w/v*	14 % w/v**

*v = volume of formic acid; **v = volume of formic acid and AmimCl mixture.

Table 4.8 - 4.9 show the morphology of an electrospun regenerated silk fibroin fiber at 14 %w/v in formic acid with different applied voltage, and the distance between tip and collector. Figure 4.8 shows an average size diameter of the fiber. These processing conditions can be utilized to produce nanofiber. Even though

the distance was adjusted to 5 cm, the fiber can be obtained with a smoother fiber. Hence, the distance was fixed at 5 cm to study the co-solvent system.

The distribution of fiber diameter are manifested in Figure 4.9 which is skewed to the left side but the values of the skewness are under acceptable limits and thus the distribution are assumed to be normal curve to carry out statistical analysis of the data. The morphology of electrospun silk fibroin in co-solvent is shown in Table 4.10-4.11 and they were connected-fiber after electrospun which was caused by the effect of high viscosity of co-solvent system with AmimCl.

At low concentration of AmimCl, the viscosity was low and the solution could be spun and silk fibroins could be formed into fibers. With an increasing the applied voltage, the fiber size was decreased due to the silk fibroin molecule was more stretched and the fiber had more beaded-fibers which was caused by the instability of an electrical charge jet during the electrospinning process. On the other hand, an increasing of AmimCl content led to high viscosity solution and the fibers were less stretched and coagulated. These effects were resulted in connected-fiber formation. This was attributed to the non-volatilization of AmimCl. However, those connected-fibers could be separated to single fibers with high enough voltage was applied during electrospinning process.

At low applied voltage, when AmimCl was increased, the fibers were tend to connect together because there was not enough electric force to pull out fibroin molecule and deposite on the collector. Contrast results were observed at higher electric forces, more single fibers were formed as there was enough electric force to pull out fibroin molecule and can be more stretched until deposited on collector.

Table 4.8 The morphology and average size diameter of electrospun RSF fiber at concentration 14 %w/v in formic acid (1).

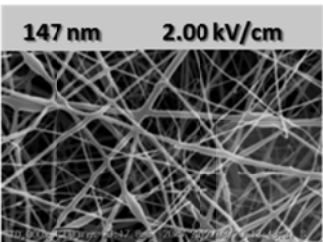
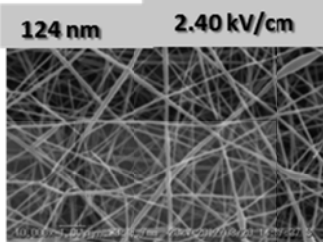
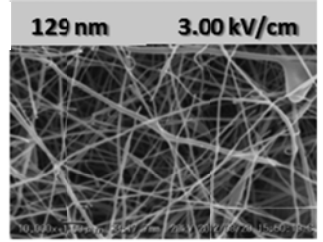
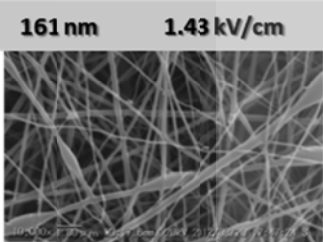
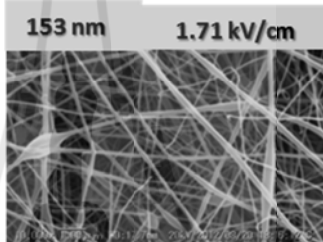
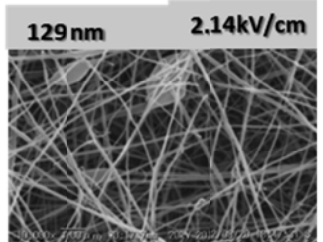
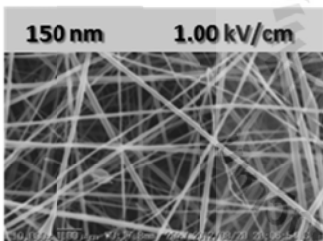
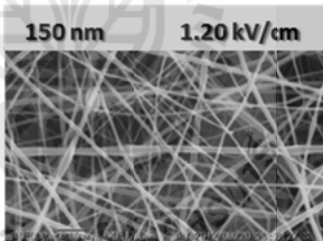
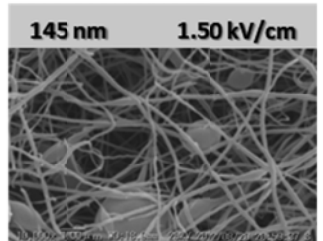
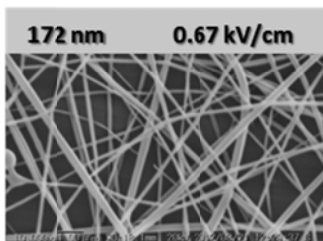
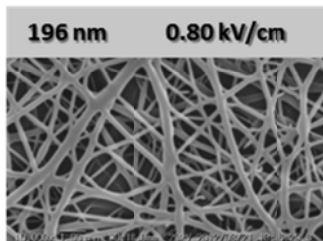
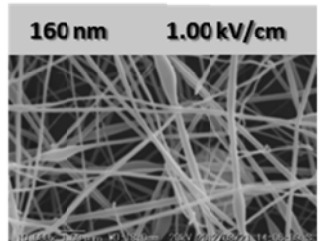
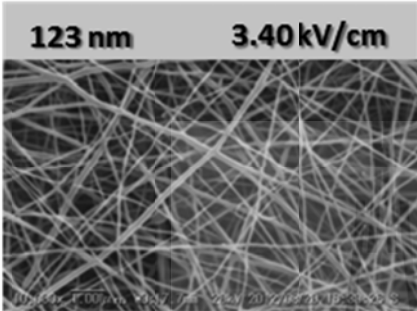
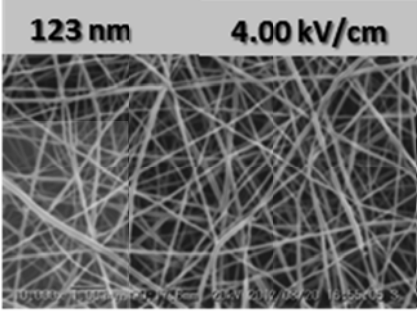
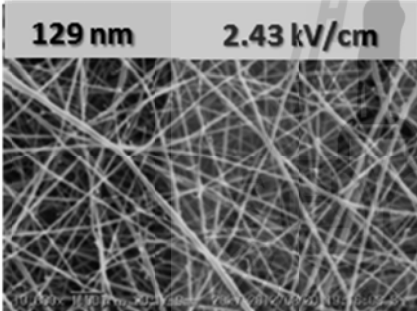
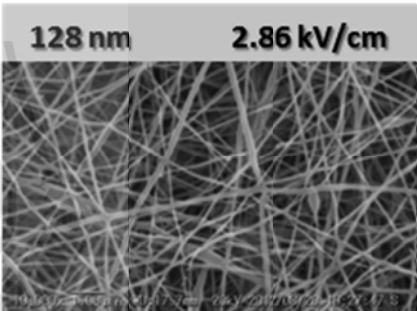
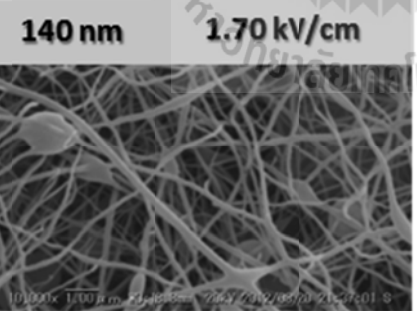
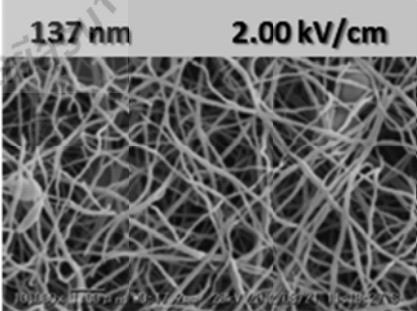
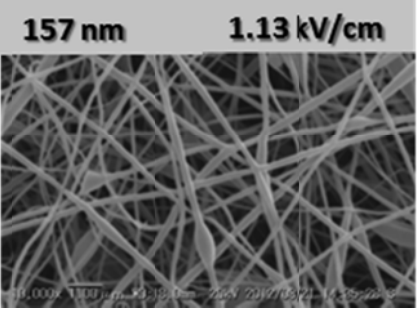
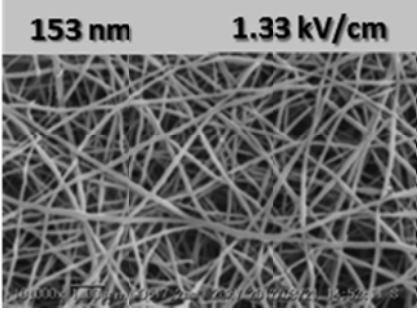
DTC	Applied Voltage (kV)		
(cm)	10	12	15
5	 <p>147 nm 2.00 kV/cm</p>	 <p>124 nm 2.40 kV/cm</p>	 <p>129 nm 3.00 kV/cm</p>
7	 <p>161 nm 1.43 kV/cm</p>	 <p>153 nm 1.71 kV/cm</p>	 <p>129 nm 2.14 kV/cm</p>
10	 <p>150 nm 1.00 kV/cm</p>	 <p>150 nm 1.20 kV/cm</p>	 <p>145 nm 1.50 kV/cm</p>
15	 <p>172 nm 0.67 kV/cm</p>	 <p>196 nm 0.80 kV/cm</p>	 <p>160 nm 1.00 kV/cm</p>

Table 4.9 The morphology and average size diameter of electrospun RSF fiber at concentration 14 %w/v in formic acid (2).

DTC	Applied Voltage (kV)	
(cm)	17	20
5	 <p>123 nm 3.40 kV/cm</p>	 <p>123 nm 4.00 kV/cm</p>
7	 <p>129 nm 2.43 kV/cm</p>	 <p>128 nm 2.86 kV/cm</p>
10	 <p>140 nm 1.70 kV/cm</p>	 <p>137 nm 2.00 kV/cm</p>
17	 <p>157 nm 1.13 kV/cm</p>	 <p>153 nm 1.33 kV/cm</p>

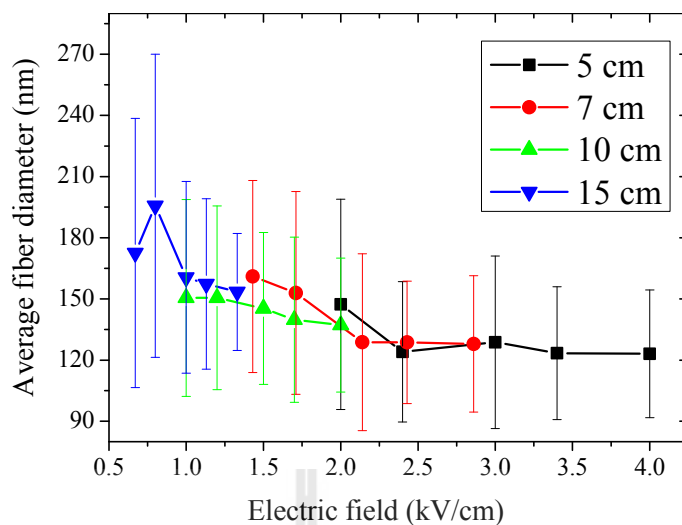


Figure 4.8 The relationship between average fiber diameter and electric field with concentration of 14 %w/v at difference spinning distance.

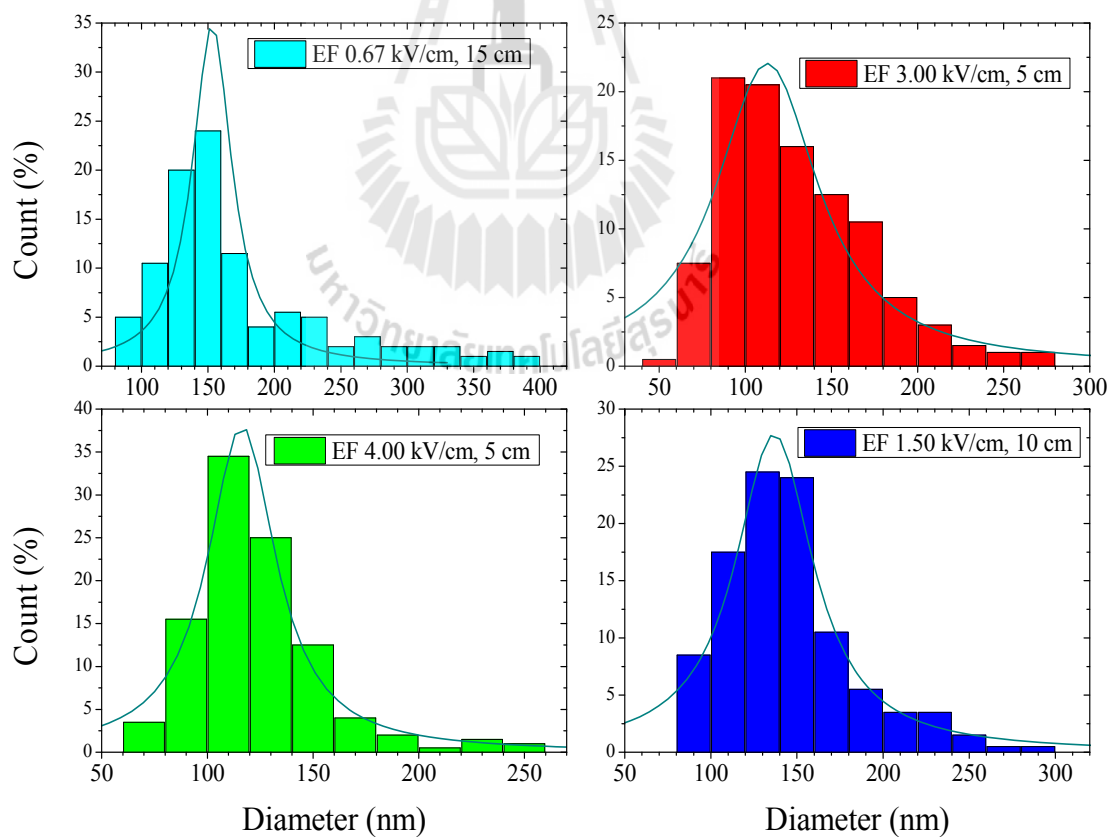


Figure 4.9 The distribution of fiber diameter of concentration of 14 %w/v with difference electric field and spinning distance.

Table 4.10 The morphology of electrospun RSF nanofibers at concentration 14 %w/v in FA/AmimCl system (1).

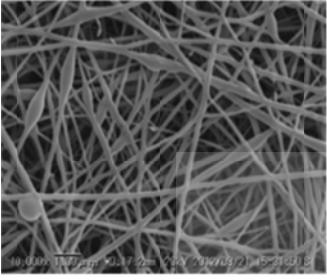
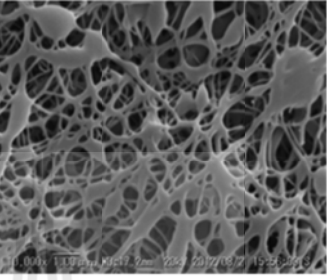
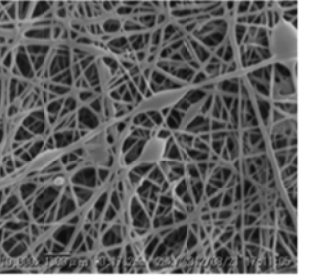
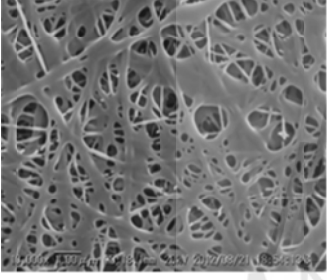
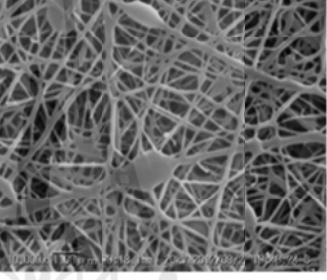
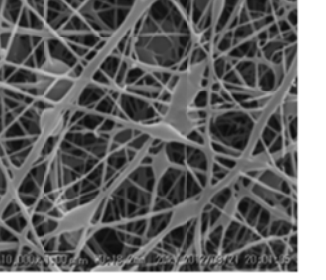
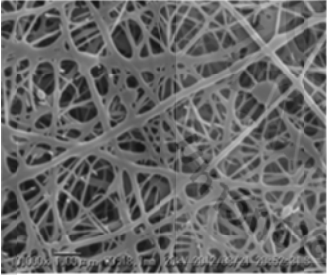
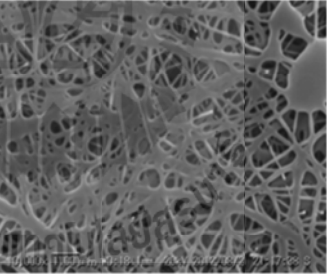
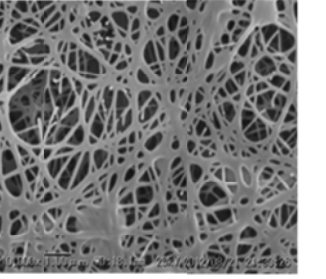
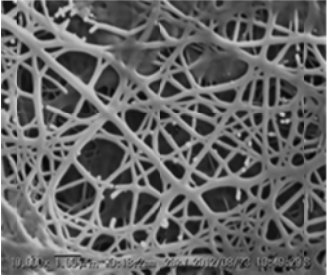
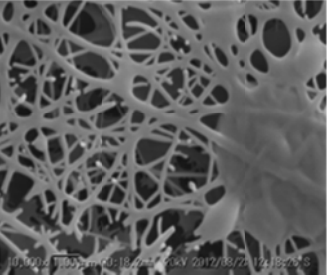
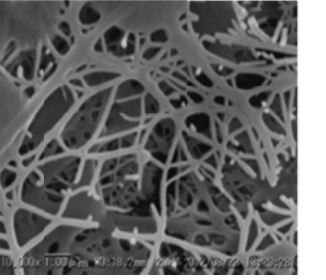
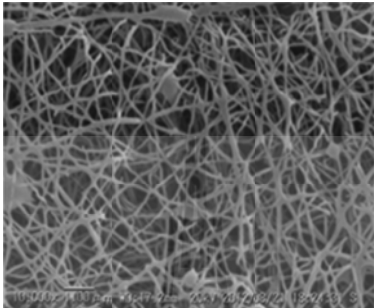
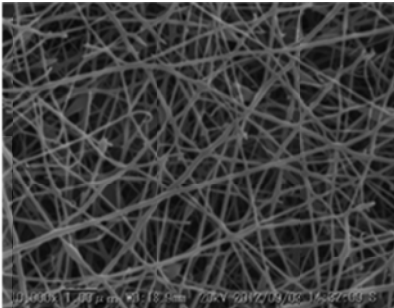
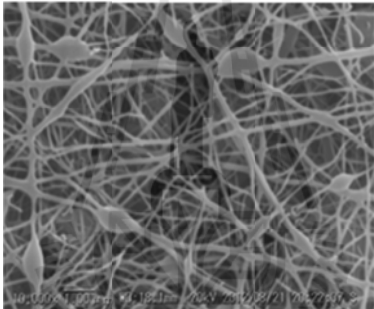
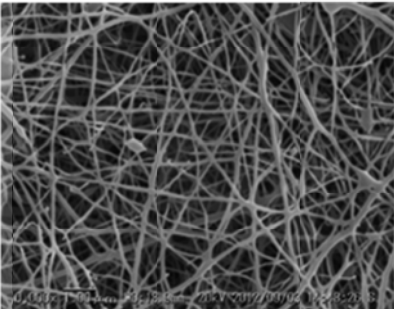
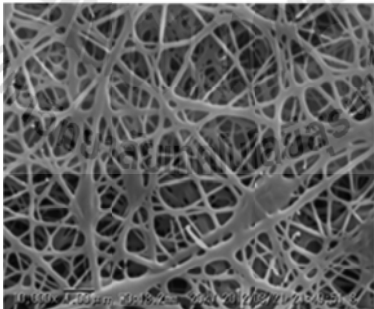
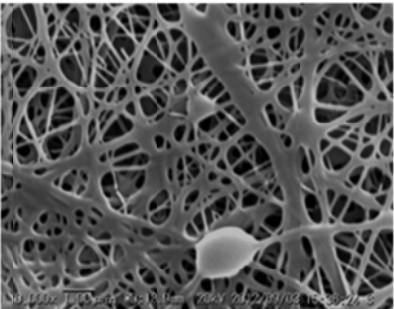
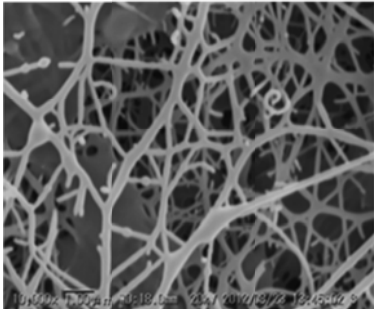
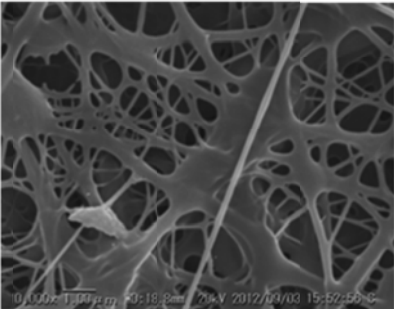
AmimCl (% v/v)	Electric field (kV/cm)		
	2.00	2.40	3.00
1			
2			
3			
4			

Table 4.11 The morphology of electrospun RSF nanofibers at concentration 14%w/v in FA/AmimCl system (2).

AmimCl (% v/v)	Electric field (kV/cm)	
	3.40	4.00
1		
2		
3		
4		

4.6 Conclusions

The electrospinning of *Bombyx mori* silk fibroin in formic acid, ionic liquid, and formic acid/ionic liquid mixed solvent were investigated. The viscosity of silk solution increased with increasing silk fibroin concentration. The rheological behavior of the solution exhibited a transition from Newtonian to non-Newtonian fluid and it formed the gelation at high concentration. The concentration, needle diameter and an electric field are parameter to affect the electrospun silk nanofiber. The fiber cannot be formed if there was insufficient molecular entanglement. There were less beaded-fiber and gradually changed to smoother fiber as increases concentration. Low electric field had no enough electric force to pull fibroin molecule and resulting in thick fibers. High applied voltage gave smaller fiber with increased spinning distance. For co-solvent with AmimCl system, the beaded-fiber was gradually changed to smoothed-fiber with increasing applied voltage and decreased AmimCl concentration. The morphology of silk fibroin slightly changed to connected-fiber with increasing AmimCl.

4.7 References

- Ayutsede, J., Gandhi, M., Sukigara, S., Micklus, M., Chen, H.-E. and Ko, F. (2005).
Regeneration of *Bombyx mori* silk by electrospinning. Part 3:
characterization of electrospun nonwoven mat. **Polymer** 46: 1625-1634.
- Ayutsede, J., Gandhi, M., Sukigara, S., Micklus, M., Chen, H. and Ko, F. (2005).
Regeneration of *bombyx mori* silk by electrospinning. part 3:
characterization of electrospun nonwoven mat. **Polymer** 46: 1625-1634.

- Chen, C., Chuanbao, C., Xilan, M., Yin, T. and Hesun, Z. (2006). Preparation of non-woven mats from all-aqueous silk fibroin solution with electrospinning method. **Polymer** 47: 6322-6327.
- Ki, C.S., Kim, J.W., Hyun, J.H., Lee, K.H., Hattori, M., Rah, D.K. and Park, Y.H. (2007). Electrospun three-dimensional silk fibroin nanofibrous scaffold. **Journal of Applied Polymer Science** 106: 3922-3928.
- Lv, Q., Cao, C., Zhang, Y., Ma, X. and Zhu, H. (2005). Preparation of insoluble fibroin films without methanol treatment. **Journal of Applied Polymer Science** 96: 2168-2173.
- Park, W.H., Jeong, L., Yoo, D.I. and Hudson, S. (2004). Effect of chitosan on morphology and conformation of electrospun silk fibroin nanofibers. **Polymer** 45: 7151-7157.
- Phillips, D.M., Mantz, R.A., Trulove, O.C. and DeLong, H.C. (2007). Regeneration of silk and silk-like fiber from ionic liquid spin dopes. United States, The United States of America as represented by the Secretary of the Air Force: 6.
- Phillips, D.M., Drummy, L.F., Conrady, D.G., Fox, D.M., Naik, R.R., Stone, M.O., Trulove, P.C., De Long, H.C. and Mantz, R.A. (2004). Dissolution and regeneration of *bombyx mori* silk fibroin using ionic liquids. **Journal of the American Chemical Society** 126: 14350-14351.
- Phillips, D.M., Drummy, L.F., Naik, R.R., De Long, H.C., Fox, D.M., Trulove, P.C. and Mantz, R.A. (2005). Regenerated silk fiber wet spinning from an ionic liquid solution. **Journal of Materials Chemistry** 15: 4206-4208.
- Sashina, E.S., Novoselov, N.P., Kuz'mina, O.G. and Troshenkova, S.V. (2008). Ionic liquids as new solvents of natural polymers. **Fibre Chemistry** 40: 270-277.

- Sill, T.J. and von Recum, H.A. (2008). Electrospinning: applications in drug delivery and tissue engineering. **Biomaterials** 29: 1989-2006.
- Wang, H., Shao, H. and Hu, X. (2006). Structure of silk fibroin fibers made by an electrospinning process from a silk fibroin aqueous solution. **Journal of Applied Polymer Science** 101: 961-968.
- Wang, Q., Yang, Y., Chen, X. and Shao, Z. (2012). Investigation of Rheological Properties and Conformation of Silk Fibroin in the Solution of AmimCl. **Biomacromolecules** 13: 1875-1881.
- Zhu, J., Shao, H. and Hu, X. (2007). Morphology and structure of electrospun mats from regenerated silk fibroin aqueous solutions with adjusting pH. **International Journal of Biological Macromolecules** 41: 469-474.

CHAPTER V

STRUCTURAL AND DYNAMIC PROPERTIES OF PP/PP BLENDS WITH DIFFERENT CHAIN TACTICITY: MONTE CARLO SIMULATION

5.1 Abstract

The conformational and dynamic properties of polypropylene (PP) chains with different tacticity were investigated based on a lattice Monte Carlo simulation of *i*PP, *a*PP and *s*PP pure melts and blends. The simulations of coarse-grained PP models were performed on a high coordination lattice, with incorporation of short range intramolecular interactions from a Rotational Isomeric State (RIS) model, and incorporation of long range interactions defined by a Lennard-Jones (LJ) potential function of propane pairs. The dynamics of PP chains in PP/PP binary mixture were simulated with the compositions of C₁₅₀H₃₀₂ at different tacticity. It was found the diffusion rate of polypropylene with different stereochemistry is generally ordered as *i*PP > *a*PP >> *s*PP. For PP/PP blend with 50:50 wt% binary mixtures, immiscibility was observed when *s*PP was introduced into the mixtures. The diffusion rate of *i*PP and *a*PP became lower after mixing, while *s*PP diffuses faster in the mixtures significantly. Intramolecular contribution does not provide any clear correlation to the diffusion changes of PP melts. Mobility of PP chains depends on both intramolecular contribution and intermolecular contribution. The effect of intramolecular

contribution (molecular size and chain stiffness) is greater than intermolecular contribution (chain packing) for *i*PP and *a*PP chains in binary mixtures. For *s*PP chain, intermolecular contribution affects the polymer dynamics greater than intramolecular interactions effects.

5.2 Introduction

Blending is one of the most effective methods to develop new materials for special applications by mixing two or more components together. This strategy is usually used to produce new polymeric materials. However, most of polymer blends are heterogeneous on mesoscale and often leads to macroscopic phase separation, due to the micro-phase separation between polymers, though macroscopically homogeneous. It is well known that the micro-phase separation structure of polymer blend is controlled by its compositions (Wang *et al.*, 2001; Peng *et al.*, 2004; Leung *et al.*, 2009). Small difference in the covalent structure of the chains is subject to strong change in the qualitative appearance of the phase diagram (Graessley *et al.*, 1995; Krishnamoorti *et al.*, 1996). The mixing behavior of polymeric hydrocarbon melts to minor structure change is illustrated by various experimental and theoretical investigations of conventional polyolefins (Choi *et al.*, 1995; Akten and Mattice, 2001).

The behavior of simple polymeric hydrocarbon pair is polyethylene (PE) and polypropylene (PP) blends, which are known to be incompatible in general (Wignall *et al.*, 1982; Freischmidt *et al.*, 2001). Phase separation in the melts consistent with short range order in liquid state of PE and PP. In case of PE, the radius of gyration of the molecules remained constant in both crystal and melt state (Ballard *et al.*, 1977;

Aharoni *et al.*, 1979). Immiscibility of PE/PP blends can be also illustrated by pair correlation function, the solubility parameter and Flory-Huggins parameter (Rajasekaran *et al.*, 1995).

PP melt provides very interesting example of the sensitivity of the mixing of polymeric hydrocarbon polymers. A binary mixture of *a*PP and *i*PP are miscible in the melts (Lohse, 1986), but immiscibility was observed when slightly replaced either species by *s*PP (Lohse, 1986; Thomann *et al.*, 1996). However, the mechanism responsible of immiscibility in PP was found to be different from PE/PP blends in the melts state. The chain dimension and the cohesive energy of PP mixtures retained approximately the same in the two-component melts as they had in the one-component melts (Haliloglu *et al.*, 1998). Moreover, it has been found that the mixing energy change of the two-component, ΔE_{AB} , is indistinguishable from zero in case of *a*PP and *i*PP, but it shows increasing of the value, greater than zero, if either component is replaced by *s*PP (Clancy *et al.*, 2000). These results agree with the transfer behavior of PP chain which the value of chemical potential, $\Delta\mu$, is indistinguishable from zero if the transferred chain is either *i*PP or *a*PP. However, $\Delta\mu$ of *s*PP is greater than zero for transferred to either *s*PP/*i*PP or *s*PP/*a*PP melts (Xu *et al.*, 2002). In addition, the pair correlation function utilized to characterize the intermolecular interaction of polymer blend, and it shows that *s*PP tends to avoid close contact with *i*PP stronger than *a*PP (Clancy *et al.*, 2000). These results were observed in experiment too, that these two blends are immiscible, with the immiscibility being stronger in *i*PP/*s*PP than in *a*PP/*s*PP blends (Maier *et al.*, 1997). In all those cases, focus was put on miscibility predictions and the miscibility behavior of the systems by statistical characterization.

The mobility of *i*PP and *s*PP were studied and found that both had similar average mobilities, where individual beads in individual chains can be departed strongly from the average. Every bead in *i*PP melt can mobile in the short time with a mean-square displacement (MSD) $> 30 \text{ \AA}^2$. In case of *s*PP melt, a few beads had not moved during the longer time. So, the correlation times for conformational transitions for *s*PP were slower than *i*PP (Antoniadis *et al.*, 1999). In *s*PP/*i*PP melts system, when the *s*PP was more strongly diluted by *i*PP, all beads of *s*PP had MSD higher than that in pure *s*PP melts. The mobilities analysis of the individual beads in *s*PP chains in blended system expressed slow mobility of *s*PP when its environment changes to *s*PP (Clancy *et al.*, 2000).

In this chapter, the dynamics change for each PP chains was investigated in PP/PP binary mixtures. The dynamical Monte Carlo simulation was utilized to examine the dynamic properties of each different tacticity PP chains in both pure melts and blend system. The different tacticity of neat PP melts and PP/PP blends with different tacticity of 50:50 %w/w binary mixtures were simulated and investigated. The structural and dynamic properties were then reported and compared between PP chains before and after mixing in PP/PP binary mixtures.

5.3 Model and method

System description

The simulation was performed with 64 PP independent parent chains and each of 50 beads in periodic boundary condition of $30 \times 30 \times 30$ lattice unit (2.5 \AA per each lattice unit). This unit cell produced a density of 0.750 g/cm^3 with 11.85% of bead occupancy on *2nnd* lattice (but the remaining from bead occupancy (88.15%))

Table 5.1 Number of chains for PP pure melts and binary mixtures (50 %w).

Systems	Number of chains		
	<i>i</i> PP	<i>a</i> PP	<i>s</i> PP
<i>i</i> PP pure melts	64	-	-
<i>a</i> PP pure melts	-	64	-
<i>s</i> PP pure melts	-	-	64
<i>i</i> PP/ <i>a</i> PP mixture	32	32	-
<i>i</i> PP/ <i>s</i> PP mixture	32	-	32
<i>a</i> PP/ <i>s</i> PP mixture	-	32	32

was not freely accessible). The system density was determined by the geometry of the high-coordination lattice and the associated mass of a $-CH_2CH(CH_3)-$ unit with each bead placed on this lattice. Simulations were reported for six compositions which composed of three systems of pure PP melts and of PP/PP binary mixtures as was expressed in Table 5.1. Monte Carlo simulation was performed by the method which was described in Chapter II.

5.4 Results and Discussion

5.4.1 Neat PP melts

The structural and dynamic changes of PP chains in neat melts are compared in Figure 5.1(a) which shows the orientation autocorrelation function of the end-to-end vector (OACF, $\langle R(t).R(0) \rangle$) of PP melts with different tacticity. *i*PP and *a*PP ($P_m = 0.5$) exhibit a complete decay from an initial value to zero within 10^7 MCS.

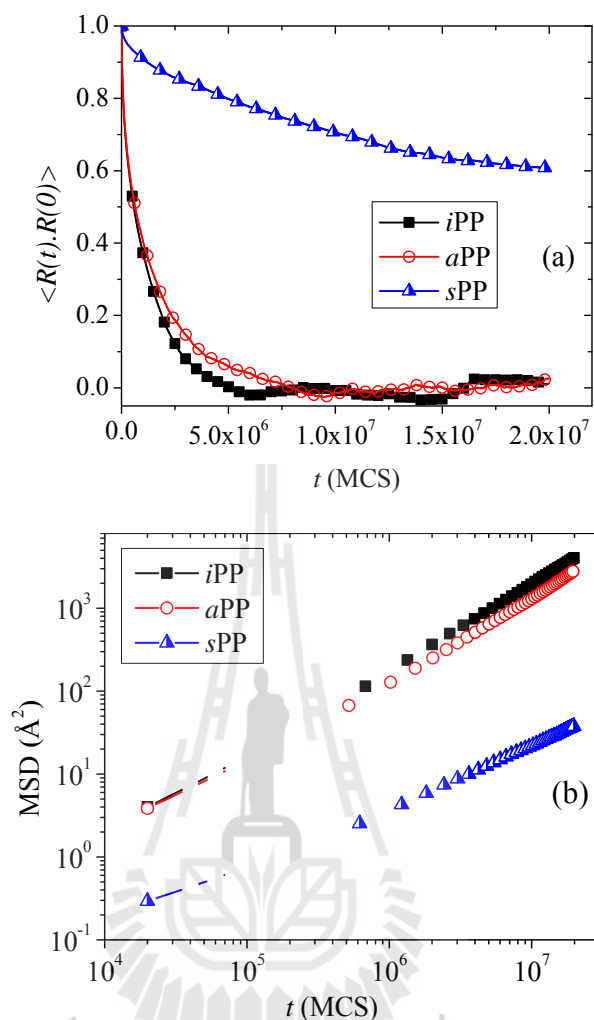


Figure 5.1 (a) Orientation autocorrelation function for the end-to-end vector and (b) Mean-square displacement of the centers-of-mass in \AA^2 for PP pure melts.

While that of *s*PP decays to only about 0.6 from an initial value. The *s*PP melts is considerably decay slower rate than others which may be caused by longer *trans* sequences in *s*PP chain. In addition, the mean-square displacement (MSD) of the centers-of-mass of PP melts with different tacticity is also given in Figure 5.1(b). Similar results to the OACF decay are observed. *i*PP diffuses faster than *a*PP and *s*PP, and the diffusion rate can be ordered as: $iPP > aPP \gg sPP$.

Table 5.2 presents typical parameters to characterize the properties of PP melts which consist of the diffusion coefficient (D), the mean square radius of gyration, $\langle R_g^2 \rangle^{1/2}$ and the characteristic ratio (C_n), which represent the system mobility, molecular size and chain rigidity, respectively. The molecular size and chain stiffness are the largest due to the *racemic* diads in *sPP* prefer to hold up in *trans* conformation and these lead to the slowest diffusion rate for *sPP* compared to others.

On the other hand, the mean square radius of gyration and characteristic ratio of *iPP* is greater than *aPP* because all *meso* diad in *iPP* chain prefer to helix conformation instead of an extended *trans* conformation. Helix conformation in *iPP* chains induces smaller chain dimension and chain stiffness. *iPP* has the largest chain dimension and an intermediate chain stiffness compared to *aPP* and *sPP*. However, *iPP* exhibits the fastest diffusion rate; therefore, an intramolecular effect (chain dimension and chain stiffness) may not be the key factors to control the dynamics of *iPP* melts. Instead, the overall mobility of PP melts can be ordered as: $iPP > aPP \gg sPP$ in both rotational and translational mode. These results suggest that not only intramolecular effect *i.e.* molecular size and chain rigidity can influence the mobility of PP chains but also the intermolecular effect (molecular packing). From the previous study in PP blend (Haliloglu and Mattice, 1999), intermolecular pair correlation functions (PCFs) of *iPP*, *aPP*, *sPP* melts were reported. PCFs data are more distinguishable from one another at in the range of 5-8 Å. *sPP* also exhibits the highest PCFs at the distance 5-8 Å compared to *aPP* and *iPP*. On the other words, *sPP* chains prefer to interact with itself more than others and have the highest chain packing density while *aPP* and *iPP* exhibit loose chain packing. These results suggest

Table 5.2 Mean square radius of gyration, $\langle R_g^2 \rangle^{1/2}$ (Å), characteristic ratio (C_n), $\langle r^2 \rangle_0/nl^2$ and diffusion coefficient, D (Å²/MCS) of PP pure melts.

Chain	$\langle R_g^2 \rangle^{1/2}$ (Å)	C_n	D (Å ² /MCS)
<i>i</i> PP	12.97	4.40	3.42E-5
<i>a</i> PP	12.72	4.23	2.35E-5
<i>s</i> PP	13.54	4.80	2.98E-7

that *s*PP melts retain more “structured” than those of *a*PP and *i*PP melts (Haliloglu and Mattice, 1999). Chain packing in *s*PP causes more difficulty for chain to move whereas *i*PP and *a*PP can move more easily. Both intramolecular and intermolecular contribution affect mainly on *s*PP while the effect of intermolecular contribution is significantly greater than intramolecular contribution in case of *a*PP and *i*PP.

5.4.2 PP/PP binary mixture

For the PP/PP blended system, the mobility of each PP chain with different tacticity compared to both pure melts and binary mixture system. The $\langle R(t).R(0) \rangle$ and MSD of PP/PP binary mixture are presented in Figure 5.2(a) and Figure 5.2(b), respectively. They represent the dynamic behavior of PP melts in overall mixtures. All PP/PP binary mixtures show the decay to about half of an initial value within 5×10^6 MCS which can be distinguishable from other systems. The overall diffusion rate of each PP mixture decreased when a half of *i*PP or *a*PP were replaced by *s*PP chains.

Similar to neat PP melts, which the chain interaction between itself is stronger than other chains with different tacticity and it leads to denser chain packing.

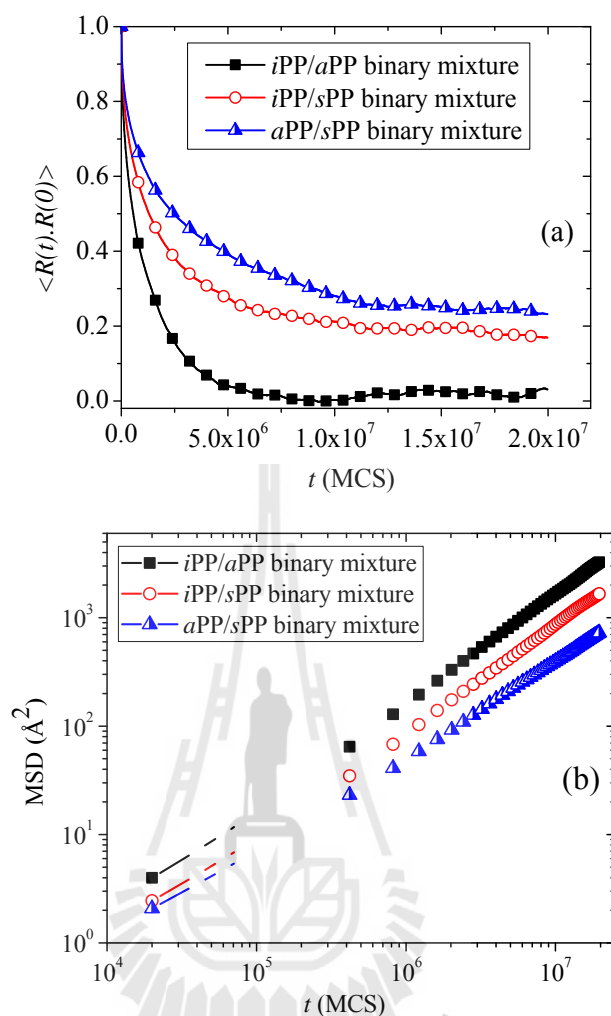


Figure 5.2 (a) Orientation autocorrelation function for the end-to-end vector and (b) Mean-square displacement of the centers-of-mass in \AA^2 for PP binary mixtures.

In addition, the PCFs of PP binary mixture indicate that beads in each chain prefer to be surrounded by beads of other PP chains with the same tacticity (Clancy and Mattice, 2001). Similarly, the iPP chains which are consisted of *meso* diad are strongly avoid *trans* conformation (iPP chains prefer helix conformation instead). iPP chains prefer to stay apart from sPP chains (due to *racemo* diad from sPP which prefer *trans* conformation). On the other hand, iPP chains do not differentiate among

themselves and *aPP* chains in the melts because those *iPP* and *aPP* chains contain some *meso* diad portion. These effects cause looser chain packing for *sPP/iPP* binary mixture and exhibit phase separation in *iPP/sPP* and *aPP/sPP* mixtures. Demixing is observed more strongly in *iPP/sPP* than in *aPP/sPP* mixture. In other words, *iPP/sPP* and *aPP/sPP* are immiscible while *iPP/aPP* mixture is miscible. *sPP* is immiscible to both *iPP* and *aPP* when it is mixed in binary PP mixture. Furthermore, the overall chain mobility of *iPP/aPP* is faster than that of *aPP/sPP* mixture and the magnitude of the overall diffusion rate for each PP binary mixtures can be ordered as: $iPP/aPP > iPP/sPP > aPP/sPP$.

The mobility change of PP chains with the same tacticity is investigated after mixing in binary PP/PP blends. All PP/PP binary systems show different dynamic behavior for each chain tacticity in the PP mixtures. The overall mobility indicates that the diffusion of *iPP* and *aPP* in the mixture are slightly decreased while the mobility of *sPP* shows significant increasing rate up to 2 and 3 times for *sPP* in *iPP/sPP* and *aPP/sPP* binary mixtures, respectively. In general, the dimension of PP chains in the binary PP mixture is slightly decreased (less than 4% except for *sPP* which has 17% decreases) after mixing with other components with different chain tacticity.

5.4.2.1 *iPP* chains in PP/PP binary mixtures

OACF of *iPP* chains in pure melts and binary mixtures are compared in Figure 5.3(a). All *iPP* chains in binary mixtures decay at slightly different rate from the others. MSD for *iPP* chains in pure melts and binary mixtures are also compared in Figure 5.3(b) and they also exhibit similar trends with OACF of

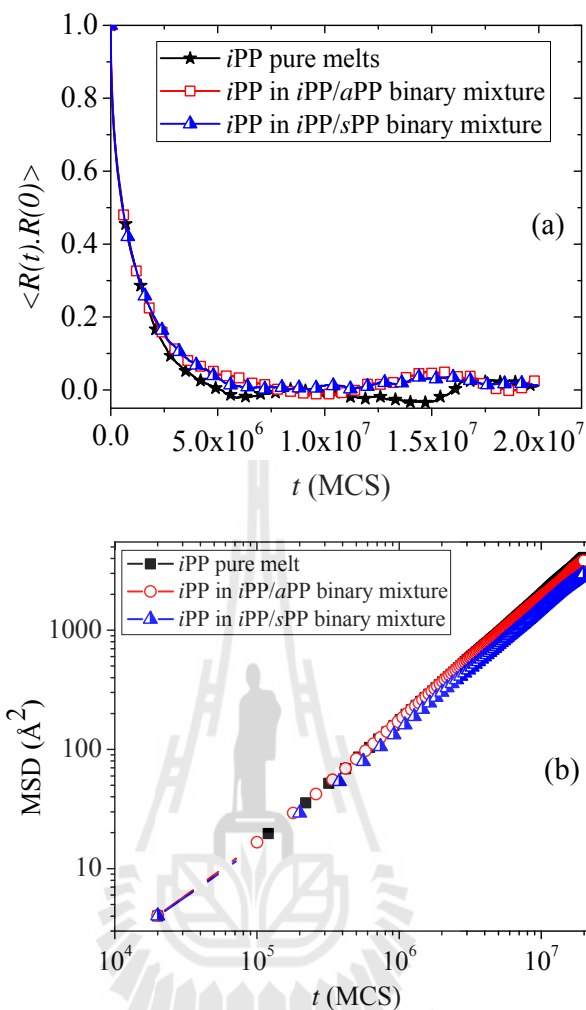


Figure 5.3 (a) Orientation autocorrelation function for the end-to-end vector and (b) Mean-square displacement of the centers-of-mass in \AA^2 for iPP chains in pure melts and binary mixtures.

PP melts. iPP chains in iPP/sPP mixture diffuse slightly slower than other binary systems for both rotational and translational motion which can be ordered as; pure $iPP \approx iPP/aPP > iPP/sPP$).

The relative values of $R_g^{2 > 1/2}$, C_n and D of PP chains in binary mixtures are presented in Table 5.3. These data obtained by comparing with those in pure PP system. iPP chains in binary mixtures diffuse slower rate than that of pure iPP

melts. The chain dimension of *iPP* chains in both *iPP/aPP* and *iPP/sPP* mixture are slightly decreased, ordering as pure *iPP* > *iPP/aPP* > *iPP/sPP*. In addition, the chain stiffness also shows similar trends with the molecular size. While both chain dimension and chain rigidity are decreased, the diffusion rate of *iPP* is instead decreased in binary mixture. These data indicate that the intramolecular effect (both molecular size and chain rigidity) is not the key factor to the dynamic behavior of *iPP* chains in PP/PP binary mixtures.

The local intermolecular packing can be obtained from PCFs of PP/PP binary mixtures which have been prior investigated by Haliloglu *et al.*, and Clancy *et al.* (Haliloglu and Mattice, 1999). It was expressed that the presence of *sPP* chains causes the *iPP* chains to aggregate slightly, relative to the situation where *iPP* shares the melt with *aPP*. There is a more substantial preferential interaction of *sPP* with other *sPP* chains and provides *iPP* and *sPP* chains try to avoid contact one another in the melts (Clancy and Mattice, 2001). This implies less intermolecular packing for *iPP/sPP* and *iPP/aPP* binary mixtures and *iPP* chains in *iPP/sPP* give the evidence for a preference contact to itself more than that in *iPP/aPP* system which is quite similar to that in pure *iPP* melts. These results contribute to slower diffusion rate of *iPP* component in *iPP/sPP* and *iPP/aPP* binary mixtures.

In addition, these results can be described in term of intramolecular effect represented by stereochemical sequence. Because the consecutive *meso* diad in *iPP* chains is significantly less mobile when there is a small amount of *racemo* diad mixed randomly in the chain *i.e.* *aPP* (Mattice *et al.*, 2007; Waheed *et al.*, 2007). In binary mixtures, when the neighboring chains of *iPP* chains are either *aPP* or *sPP*, the *mmm* tetrad in *iPP* chains in the mixture has slightly slower mobility than in pure *iPP*

Table 5.3 Relative value of mean square radius of gyration, characteristic ratio and diffusion coefficient of the chains in PP binary mixtures (50%w).

Chain	Mixture system	$\langle R_g^2 \rangle_{\text{mix}}^{1/2} / \langle R_g^2 \rangle_{\text{pure}}^{1/2}$	$C_{n(\text{mix})} / C_{n(\text{pure})}$	$D_{\text{mix}} / D_{\text{pure}}$
<i>i</i> PP	<i>i</i> PP/ <i>a</i> PP	0.98	0.95	0.94
	<i>i</i> PP/ <i>s</i> PP	0.95	0.91	0.74
<i>a</i> PP	<i>i</i> PP/ <i>a</i> PP	0.98	0.97	0.91
	<i>a</i> PP/ <i>s</i> PP	0.96	0.93	0.43
<i>s</i> PP	<i>i</i> PP/ <i>s</i> PP	0.83	0.68	2.06
	<i>a</i> PP/ <i>s</i> PP	0.94	0.89	2.90

melts. *i*PP/*s*PP mixtures are stronger different in their stereochemistry composition than those in *i*PP/*a*PP mixture. *i*PP chains in *i*PP/*a*PP mixture have more mobility than *i*PP/*s*PP mixture. This is because *s*PP has longer consecutive *r* diad than *a*PP. Hence, *s*PP should have more all-*trans* crystal-like sequence which retards the mobility of other chains in binary mixture.

5.4.2.2 *a*PP chains in PP/PP binary mixtures

Figure 5.4(a) demonstrates a plot of an OACF of *a*PP chains in pure PP melts and PP/PP binary mixtures. Each *a*PP decays at quite different from each other. Similar trends were also observed in the MSD data for *a*PP chains in both pure melts and binary mixtures as shown in Figure 5.4(b). *a*PP chains in *a*PP/*s*PP mixture have less mobility (rotational and translational mode) than those in pure *a*PP melts and *i*PP/*a*PP mixture whereas the mobility of *a*PP in their pure melts and in *i*PP/*a*PP system are not distinguishable from each other.

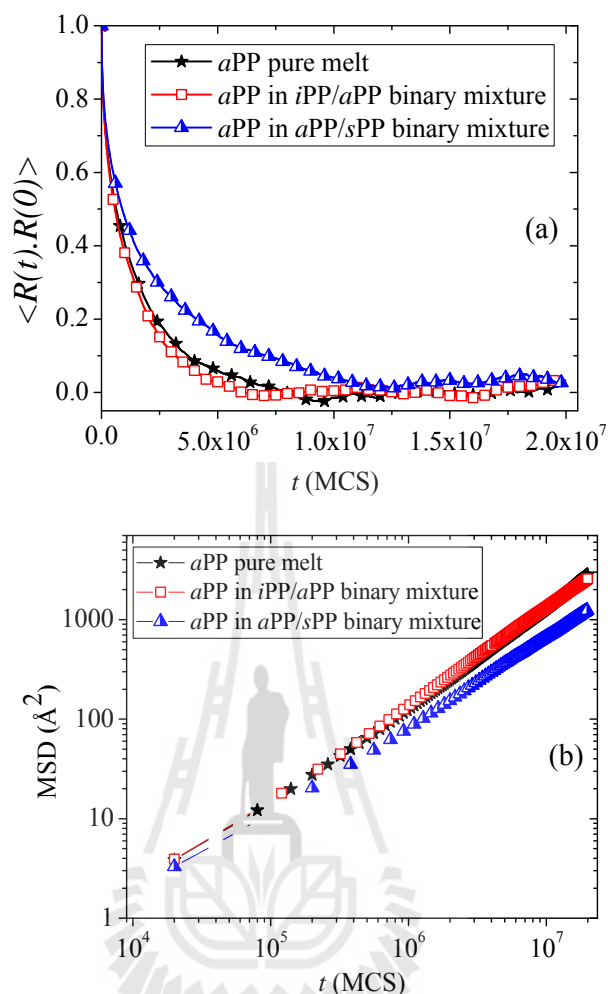


Figure 5.4 (a) Orientation autocorrelation function for the end-to-end vector and (b) Mean-square displacement of the centers-of-mass in \AA^2 for *aPP* chains in pure melts and binary mixtures.

Similar to *iPP* chains, the mobility of *aPP* chains in binary mixtures is slower than that of *aPP* in pure melts. Both molecular size and chain stiffness are decreased in the blended systems. Both chain dimension and chain rigidity of *aPP* chains in *iPP/aPP* mixture are slightly greater than those in *aPP/sPP* binary mixture. This leads to slower diffusion rate of *aPP* chains in *iPP/aPP* and *aPP/sPP* mixtures. *aPP* chains in *aPP/sPP* mixture diffuse slightly slower than in

iPP/aPP mixture while *aPP* chain has approximately the same molecular size and chain rigidity in both *iPP/aPP* and *aPP/sPP* systems. These results indicate that both molecular size and chain rigidity (intramolecular effect) are not only the key factor that affects the dynamic behavior of *aPP* chains in binary mixtures.

Haliloglu *et al.* reported that the PCFs is slightly decreased in binary PP/PP mixture when half of all chains were replaced by *aPP* chains. From those PCFs data, *iPP/aPP* melt is miscible while *aPP/sPP* blend is immiscible, which leads to inhomogeneity of *aPP/sPP* system. This contributes to slower diffusion rate of *aPP* in *aPP/sPP* than that in *iPP/aPP* mixture.

These results can also be described by the effect of intramolecular interaction from the stereochemical configuration of tetrad sequences in PP chains. The mobility of some tetrad sequences in *aPP* was depended on their counterpart environment. When tetrad sequences are surrounded by the same tetrad from different *aPP* chains, there is a greater intermolecular contribution resulting in looser chain packing. *aPP/sPP* binary mixture is consisted of quite different stereochemical composition compared to those in *iPP/aPP* mixture and it leads to slower mobility of the random tetrad in *aPP* chains in *aPP/sPP* binary mixture than that in pure *aPP* melts.

5.4.2.3 *sPP* chains in PP/PP binary mixtures

Figure 5.5(a) and 5.5(b) show OACF and the MSD for *sPP* chains in pure melts and binary PP/PP mixtures, respectively. Similar dynamic features of *sPP* are observed in both rotational and translation mode. Each *sPP* OACF decays and MSD are quite different from each other. *sPP* in binary PP/PP blend has more

mobility than that of its pure melts. For *iPP/sPP* binary mixture, due to the aggregation of *iPP* chains, this binary mixture exhibits an inhomogeneity. Hence, *sPP* chains in *iPP/sPP* system diffuse faster than *sPP* in *aPP/sPP* binary mixture.

The relative values for molecular size, chain rigidity and diffusion coefficient of *sPP* chains in binary PP/PP mixture are presented in Table 5.3. These values are quite similar trends for *iPP* and *aPP* in their binary PP/PP mixtures. The chain dimension and chain rigidity of *sPP* chains in *iPP/sPP* mixture are smaller and more flexible, respectively, than those in *aPP/sPP* binary mixture. Hence, *sPP* chains in binary mixtures can diffuse faster than those of pure *sPP* melts, ordering as: *aPP/sPP* > *iPP/sPP* > pure *sPP* melts. The dynamic behavior of *sPP* chain in binary mixture does not result from the intramolecular effect (the molecular size and chain stiffness)

The PCFs of PP binary mixtures depicts the general features for the *sPP* chains are similar to those of *iPP* chains but all three PCFs are clearly distinguishable (Haliloglu and Mattice, 1999). *sPP* chains are more closed packed in *iPP/sPP* mixture than those in *aPP/sPP* mixture and pure *sPP* melts. In addition, both *iPP* and *sPP* chains are avoided to contact one another and it leads to an *iPP* aggregation in binary mixture. It also causes slightly aggregation of *aPP* chains in binary mixtures. An inhomogeneity of binary PP/PP mixture is caused by preferential interaction of *sPP* to other *sPP* chains in the system. This preferential interaction forces the *sPP* chains trend to separate themselves from *iPP* chains in *iPP/sPP* mixture (Clancy and Mattice, 2001) and stronger than the separation of *aPP* in *aPP/sPP* blend system.

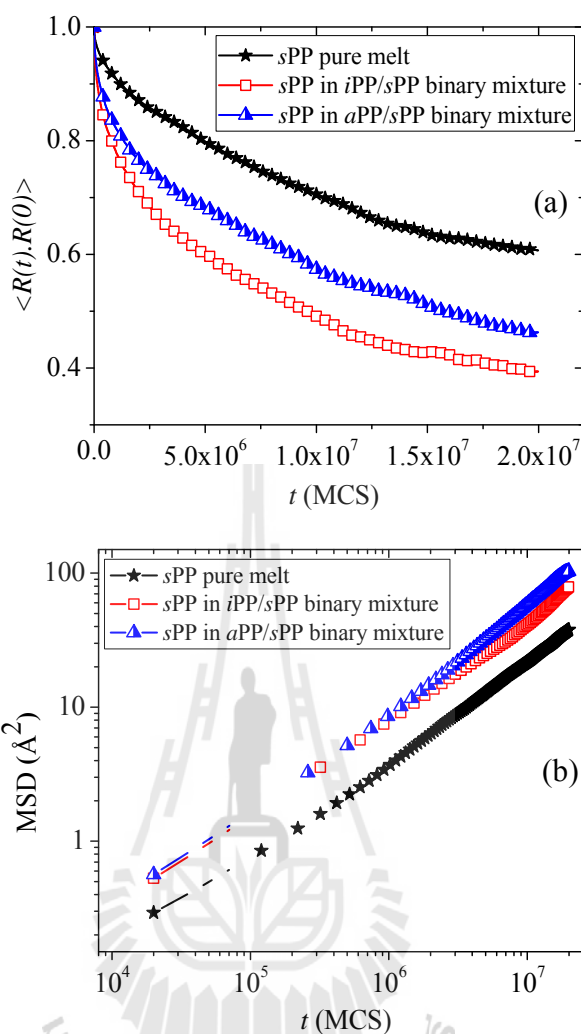


Figure 5.5 (a) Orientation autocorrelation function for the end-to-end vector and (b) Mean-square displacement of the centers-of-mass in \AA^2 for *s*PP chains in pure melts and binary mixtures.

The intramolecular interaction of tetrad in the PP chain is also utilized to describe the mobility of PP chains. When the neighboring chains consist of random tetrad, the *rrr* tetrad is more mobile than that in pure stereochemicals PP chains. *s*PP chains are more mobile in *a*PP/*s*PP mixture than those in *i*PP/*s*PP mixture. An increased mobility for *s*PP (2-3 times higher than that of the pure *s*PP melts) in blends may be related to both a reduction of molecular size and intermolecular

contribution when *rrr* tetrad is surrounded by different type of tetras. All these causes slower diffusion rate of *sPP* chains in *iPP/sPP* mixture than that in *aPP/sPP* mixture.

5.5 Conclusions

The structural and dynamic properties of polypropylene (PP) melts with different tacticity were elucidated by lattice Monte Carlo simulation. The molecular size, chain rigidity and diffusion of PP chains were investigated in both pure PP melts and PP/PP binary mixtures. The diffusion coefficients obtained from simulation results suggested both contribution from the intermolecular contribution (intermolecular pair correlation functions) and intramolecular contribution (the molecular size and chain rigidity).

In neat PP melts system, the diffusion of PP with different tacticity is generally ordered as $iPP > aPP > sPP$. Both molecular size and chains rigidity provided no clear evidence contribution to diffusion of PP melts. Mobility of PP chains depends not only on an intramolecular but also intermolecular contribution between neighboring chains.

Binary mixtures of 50:50 wt% PP/PP melts were studied for both the miscibility prediction and the transformation of chains in comparison with the pure PP melts system. The melts of PP blend was found miscibility of *iPP/aPP* binary mixture but *iPP/sPP* and *aPP/sPP* mixtures are immiscible. In general, molecular size and chains rigidity became lower when different tacticity was added in the PP mixtures. The diffusion rate of *iPP* and *aPP* chains in binary mixtures was rather decreased, regarding to the effect of intramolecular contribution which correlates to molecular size and chain stiffness, cooperates with intermolecular contribution which is

represented by intermolecular pair correlation functions. In case of *s*PP chains, the diffusion rate of *s*PP chains in the mixtures is higher than in pure *s*PP melts system as a result of the intermolecular contribution of other chains influence the dynamics greater than intramolecular interactions in PP chain.

5.6 References

- Aharoni, S.M., Kramer, V. and Vernick, D.A. (1979). Instantaneous Shape and Segmental Density of Individual Flexible Linear Macromolecules. 4. Tagged in Untagged Crystallizable Polymers. **Macromolecules** 12: 265-271.
- Akten, E.D. and Mattice, W.L. (2001). Monte Carlo Simulation of Head-to-Head, Tail-to-Tail Polypropylene and Its Mixing with Polyethylene in the Melt. **Macromolecules** 34: 3389-3395.
- Antoniadis, S.J., Samara, C.T. and Theodorou, D.N. (1999). Effect of Tacticity on the Molecular Dynamics of Polypropylene Melts. **Macromolecules** 32: 8635-8644.
- Ballard, D.G.H., Cunningham, A. and Schelten, J. (1977). Small-angle neutron scattering studies of polyethylene crystallized at high pressure. **Polymer** 18: 259-261.
- Choi, P., Blom, H.P., Kavassalis, T.A. and Rudin, A. (1995). Immiscibility of poly(ethylene) and poly(propylene): A molecular dynamics study. **Macromolecules** 28: 8247-8250.
- Clancy, T.C. and Mattice, W.L. (2001). Miscibility of Poly(vinyl chloride) Melts Composed of Mixtures of Chains with Differing Stereochemical

- Composition and Stereochemical Sequence. **Macromolecules** 34: 6482-6486.
- Clancy, T.C. and Mattice, W.L. (2001). Role of the attractive portion of the Lennard-Jones potential in the homogeneity of melts of isotactic and syndiotactic polypropylene. **The Journal of Chemical Physics** 115: 8221.
- Clancy, T.C., Pütz, M., Weinhold, J.D., Curro, J.G. and Mattice, W.L. (2000). Mixing of Isotactic and Syndiotactic Polypropylenes in the Melt. **Macromolecules** 33: 9452-9463.
- Freischmidt, H.M., Shanks, R.A., Moad, G. and Uhlherr, A. (2001). Characterization of polyolefin melts using the polymer reference interaction site model integral equation theory with a single-site united atom model. **Journal of Polymer Science Part B: Polymer Physics** 39: 1803-1814.
- Graessley, W.W., Krishnamoorti, R., Reichart, G.C., Balsara, N.P., Fetters, L.J. and Lohse, D.J. (1995). Regular and Irregular Mixing in Blends of Saturated Hydrocarbon Polymers. **Macromolecules** 28: 1260-1270.
- Haliloglu, T., Cho, J. and Mattice, W.L. (1998). Simulations of rotational isomeric state models for poly(propylene) melts on a high coordination lattice. **Macromolecular Theory and Simulations** 7: 613-617.
- Haliloglu, T. and Mattice, W.L. (1999). Detection of the onset of demixing in simulations of polypropylene melts in which the chains differ only in stereochemical composition. **Journal of Chemical Physics** 111: 7.
- Krishnamoorti, R., Graessley, W.W., Dee, G.T., Walsh, D.J., Fetters, L.J. and Lohse, D.J. (1996). Pure Component Properties and Mixing Behavior in Polyolefin Blends. **Macromolecules** 29: 367-376.

- Leung, B.O., Hitchcock, A.P., Brash, J.L., Scholl, A. and Doran, A. (2009). Phase Segregation in Polystyrene-Polylactide Blends. **Macromolecules** 42: 6.
- Lohse, D.J. (1986). The melt compatibility of blends of polypropylene and ethylene-propylene copolymers. **Polymer Engineering & Science** 26: 1500-1509.
- Maier, R.-D., Thomann, R., Kressler, J., Mülhaupt, R. and Rudolf, B. (1997). The influence of stereoregularity on the miscibility of poly(propylene)s. **Journal of Polymer Science Part B: Polymer Physics** 35: 1135-1144.
- Mattice, W.L., Tatek, Y.B. and Waheed, N. (2007). Variability in the Persistence Length of an Atactic Polymer Due to Quenched Randomness, As Illustrated by Atactic Polystyrene. **Macromolecules** 40: 379-383.
- Peng, C.J., Li, J.K., Liu, H.L. and Hu, Y. (2004). Monte Carlo simulation for the adsorption of symmetric triblock copolymers. **Chinese Journal of Chemical Engineering** 12: 357-362.
- Rajasekaran, J.J., Curro, J.G. and Honeycutt, J.D. (1995). Theory for the Phase Behavior of Polyolefin Blends: Application to the Polyethylene/Isotactic Polypropylene Blend. **Macromolecules** 28: 6843-6853.
- Thomann, R., Kressler, J., Setz, S., Wang, C. and Mülhaupt, R. (1996). Morphology and phase behaviour of blends of syndiotactic and isotactic polypropylene: 1. X-ray scattering, light microscopy, atomic force microscopy, and scanning electron microscopy. **Polymer** 37: 2627-2634.
- Waheed, N., Mattice, W.L. and von Meerwall, E.D. (2007). Enhanced Diffusion at Intermediate Stereochemical Composition in Polypropylene by Dynamical Monte Carlo. **Macromolecules** 40: 1504-1511.

- Wang, B., Cai, J., Liu, H. and Hu, Y. (2001). Monte Carlo Simulations of Density Profiles for Hard-Sphere Chain Fluids Confined Between Surfaces. **Chin.J.Chem.Eng.** 9: 156-161.
- Wignall, G.D., Child, H.R. and Samuels, R.J. (1982). Structural characterization of semicrystalline polymer blends by small-angle neutron scattering. **Polymer** 23: 957-964.
- Xu, G., Clancy, T.C., Mattice, W.L. and Kumar, S.K. (2002). Increase in the Chemical Potential of Syndiotactic Polypropylene upon Mixing with Atactic or Isotactic Polypropylene in the Melt. **Macromolecules** 35: 3309-3311.



CHAPTER VI

EFFECT OF STEREOCHEMICAL SEQUENCE ON STRUCTURAL AND DYNAMIC PROPERTIES OF *ATACTIC* POLYPROPYLENE MELTS

6.1 Abstract

Static and dynamics properties of *a*PP melts were studied by Monte Carlo simulation of coarse-grained PP model at 473 K with C₁₉₂H₅₇₈ at the same stereochemical composition but different sequences. *a*PP with alternate *meso* diad sequence have a tendency to diffuse faster than other sequences. Diffusion of polymer melts is depended not only on an intramolecular but also intermolecular contribution resulting from stereochemical sequence. At an intermediate stereochemical composition, *m* and *r* diad have more mobility when there are small amounts of mixed random sequence. The chains with long consecutive diad and with the same sequence diffuse slower than the mixed stereochemical sequence. The effect of intramolecular contribution is greater than the effect of intermolecular interaction at the stereochemical composition containing *meso* diad close to $P_m = 0.0$ (all *racemo* or *syndiotactic* chain). For P_m close to 1.0, the intermolecular contribution affects the diffusion greater than the intramolecular effects.

6.2 Introduction

The development in metallocenes catalysts provides the great potential opportunity to control the stereoregular and partial regular homopolymer and copolymers (Soga and Shiono, 1997; Busico and Cipullo, 2001). This control is not only on the preparation of pure tacticity vinyl polymers, which there are only m or r diad, respectively, but also to synthesize chains in which the fundamental repeat for the stereochemical sequence extends over a range longer than diad with only types, e.g., mmr , rmr , etc. *Atactic* chains, are actually random copolymers (Flory, 1969). Even monodisperse *atactic* chains usually have different fractions of m and r diad, indicating that each isomer has a unique conformational partition function (Mattice *et al.*, 2007).

Tacticity of PP can affect many properties such as the thermal properties, diffusion and crystallization (Chen *et al.*, 2006). It is well-known that *i*PP chain with tg conformers diffuses faster than *s*PP chain with tt conformers but the maximum rate was found for the diffusion of *a*PP chain which exhibits an intermediate behavior (Antoniadis *et al.*, 1999). *a*PP is an amorphous rubbery material, it has an irregular structure which inhibits the regular packing required to create crystallites whereas *i*PP and *s*PP are semi-crystalline. The crystallization and the melting point of *i*PP and *s*PP were strongly are influenced by their stereochemical defected structure (Madkour and Mark, 1997).

Computer simulation of polymeric materials presents a formidable challenge due to the considerable range of length and time scales relevant in these physical systems. Coarse-grained lattice models have traditionally been applied to allow for an efficient simulation of polymers. Simulation of vinyl polymers on the high-

coordination *2nm*d lattice (Mattice and Clancy, 1999; Akten and Mattice, 2001) retains sufficient detail to enable distinction of the precise chemical composition of the polymers being simulated, yet allows for the efficient study of large polymer systems which cannot be equilibrated on reasonable time scale with an atomistic simulation (Antoniadis *et al.*, 1998; Logotheti and Theodorou, 2007). This technique has been used to study the effect of stereochemistry of polymer chain on various properties. It was found that the stereochemical sequence of *atactic* chain with quenched randomness affects samples with intermediate stereochemical composition at the probability of *meso* diad, P_m (Chen *et al.*, 2007), and it makes *meso* and *racemo* sequences in *aPP* chain to diffuse faster than that of *iPP* and *sPP* chain when each *atactic* chain is composed of different stereochemical pattern of *r* and *m* diad with random sequence on each chain. Stereochemical effect are well understood for mixtures of small-molecule enantiomers (Mattice and Waheed, 2006) but to understand polymer dynamic properties, we need to know the fundamental aspects of the stereochemistry of polymer chain. Therefore, there is a need for a more comprehensive study of this effect on structural and dynamic properties in relative to the specific stereochemical sequences of vinyl polymer chains.

The subject of interest in this part is the effect of stereochemical sequence of *aPP* at the fixed P_m on the physical properties of *aPP*. Dynamic MC simulation was utilized to study structural and dynamic properties of *aPP* melt with the same stereochemical compositions. P_m for each *aPP* are fixed at 0.25, 0.50 and 0.75 but different stereochemical sequence to find how each specific sequence can affect molecular properties and chain dynamics.

6.3 Computational method

System descriptions

*a*PP were modeled by a chain of beads, each bead represents a propane unit. The simulation placed 29 chains, each with 64 beads, in a $25 \times 25 \times 25$ lattice unit. The stereochemical sequence of *a*PP chain was described using *m* and *r* diad with P_m were fixed at 0.25, 0.50 and 0.75. The repeating sequence of each stereochemical sequence chains were listed in Table 6.1, 6.2 and 6.3, respectively. Monte Carlo simulation was performed by method which was described in Chapter II.

6.4 Results and discussion

The orientation autocorrelation function (OACF) of the end-to-end vector (\vec{R}) ($\langle R(t) \cdot R(0) \rangle$) and the mean-square displacement (MSD) of the centers-of-mass for *a*PP at the $P_m = 0.25, 0.50$ and 0.75 with random *m* and *r* diad are presented in Figure 6.1(a) and 6.1(b), respectively. The order of decay rate can be observed as $P_m = 0.75 > 0.50 > 0.25$, respectively. These results are in good agreement with recent report, which the maximum diffusion was seen at an intermediate stereochemical composition (Waheed *et al.*, 2007). In addition to the previous study, the compositions at the same diad as shown in Figure 6.1 but constraints number of *m* and *r* diad for each fixed P_m to investigate the effect of specific stereochemistry sequence of *a*PP chain.

6.4.1 Atactic polypropylene at $P_m = 0.25$

OACF of the end-to-end vector and MSD for *a*PP at $P_m = 0.25$ which has the same stereochemical composition but different stereochemical sequences are

shown in Figure 6.2. The MRRRMRRR sequence decays at considerably faster rate while MMRRRRRR sequence gives a slower decay rate. The MSD also gives similar trends with the decay of the end-to-end vector *i.e.* MRRRMRRR sequence has a faster mobility for both rotational and translational mode. Other stereochemical sequences have similar dynamic characteristics.

Table 6.1 presents the diffusion coefficient which can be divided into two groups, A and B which denote the fast and slow diffusion, respectively. For group A, MRRRMRRR sequence diffuses faster than MRRMRRRR sequence. The radius of gyration and the characteristic ratio, representing the size and chain rigidity, respectively, of MRRRMRRR sequence gives minimum values indicating that both size and chain rigidity are influent chain mobility. In general, polymer chain with smaller size and more flexible chain should have higher molecular mobility. On the other hand, for the slower dynamics in group B, MMRRRRRR sequence moves faster than MRRMRRRR sequence. Even though both patterns have the same chain stiffness but MRRMRRRR sequence has smaller molecular size.

The Local intermolecular packing can be obtained from pair correlation functions (PCFs) as demonstrated in Figure 6.3. The intermolecular PCFs for MMRRRRRR and MRRMRRRR sequence are similar to each other while the other two sequences, MRRMRRRR and MRRRMRRR, are quite distinguishable. These results provide an evidence for a preference of each block to interact with itself. All four sequences have weak local maximum in the sixth shell and weak local minimum in the fourth shell but MRRMRRRR and MRRRMRRR sequence exhibit lower PCFs values from the third to the ninth shell. In other words, MRRMRRRR sequence prefers to interact with itself less than MRRRMRRR, MMRRRRRR and

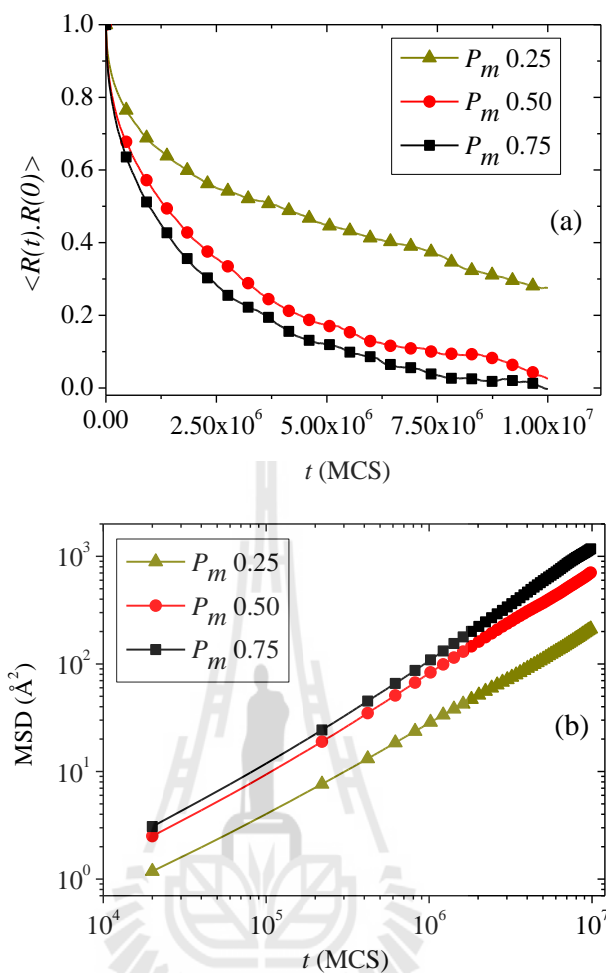


Figure 6.1 (a) Orientation autocorrelation function for the end-to-end vector and (b) Mean-square displacement for melts of *a*PP, $P_m = 0.25, 0.50$ and 0.75 .

MRRMRRRR sequence, respectively. This result implies that the chain packing of MRMRRRRR sequence is less effective than other three sequences which should lead to faster dynamics but it gives the slowest diffusion rate. The MRMRRRRR sequence has a packing efficiency close to MRRRMRRR sequence (the fastest mobility) but it is the smallest size and the most rigid chain which should be related to the effect of stereochemical sequence. The more orderly MRRRMRRR sequence has a smaller molecular size and the chains pack much looser than the MRRMRRRR sequence.

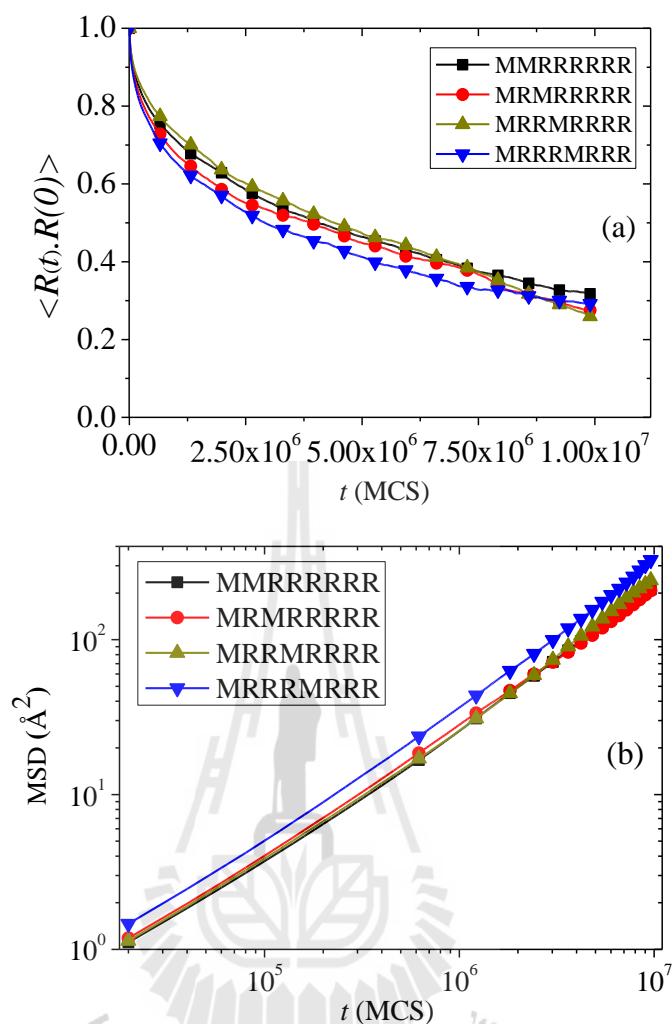


Figure 6.2 (a) Orientation autocorrelation function for the end-to-end vector and (b) Mean-square displacement for *a*PP melt, $P_m = 0.25$, with different stereochemical sequences pattern.

The acceptance rate can be used to elucidate the diffusion of sequence by the mobility of *tetrad* in the same stereochemistry (Waheed *et al.*, 2007). Because the acceptance of moves in isolated chains is a factor of an intramolecular contribution, it should cause similar effect on the acceptance rate. The *rrr* tetrad is more mobile when there is a small amount of *m* diad to break the helix formation and enhance the chain aggregation (Destrée *et al.*, 2000). For group A, MRRRMRRR sequence has more

Table 6.1 Repeating sequences, mean square radius of gyration, characteristic ratio, and relative intermolecular PCFs in the third shell and diffusion coefficient of *aPP* at $P_m = 0.25$ with different stereochemical sequences pattern in parent chain.

Group	Repeating sequences	$\langle R_g^2 \rangle^{1/2}$	C_n (RIS)	relative $g_{total}(3)$	relative D
A	MRRRMRRR	14.25	5.54	1.00	1.00
	MRRMRRRR	14.46	5.62	1.09	0.77
B	MMRRRRRR	14.64	5.80	1.08	0.65
	MRMRRRRR	13.89	5.80	0.99	0.63

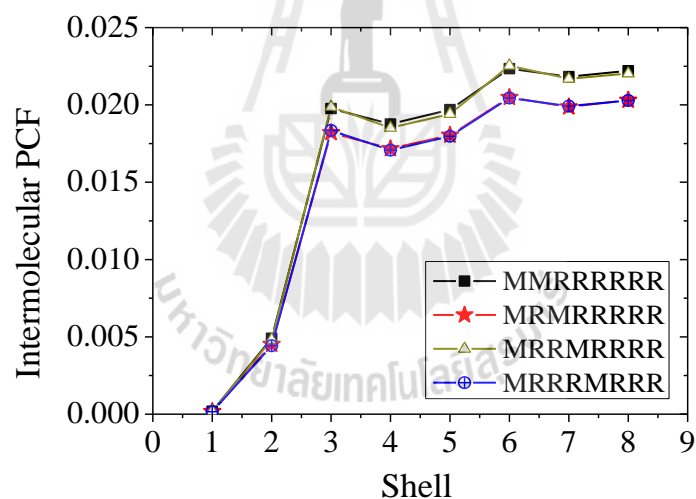


Figure 6.3 Intermolecular PCFs of total block for *aPP* melts, $P_m = 0.25$, with different stereochemical sequence.

m diad in linking to *r* diad than MRRMRRRR sequence. This leads to an ascending of the acceptance rate of *rrr* tetrad and results in higher diffusion coefficient. When the neighboring chain consists of random tetrad, the *rrr* tetrad is more mobile than in the regular stereochemistry chain. For group B, there is more consecutive *r* diad in the

chain. Even if MMRRRRRR and MRMRRRRR sequence have the same chain stiffness, MMRRRRRR sequence diffuses faster. This MMRRRRRR sequence also has a larger molecular size and closer local chain packing which is caused by the stereochemical sequence of *rrr* tetrad when long consecutive *r* diad instructs all-trans crystal-like sequence (Clancy and Mattice, 2000; Clancy and Mattice, 2001).

6.4.2 Atactic polypropylene at $P_m = 0.50$

Figure 6.4(a) shows an OACF for the end-to-end vector for *a*PP ($P_m = 0.50$) with different stereochemical sequence. All systems achieve an equilibration quite fast and have little difference from others. The corresponding MSDs are displayed in Figure 6.4(b) manifested similar results with the decay of the end-to-end vector. It was found that the first two systems are distinguishable from other seven systems due to their lower mobility. The alternate sequence *i.e.* MRMRMRMR, has the fastest mobility and other systems have similar dynamic characteristics.

For the diffusion behavior in group C (in Table 6.2), MMRMMRRR and MRMMRRMR systems have the same diffusion rate while MMRMRMRR and MMRRMMRR systems diffuse slower, respectively. The chain rigidity, molecular size and packing density of MMRMMRRR system are higher than others. *rrr* tetrad is more mobile when they are mixed with some *m* diad and surrounded by different stereochemical diad (Waheed *et al.*, 2007). For three remaining patterns, MRMMRRMR and MMRRMMRR sequence have similar molecular size and chain rigidity closed to each other because they have the same MM and RR triads in the middle of sequence while the MMRMRMRR sequence has RM triads in the middle of chain; making it more flexible than the other two sequences. Moreover, the local

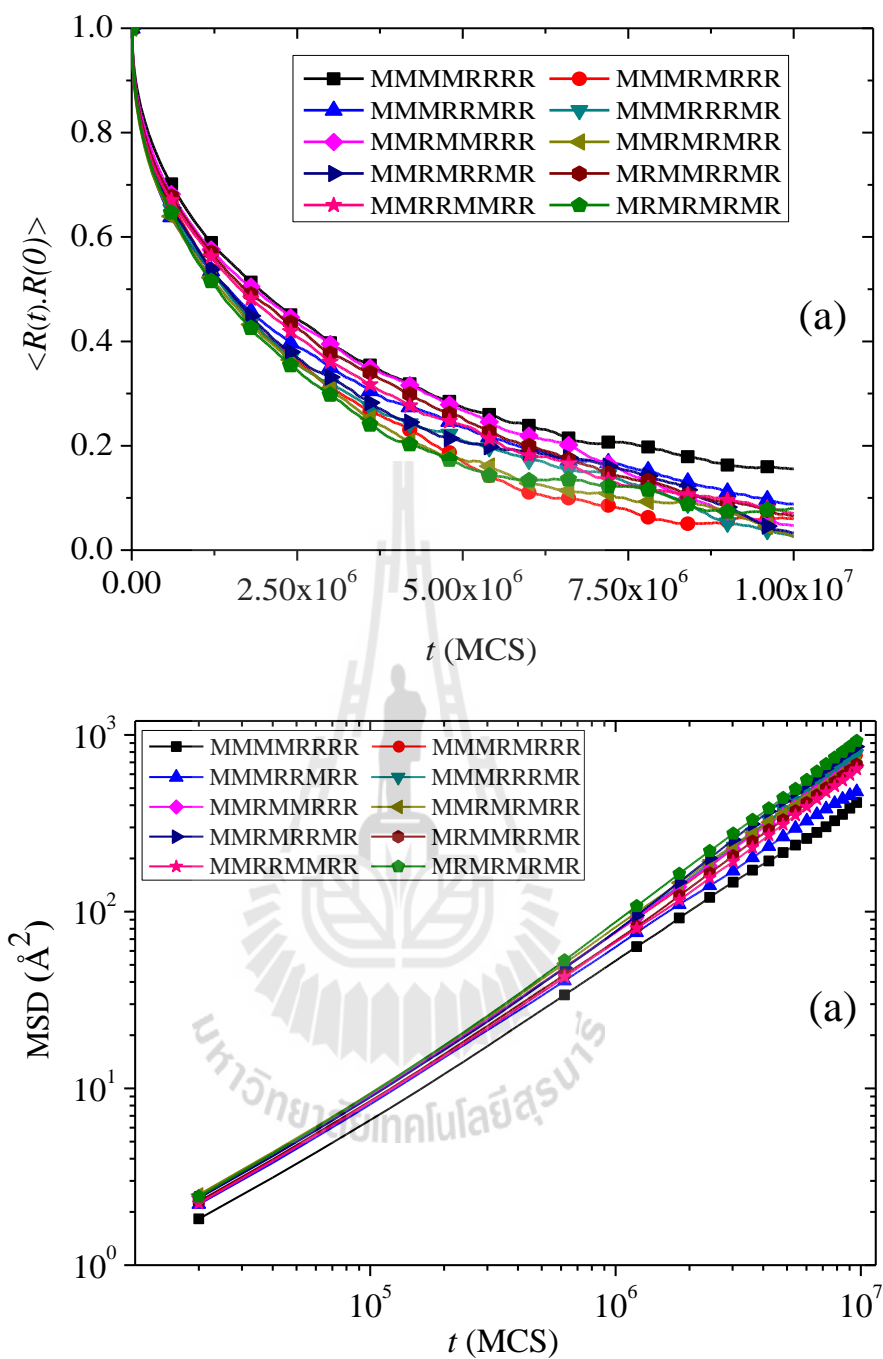


Figure 6.4 (a) Orientation autocorrelation function for the end-to-end vector and (b) Mean-square displacement for *a*PP melt, $P_m = 0.50$, with different stereochemical sequence.

Table 6.2 Repeating sequences, mean square radius of gyration, characteristic ratio, and relative intermolecular PCFs in the third shell and diffusion coefficient of *aPP* at $P_m = 0.50$ with different stereochemical sequences pattern in parent chain.

Group	Repeating sequences	$\langle R_g^2 \rangle^{1/2}$	C_n (RIS)	relative $g_{total}(3)$	relative D
A	MRMRMRMR	14.67	4.17	1.00	1.00
	MMRMRRMR	14.47	4.59	0.97	0.94
B	MMMRRRMR	14.84	5.71	1.09	0.84
	MMMRMRRR	14.86	5.44	1.08	0.83
C	MMRMMRRR	15.42	5.07	0.99	0.73
	MRMMRRMR	14.62	4.74	0.91	0.73
	MMRMRRMR	14.24	4.42	1.09	0.72
	MMRRMMRR	14.43	4.99	1.20	0.69
D	MMMRMMRR	14.02	5.54	1.19	0.51
	MMMMRRRR	14.58	6.58	1.20	0.42

intermolecular packing are demonstrated in Figure 6.5. The MMRRMMRR system has denser local packing efficiency than others in this group, resulting in the slowest diffusion. For the last group, MMMRRMRR system diffuses faster than the MMMMRRRR system as the consecutive *r* diad are broken by *m* diad. The molecular size is smaller with less chain rigidity and the intermolecular chain packing is lower than those of the MMMMRRRR system, resulting in a faster diffusion rate.

The acceptance rate can be utilized to confirm the chain diffusion by comparing the mobility of *mmm* and *rrr* tetrad. At an intermediate stereochemical composition, moving of *tetrad* is depended on their counterparts in the stereochemistry when these tetrads are surrounded by like tetrads, indicating greater intermolecular contribution. The *rmr* and *mrn* tetrad are the fastest mobility when they are in the same stereochemical composition and decrease in the order from *rmr* (or *mrn*), *mmr* and *mrr*, respectively (Waheed *et al.*, 2007). These results imply that the diffusion of *aPP* with MRMRMRMR system diffuses faster than others because it contains more *rmr* or *mrn* tetrad as well as it has higher chain flexibility. The diffusion of *aPP* melts depends not only on intramolecular contribution but also on the intermolecular contribution. The effect of intramolecular contribution is greater than an intermolecular contribution at an intermediate stereochemical composition ($P_m = 0.25$ and 0.50).

6.4.3 Atactic polypropylene at $P_m = 0.75$

Figure 6.6(a) demonstrates the decay for *aPP* at P_m 0.75. RMMMRMMM and RMMRMMMM systems decay at considerably similar rate and faster than those of RMRMMMMM and RRMMMMMM systems. The corresponding MSD of these sequences are displayed in Figure 6.6(b). The RMMMRMMM system exhibits the fastest mobility and followed by RMMRMMMM, RMRMMMMM and RRMMMMMM systems, respectively. The diffusion coefficients presented in Table 6.3 reveal that *aPP* with RMMMRMMM system diffuses faster than others and decreases as RMMRMMMM, RMRMMMMM and RRMMMMMM systems, respectively.

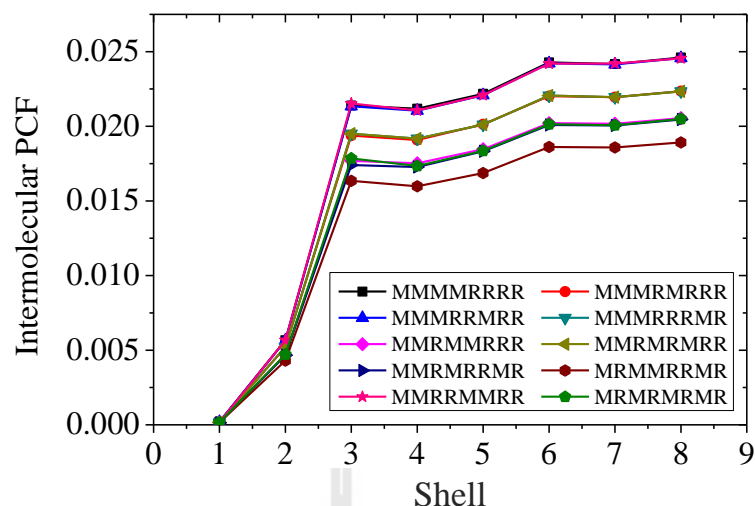


Figure 6.5 Intermolecular PCFs of total block for *a*PP melts, $P_m = 0.50$, with different stereochemical sequence.

Table 6.3 Repeating sequences, mean square radius of gyration, characteristic ratio, and relative intermolecular PCFs in the third shell and diffusion coefficient of *a*PP at $P_m = 0.75$ with different stereochemical sequences pattern in parent chain.

Repeating sequence	$\langle R_g^2 \rangle^{1/2}$	C_n (RIS)	relative $g_{total}(3)$	relative D
RMMRMMM	14.81	5.58	1.00	1.00
RMMRMMM	14.90	5.08	1.09	0.87
RMRMMMM	14.43	5.13	1.20	0.51
RRMMMMM	14.91	6.15	1.34	0.43

RRMMMMMM system has the largest size, the most chain rigidity and the most dense intermolecular packing efficiency, due to the helix-like conformation of long consecutive *m* diad, which leads to the slow moving rate. Similar to the case for $P_m = 0.25$, the long consecutive *r* diad cause the all-*trans* crystal-like sequence

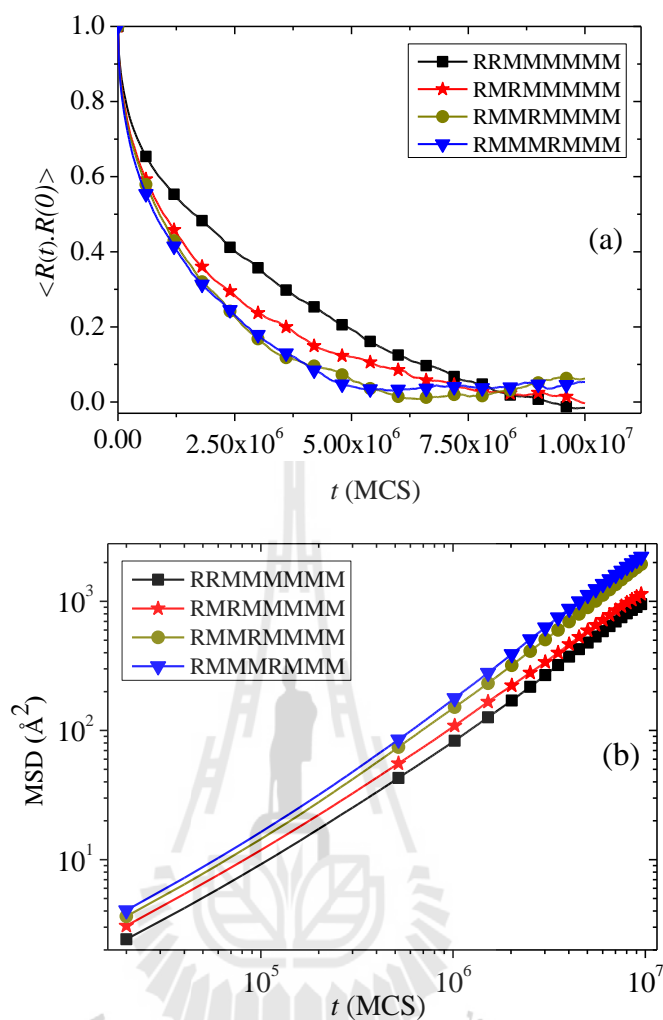


Figure 6.6 (a) Orientation autocorrelation function for the end-to-end vector for *a*PP melts and (b) Mean-square displacement for *a*PP melts, $P_m = 0.75$, with different stereochemical sequence .

(Clancy *et al.*, 2000; Choi and Mattice, 2004) but, in this case, the long consecutive *m* diad cause more chain to aggregate and less mobility (Waheed *et al.*, 2007). Despite the size RMMMRMMM chains is close to that of RRMMMMMM system, it moves faster than others which are attributed to an increasing of the acceptance rate for *mmm* tetrad when some *r* diad are mixed in this stereochemical sequence. In addition, the most flexible chain was found for RMMRMMMM sequence which has the smallest

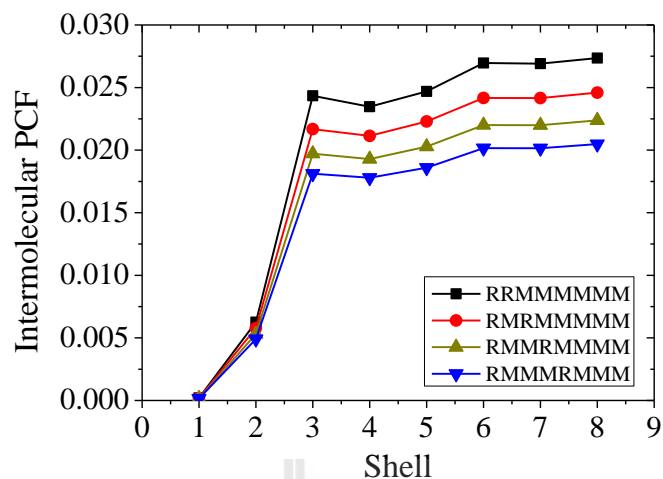


Figure 6.7 Intermolecular PCFs of total block for *a*PP melts, $P_m = 0.75$, with different stereochemical sequence.

size due to long consecutive *m* diad.

The intermolecular PCFs for four sequences are shown in Figure 6.7. The intermolecular PCFs of all four sequences were indistinguishable. All four systems exposed a weak local maximum in the sixth shell and a weak local minimum in the fourth shell but the values of PCFs curves slightly increase from RMMMRMMM, RMMRMMMM, RMRMMMMM to RRMMMMMM systems, respectively. This result elucidates that RMMMRMMM system prefers to interact with itself much more than others. Hence, the diffusion of polymer with *meso* diad closes to $P_m=1.0$ should be influenced by an intermolecular contribution more than intramolecular contribution.

6.5 Conclusions

The effect of stereochemical sequence on the structural and dynamic properties of stereo isomer PP was illustrated by MC simulation of *a*PP model with fixed P_m at 0.25, 0.50 and 0.75. The molecular size and motion of the *a*PP melts were studied

with different stereochemical composition and sequence. The diffusion coefficients obtained from simulation results suggest that there are the effects from an intramolecular contribution (molecular size and chain flexibility) and intermolecular contribution (intermolecular pair correlation functions). At an intermediate stereochemical composition, m and r diad have more mobility when small amount of diad randomness is mixed in compared with 100% *isotactic* and *syndiotactic* pattern. The chain with long consecutive diad with orderly sequence diffuses slower than the mixed stereochemical sequence. The stereochemical composition that contains m diad in equivalent to r diad, an intramolecular contribution affects the diffusion slightly greater than intermolecular contribution. The effect of intermolecular contribution is greater than intramolecular contribution at the stereochemical composition that contains m diad close to $P_m = 0.0$. On the other hand, for the stereochemical composition at P_m close to 1.0, intermolecular contribution affects more on the diffusion of polymer melts than an intramolecular effect.

6.5 References

- Akten, E.D. and Mattice, W.L. (2001). Monte Carlo Simulation of Head-to-Head, Tail-to-Tail Polypropylene and Its Mixing with Polyethylene in the Melt. **Macromolecules** 34: 3389-3395.
- Antoniadis, S.J., Samara, C.T. and Theodorou, D.N. (1998). Molecular Dynamics of Atactic Polypropylene Melts. **Macromolecules** 31: 7944-7952.
- Antoniadis, S.J., Samara, C.T. and Theodorou, D.N. (1999). Effect of Tacticity on the Molecular Dynamics of Polypropylene Melts. **Macromolecules** 32: 8635-8644.

- Busico, V. and Cipullo, R. (2001). Microstructure of polypropylene. **Progress in Polymer Science** 26: 443-533.
- Chen, X., Kumar, S.K. and Ozisik, R. (2006). Monte Carlo simulations of the crystallization of isotactic polypropylene. **Journal of Polymer Science Part B: Polymer Physics** 44: 3453-3460.
- Chen, X., Ozisik, R., Kumar, S.K. and Choi, P. (2007). Influence of stereoerrors on the formation of helices during early stage crystallization of isotactic polypropylene. **Journal of Polymer Science Part B: Polymer Physics** 45: 3349-3360.
- Choi, P. and Mattice, W.L. (2004). Molecular origin of demixing, prior to crystallization, of atactic polypropylene/isotactic polypropylene blends upon cooling from the melt. **The Journal of Chemical Physics** 121: 8647.
- Clancy, T.C. and Mattice, W.L. (2000). Rotational isomeric state chains on a high coordination lattice: dynamic monte carlo algorithm details. **Journal of Chemical Physics** 112: 10049-10055.
- Clancy, T.C. and Mattice, W.L. (2001). Miscibility of Poly(vinyl chloride) Melts Composed of Mixtures of Chains with Differing Stereochemical Composition and Stereochemical Sequence. **Macromolecules** 34: 6482-6486.
- Clancy, T.C., Pütz, M., Weinhold, J.D., Curro, J.G. and Mattice, W.L. (2000). Mixing of Isotactic and Syndiotactic Polypropylenes in the Melt. **Macromolecules** 33: 9452-9463.

- Destrée, M., Lauprêtre, F., Lyulin, A. and Ryckaert, J.P. (2000). Local dynamics of isotactic and syndiotactic polypropylene in solution. **The Journal of Chemical Physics** 112: 9632.
- Flory, P.J. (1969). **Statistical Mechanics of chain Molecules**. Wiley, Newyork.
- Logotheti, G.E. and Theodorou, D.N. (2007). Segmental and Chain Dynamics of Isotactic Polypropylene Melts. **Macromolecules** 40: 2235-2245.
- Madkour, T.M. and Mark, J.E. (1997). Modeling of the crystallization of isotactic polypropylene chains. **Journal of Polymer Science Part B: Polymer Physics** 35: 2757-2764.
- Mattice, W.L. and Clancy, T.C. (1999). Unperturbed Dimensions and Local Stiffness of Poly(vinyl chloride) with Stereochemical Sequences Composed of Repeating Units. **Macromolecules** 32: 5444-5449.
- Mattice, W.L., Tatek, Y.B. and Waheed, N. (2007). Variability in the Persistence Length of an Atactic Polymer Due to Quenched Randomness, As Illustrated by Atactic Polystyrene. **Macromolecules** 40: 379-383.
- Mattice, W.L. and Waheed, N. (2006). An Assessment of the Role of Quenched Randomness in the Stereochemical Sequences of Atactic Vinyl Polymers. **Macromolecules** 39: 2380-2387.
- Soga, K. and Shiono, T. (1997). Ziegler-Natta Catalysts for olefin Polymerizations. **Progress in Polymer Science** 22.
- Waheed, N., Mattice, W.L. and von Meerwall, E.D. (2007). Enhanced Diffusion at Intermediate Stereochemical Composition in Polypropylene by Dynamical Monte Carlo. **Macromolecules** 40: 1504-1511.

CHAPTER VII

MONTE CARLO SIMULATION OF POLYETHYLENE END-GRAFTED ON AN INTERACTING SOLID SUBSTRATE

7.1 Abstract

The coarse-grained polymer model was applied to simulate polyethylene (PE) brushes that were grafted on an interacting solid substrate by lattice Monte Carlo simulation. Monodisperse and bidisperse PE brushes composed of a mixture of the short and long PE chains grafted on interacting surface were investigated. The temperature effect on the structure of monodisperse PE brush on an interacting surface was also studied. The structural, conformational and orientational properties of PE brush with $40 < C < 120$ at grafting density in the range of $0.92\text{-}1.85\text{ nm}^{-2}$ were investigated. The temperature was set in the range of $298\text{-}473\text{ K}$. The results were in good agreement with prior numerical and theoretical results. For monodisperse PE brush, the PE chains were more stretched in the outer layer with increasing both grafting density and PE chain length. An increasing temperature can lead to a more stretching of PE chains at the outer region and the density was decreased. The temperature at 298 K could induce the crystallization of PE chains and caused high density at the vicinity near solid surface. For bimodal PE brushes, the long chains at the outer layer were more stretched while the shorter chains were compressed in the

inner layer of the bidisperse PE brushes. The chain stretching was also found to depend on the nature of an interaction between PE chains and the solid grafting wall. There was larger chain stretching for both long and short chains when PE chains were grafted on the repulsive surface than other interacting wall systems. The influence of an interacting surface on properties of PE brush can be ordered as: repulsive > neutral > attractive wall system. However, there was similar effect of an interaction between polymer chains and the solid substrate on properties of high molecular weight PE brushes.

7.2 Introduction

Polymer brush is the polymer with packed of densely chains, or high surface coverage, which are arrayed on hard surface by attaching one end to an interface. It usually deforms and stretches out in the perpendicular direction to form a brush at the surface, if no adsorption between solid surface and polymer chains (de Gennes, 1980; Milner, 1991). Brush polymers have been the subject to be studied by both experiment and theory in the past decade, mainly because of an important to various applications. In practice, the structural properties of brush surface is important and has been investigated for a wide range of applications, such as surface modification, lubrication, adhesion, colloidal stability, biocompatibility and biotechnology.

Various study of polymer brush based on Self-Consistent Field (SCF) method because this theory is a powerful tool for the quantitative understanding of polymer brushes beyond scaling theory. The most successful method to analyze the grafted polymer is the SCF equations which give a valid mean-field description at high grafting density system (Zhulina *et al.*, 1991). The simplified SCF method has been

developed based on the assumption of long, strongly stretched chains and weak excluded-volume interactions, and is argued to be exact in the long-chain limit. Hence, it was found a parabolic form for the density profile and supported by Monte Carlo simulation in the case of non-adsorption wall (Skvortsov *et al.*, 1988). There is a good agreement to parabolic form except a depletion zone very closed to the grafting surface. It was also found the free ends of the chain are included in the region very near the grafting surface (Chakrabarti *et al.*, 1992). In contrast, the parabolic form for convex surface and melts condition no longer exist and indicating that the free ends are excluded from the grafting surface zone in order to regain self-consistency (Toral and Chakrabarti, 1993). Moreover, it was found the existence of an exclusion zone from which the free chain ends are expelled (Ball *et al.*, 1991).

Initial investigation of polymer brushes focused on only monodisperse polymers by the monomer density profile shows a depletion layer near the grafting surface in agreement with phenomenological theories. Beyond that depletion layer, the density profile can be represented by a parabolic form. This result is in agreement with SCF calculation rather than with the scaling arguments that predict a plateau region for the density profile. The chain-end density is also found to be consistent with the SCF calculation. The free ends of the grafted chains are not excluded from the regions near the grafting surface (Chakrabarti and Toral, 1990). Moreover, the region close to the substrate is fully occupied by segments belonging to grafted chains. As high grafting density, free chains are progressively expelled from the surface region. In addition, the local melt density in the region closest to the interface illustrates systematically higher values than in the bulk, exhibiting distinct local maxima due to polymer adsorption. Moreover, the chain conformation tensor demonstrates that chains are

significantly stretched in the direction perpendicular to the surface. Furthermore, the chain-end density profile exhibits universal behavior in agreement with the prediction by the SCF theory (Daoulas *et al.*, 2002).

However, it is often unavoidable feature of the polydispersity system, mostly molecular weight distribution, on polymer brush structure in an experiment. This is an important motivation to study a polydisperse brush in theoretical method. It is necessary to investigate the relationship between molecular weight distribution and brush properties in both purely scientific reasons and engineering applications (Terzis, 2002), however, polydispersity can be used to one of an advantage in tailoring specific brush structure.

The first exploration of bimodal polymer brushes was investigated in the limit of strong stretching and for infinite molecular weight. The prototype of bimodal brushes has been examined in great detail by means of numerical SCF calculations (Dan and Tirrell, 1993). From uniform distribution polymers, there is completely change of density profile (Chakrabarti and Toral, 1990) but in the system where the difference in molecular weight between the two chains is small, the longer chain ends are localized at the brush edge and also suggests that the segment density profiles of two symmetrical brushes compresses together show stratification persists under compression (Descas *et al.*, 2006).

Moreover, the agreement between the experimental results and SCF result is very good. An investigation of bidisperse polymer brushes also provides the detail of the structure. The inner structure is described by the bottom region, formed by a mixture of long and short chains, and the top region is composed only of segment of the longer chains. The inner structure approximately scales with the total brush height,

although small deviation occurs. The width of the transition zone between two regions seems to be independent of the brush height (Terzis, 2002). Furthermore, bimodal polymer brush has a compression close to the grafting interface for short chains, whereas the longer chains have a characteristic flower-like distribution. Similar to the previous study, these longer chains stretch strongly (stem) when surrounded by smaller chains and decrease their stretching (crown) when only surrounded by longer chains (de Vos and Leermakers, 2009).

In addition, for a flat grafting surface and in good solvent condition, the short and long chains segregate vertically and the long chains stretch more in the coexisting region (Chen and Chakrabarti, 1995). The situation is different from the good solvent case where the stretching of the short chains increases as the short chain fraction increases (Chen and Chakrabarti, 1995).

The SCF method have been utilized to study polymer grafted on both non-interacting (He *et al.*, 2010) and interacting flat surface (Chakrabarti *et al.*, 1992), for both attractive and repulsive interactions. The layer thickness of polymer grafted on attractive interacting surface is depended on the total strength of the interaction potential without dependence on the particular shape of the potential well. On the other hand, for repulsive interaction, the exclusion zone was found from which the free chain ends are excluded by SCF calculations, similar with the convex non-interacting surface system. It should be noted that z_0 plays an important role to govern the structure of the polymer brush (Ball *et al.*, 1991).

In this work, polymers with all chain-ends attached to an interacting solid surface were investigated by MC simulation. Many of these studies were focused on PE model grafted on both non-interacting and interacting solid surface. Monodisperse

brush is investigated for end grafted on the surface with and without interactions. In addition, the temperature effect on monodisperse PE brush was also investigated. Finally, the grafted polymer with different molecular weight distribution was also studied in term of the effect of bimodal brushes consisting of a mixture of long and short PE chains. The density profile and the density of free end were analyzed. Moreover, conformational and orientation properties of all simulation were reported. All results would be presented for neutral (no interactions between surface and ethylene monomer), repulsive and attractive interaction to PE chains.

7.3 Model and method

System description

The grafted polymer systems contain ethylene units $(-CH-CH-)_n$, with $40 \leq C \leq 80$ and $80 \leq N \leq 160$ when C is the number of carbon in the chain and N is the number of PE chains. The periodic boundary condition was chosen in the x and y directions, while the two boundaries in z direction were treated as hard impenetrable walls. The total number of available surface sites was 40×40 lattice unit (surface area = 86.6 nm^2). The grafting density (σ) was varied from 0.92 - 1.85 nm^{-2} . The solid substrate was located at $z = 0$ and $z = M$, where $M > C$. All beads were not allowed to move from $z = 0$ to -1 . The simulations were done in the temperature range of 298 - 473 K to investigate the temperature effect on properties of polymer brushes on an interacting solid surface. The interaction between polymer and surface was applied with repulsive and attractive interaction in comparison to non-interaction surface. The solid substrate was incorporated by introducing an external polymer-substrate interaction term. A modified Lennard-Jone potential for ethylene units was employed

with the well depth was $\varepsilon = 370, 185,$ and 18.5 kJ/mol in simulation to represent the attractive, neutral and repulsive interaction for the solid substrate-polymer interaction, respectively. Monte Carlo simulation was performed by the method previously described in Chapter II.

7.4 Results and discussion

7.4.1 Monodisperse polyethylene melt brushes

7.4.1.1 Local melt density

The density profiles as a function of distance from the grafting surface (z) for several values of the surface coverage, σ , is shown in Figure 7.1(a). It depicts the variation of monomer density distribution with different polymer-surface interaction. For PE chains in higher grafting density, the chains are more stretching in the coexisting region and corresponded to a plateau region of density profiles which indicate the polymer bulk region throughout the inner layer. In the bulk region, the densities for all systems do not different but the widths of the bulk region are dramatically increased with increasing grafting density. Moreover, the polymer chains which are grafted on an attractive surface have more local degree of stretching in the inner layer than polymer chains that are grafted on neutral and repulsive interacting surface.

For all values of grafting densities considered here, the density profiles have similar behavior which exhibit two main zones corresponding to the two boundaries. There are polymer/wall interface at the bottom region and at upper region with polymer/vacuum interfaces. At the upper region far from the grafting surface where polymer is subjected to gradually ramp-like descended, the sigmoidal shape

and the width of the profile of the melt is typically observed. The width of the density profile in three different interacting walls is distinguishable among attractive, neutral and repulsive wall system. For an attractive interaction surface, there is more compression of polymer chain than that in the neutral and repulsive wall, respectively. Moreover, the difference of depletion layers width, depletion zone, in the vicinity of the substrate surface are also observed.

Interestingly, there were strong dependence of ρ on z , practically, in the first layers where monomer density achieves values considerable higher than in the bulk region, especially, in the attractive wall system, attributable to an adsorption of polymer chains which is found more for an attractive interacting wall than that in the neutral wall system. In contrast, for repulsive wall system, the depletion zone was lower than in the bulk region and lower than that in other interacting surface cases, which are attributed to the repulsion of substrate surface to polymer chains at the surface.

In addition, similar results were found when grafting density was fixed with different chain lengths (in Figure 7.1(b)). The density profile shows an interested stretching of polymer chains with an increasing chain length. The local chains with longer lengths are more stretched in the bulk region with distinguishable for three different interactions between polymer and grafting surface. The density profile of polymer chains grafted on an attractive surface became slightly broader than that in neutral and repulsive surface, respectively, which is contributed to more chain stretching than other two systems.

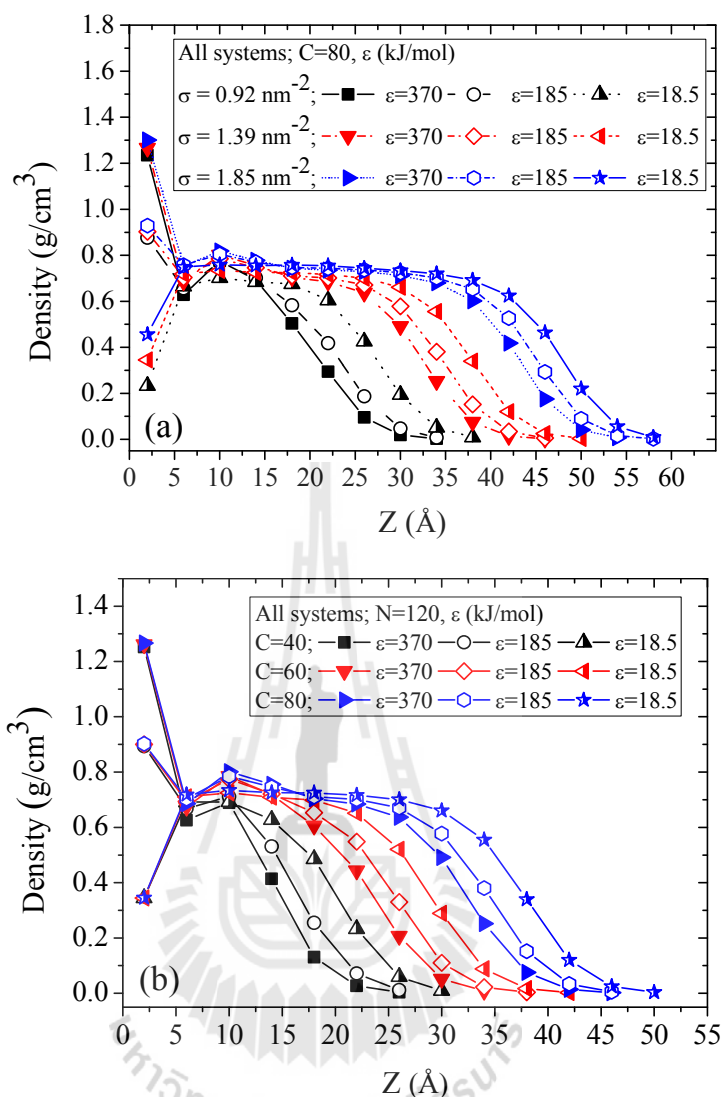


Figure 7.1 Density profile as a function of the distance from the grafting plane of PE grafted on a hard interacting substrate with different ϵ ; (a) C₈₀, $\sigma = 0.92$, 1.39 and 1.85 nm⁻², (b) C₈₀, C₁₂₀ and C₁₆₀, $\sigma = 1.39$ nm⁻².

7.4.1.2 Conformational properties

The conformation properties of polymer chains grafted on the substrate can be characterized by grouping atoms along the chain according to their scaled coordinated, i/N . Hence, those atoms are considered to be equivalent and are

plot against the reduced mean height $\zeta(s)$ which is defined by $\langle z(i)/z(l) \rangle$. It should have a universal curve in case of σ independent according to the prediction by SCF theories for polymer brush (Milner *et al.*, 1988).

It is very interesting that all curves do not superimpose for all values of grafting density as presented in Figure 7.2(a). The superimposed can exist when the surface coverage achieve a high enough values and the curve are downward without any back folding. Moreover, the attractive interacting causes more chain compression than that in neutral and repulsive wall, respectively. At low grafting density, $\sigma = 0.92 \text{ nm}^{-2}$, the curves of all three interacting surfaces are changed from an upward at the vicinity of the substrate surface to a downward at the distance far from the grafting surface, which is strongly affected by the nature of an interacting surface to chain characteristics. It is also found more chain stretching for grafted chains on repulsive wall and chain contraction in the case of an attracting wall.

There is an important effect from the interaction between polymer and the substrate. So, to confirm this effected on conformational properties of grafted polymer. Figure 7.2(b) shows a reduced mean height of PE grafted at $\sigma = 0.92 \text{ nm}^{-2}$ with different chain length and type of an interacting wall. The interacting wall influences the conformation similar to prior results and the superimposition can be seen when the chain length is increased. Similarly, as the chain length decreases, the chains at the upper region are folded to downward in all interacting surface system. The downward folding of chains is attributed to the strong effect of interacting wall on grafted polymers while a slightly different of curve at superimpose region can be attributed to the difference of an analytical details (Milner *et al.*, 1989).

7.4.1.3 End bead distributions

Figure 7.3 shows the distribution of end beads for grafted polymer on the substrate with different grafting density and interacting surface. It was found that end beads can be located anywhere in polymer brush. All curves were a systematic deviation from the SCF theory which predicts no end bead at the substrate surface, $z = 0$. The distribution near the substrate surface is dependent on the nature of an interaction between polymer chains and the wall. With an increased grafting density (in Figure 7.3(a)), the maximum peak of end bead profiles shift away from the grafting wall and exhibits a rather concave curve at the inner region, which is attributed to an extension of polymer chains in the z direction and force the end beads to extend a larger distance, which agree well with the density profile. Similarly, an attractive interacting wall causes larger values of the distribution of end bead than that in neutral and repulsive wall systems, respectively.

In contrast, when the grafting density was fixed (Figure 7.3(b)), the density of end bead was decreased with increasing chain length and the profile are shifted to the outer region caused by chain stretching while decreasing chain length causes the contraction in the inner region near the grafting surface. The results of an interacting wall provide that there was more chain extension grafted chains on an attractive wall than that in the neutral and repulsive wall case, respectively.

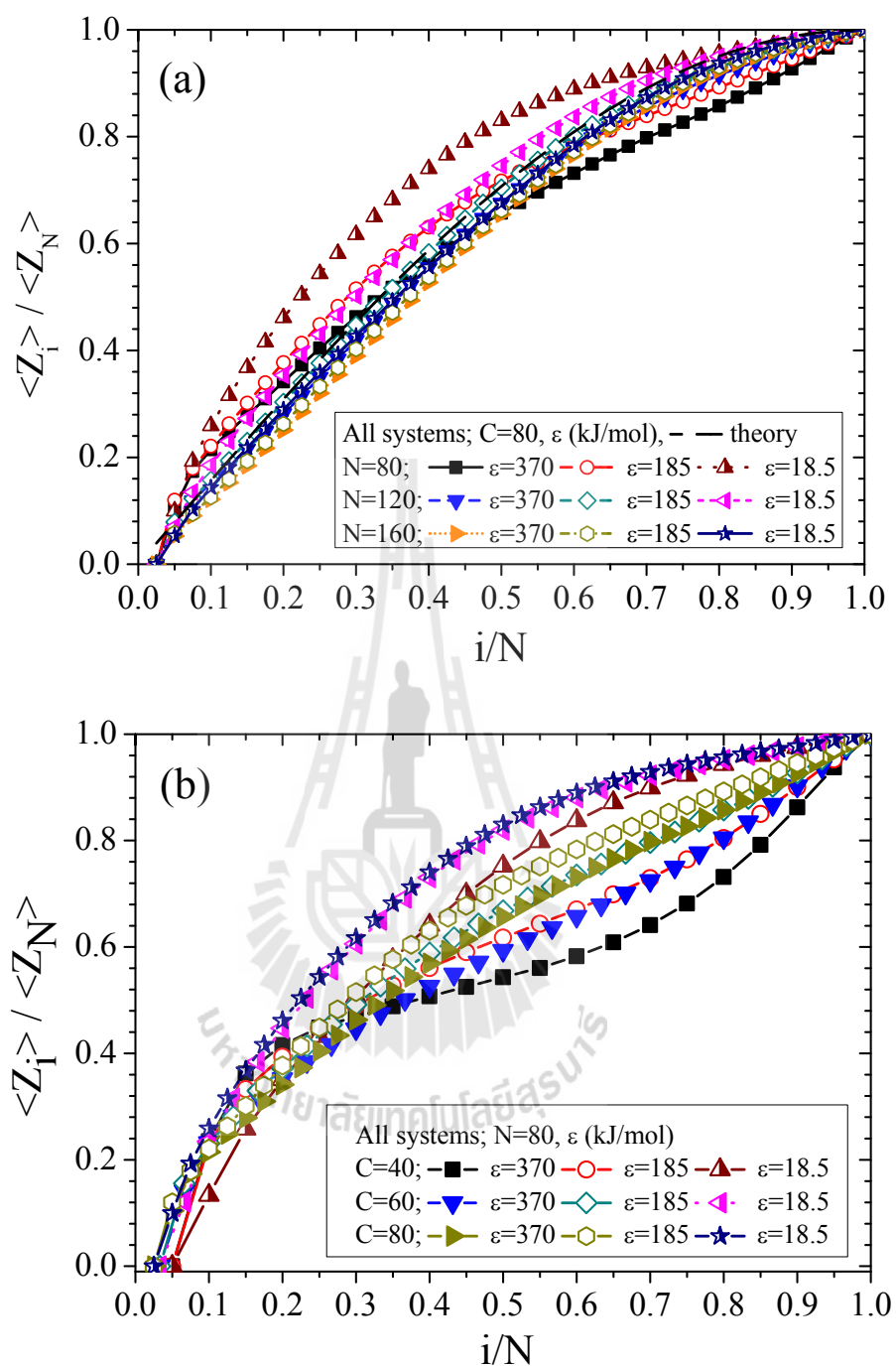


Figure 7.2 The normalized mean height $z(s)$ as a function of the normalized bead coordinate s along chain contour of PE grafted on a hard substrate with different ϵ ; (a) C_{80} , $\sigma = 0.92, 1.39$ and 1.85 nm^2 , (b) C_{40} , C_{60} and C_{80} , $\sigma = 0.92 \text{ nm}^2$. The solid line is the Milner *et al.* theory.

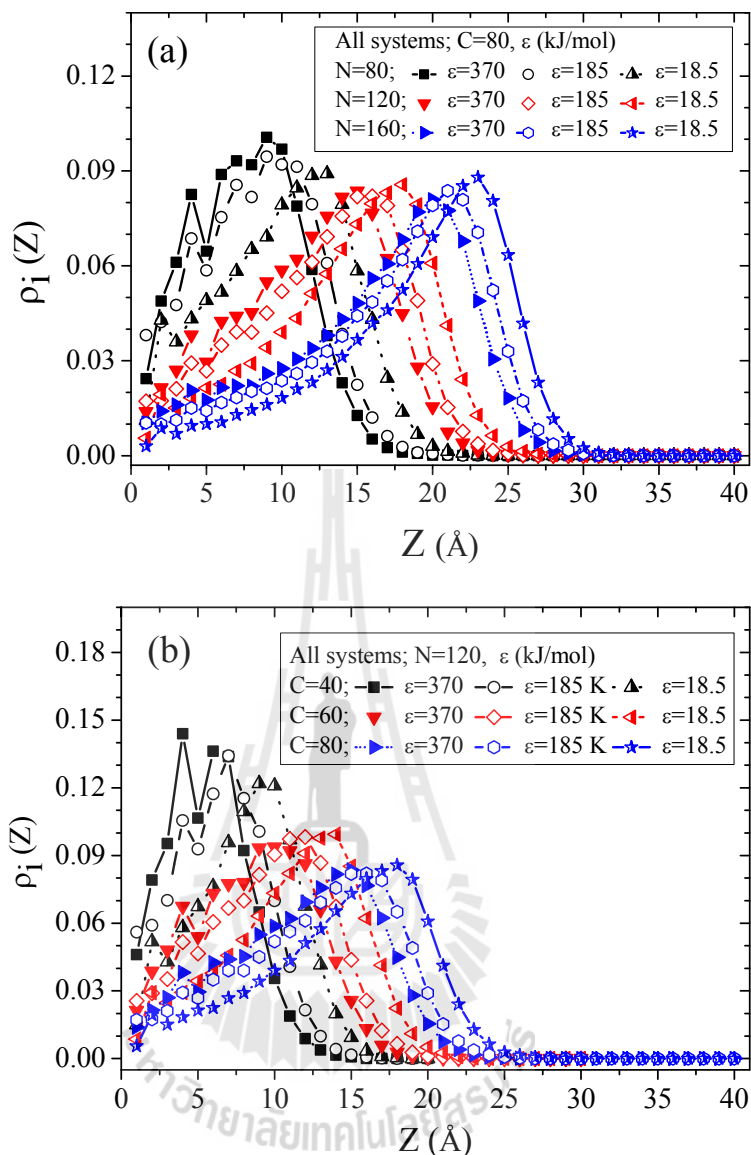


Figure 7.3 Distribution of free ends of PE grafted on a hard substrate with different ϵ ;

(a) C_{80} , $\sigma = 0.92, 1.39$ and 1.85 nm^{-2} , (b) C_{40}, C_{60} and C_{80} , $\sigma = 1.39 \text{ nm}^{-2}$.

7.4.1.4 Orientation of bond

Another parameter to determine of the chain stretching at the local scale is the orientation of bond which is represented by $\langle \cos(\theta_i) \rangle$ as a function of the normalized bead coordinate along chain contour. From Figure 7.4(a), it is clearly seen that all chains are extended to the outer region with an increasing grafting density but

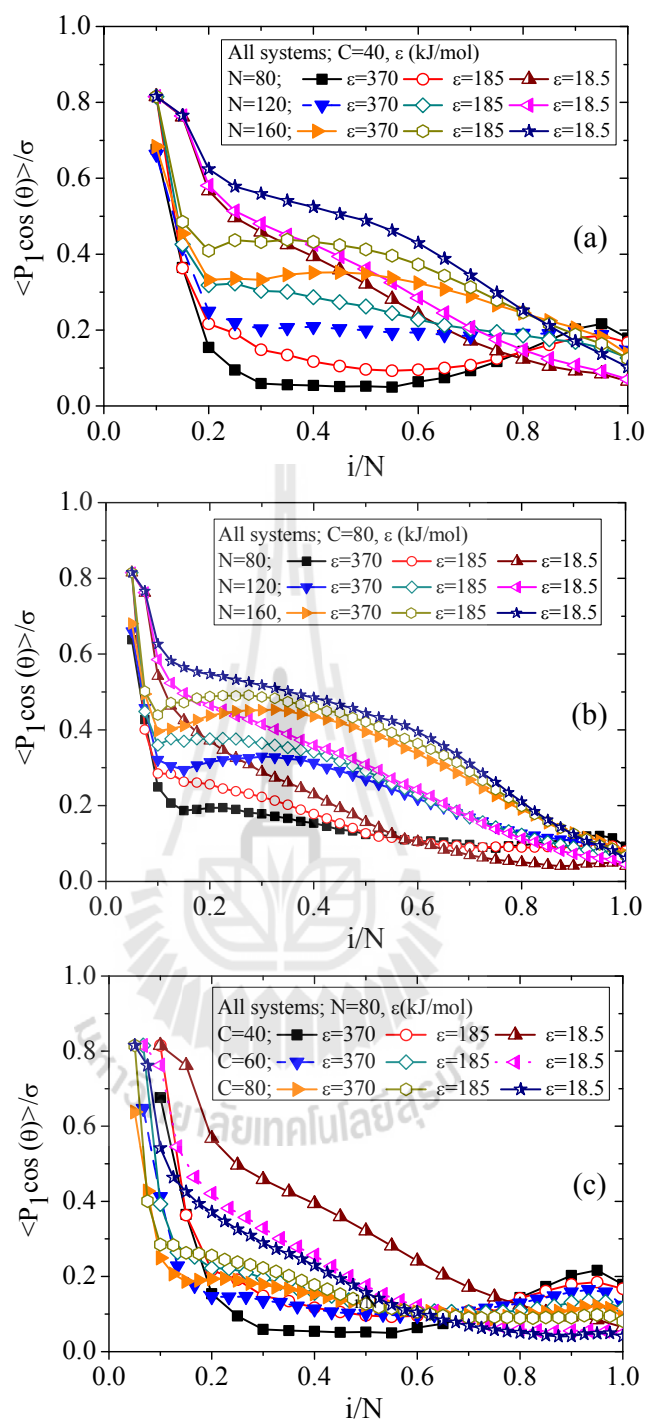


Figure 7.4 The chord-order parameter as a function of distance from grafting substrate of PE grafted on a hard substrate with different ϵ ; (a) C_{40} , $\sigma = 0.92, 1.39$ and 1.85 nm^{-2} , (b) C_{80} , $\sigma = 0.92, 1.39$ and 1.85 nm^{-2} , (c) C_{40}, C_{60} and C_{80} , $\sigma = 0.92 \text{ nm}^{-2}$.

PE chains at the vicinity of the polymer/vacuum interface of low grafting density system were more stretching.

There is also the wall effect on the orientation of polymer bond. Due to an attractive interaction between polymer chains and the grafting surface, the chains are less stretched while the chains grafted on the neutral and repulsive surface are more and most stretched, respectively. Moreover, when the chain length is increased as displayed in Figure 7.4(b), similar results are seen and the curve for these three surfaces are closed to each other and the stretching of short chain is disappeared at the upper interface. This is attributed to the less effect of solid surface on the long chain length system. Also, the polymer brushes at high grafting density ($N = 160$, $40 < C < 80$) are more stretched in the inner layer but become less stretched at outer region, in Figure 7.4(c).

7.4.2 Temperature effect on monodisperse polyethylene brush

The temperature was set in the range 298-473 K starting from high temperature and was decreased to equilibrate structure at lower temperature from 473 K \rightarrow 450 K \rightarrow 390 K \rightarrow 298 K.

7.4.2.1 Local melt density

The density profiles of monodisperse PE brush as a function of distance from the grafting surface with different temperature are displayed in Figure 7.5. It depicts the variation of ethylene density distribution with different $\varepsilon = 370$, 185 and 18.5 kJ/mol which are noted as an attractive, neutral and repulsive wall interaction, respectively. In all cases, studies are assumed an overall grafting density

of $\sigma = 1.39 \text{ nm}^{-2}$ ($N = 120$ chains and $C = 60$ units). For all values of temperature considered here, the density profiles show different behavior for each different interacting wall which is distinguishable for an attractive, neutral and repulsive wall interaction system.

Similar to monodisperse PE brush system, there are strong dependence of ρ on z in the first layer in which the monomer density is higher than that in the bulk region. Especially, in an attractive wall system, this is attributed to an adsorption of polymer chains on solid surface which is larger for an attractive surface than that in the neutral wall system. In contrast, for the repulsive wall system, its depletion zone is lower than that in the bulk region and also lower than other cases.

For an attractive wall (Figure 7.5(a)), density of PE at the vicinity near the solid substrate is increased about 2 times when the temperature is decreased from 473 K to 298 K. There is also a compression of polymer chains at the inner layer resulting from segregation of PE chains near the substrate surface. This behavior is caused by both temperature and wall interaction. It also leads to the structural formation of PE chains at the region near the grafting surface as most PE chains transform to an all-*trans* crystal like conformation and have higher density at lower temperature. Figure 7.5(b) presents the density profile of PE chains which are grafted on the neutral surface. PE chains grafted on the neutral surface are more stretched in the outer layer than those with an attractive surface. The density of PE brush at the surface is slightly increased with lower temperature. It also expresses a few ordered layers in the bulk region with different densities. At lower temperature, the density is more increased at the inner layer and the polymer chains are more compressed at the outer layer.

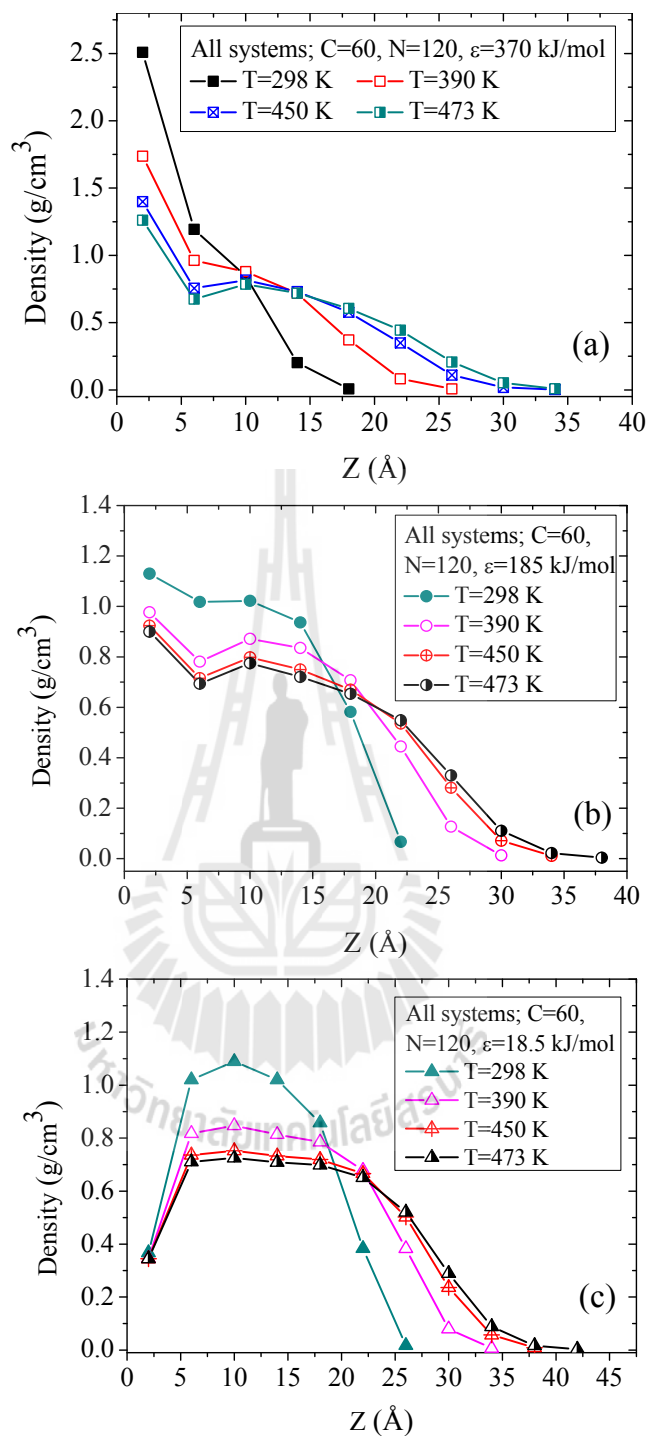


Figure 7.5 Density profile as a function of the distance from the grafting plane of C_{60} PE brush with different temp.; (a) $\epsilon = 370 \text{ kJ/mol}$, (b) $\epsilon = 185 \text{ kJ/mol}$, and (c) $\epsilon = 1.85 \text{ kJ/mol}$.

Similarly, the density of PE chains in the repulsive wall system is shown in Figure 7.5(c). It has similar behavior as the neutral wall case which the chains are more stretched at the outer region. A “plateau” region of density profiles is seen and it indicates that there is the bulk region throughout an inner layer. It is seen that the density of bulk region is dramatically increased with lowering temperature. Moreover, the density profiles of polymer chains become slightly narrower when the temperature of system decreased. This leads to the contraction of polymer chains to the inner layer. Besides, at lower temperature, the polymer chains grafted on the repulsive wall has more local degree of stretching in the inner layer than those chains grafted on neutral and attractive interface.

7.4.2.2 Conformational properties

It is very interesting that all curves for the conformational properties do not superimpose anymore for all kinds of interface. From Figure 7.6, the curves are superimposed when the temperature achieves a high enough value and there is upward and downward with some folding shape for every curve. The attractive wall shows the largest compression of polymer chains than other cases. In an attractive wall system, the curve in Figure 7.6(a) is changed to downward at the distance far from the grafting surface when temperature is decreased. This is attributed to the compression of polymer chains at the outer layer for low temperature system. These data agree well with the density profile in the previous section. In contrast, the conformational properties for the neutral wall system are given in Figure 7.6(b). The PE chains upward at the lower region but fold to downward at the upper region which is attributed to polymer chains are more stretched in the region near the

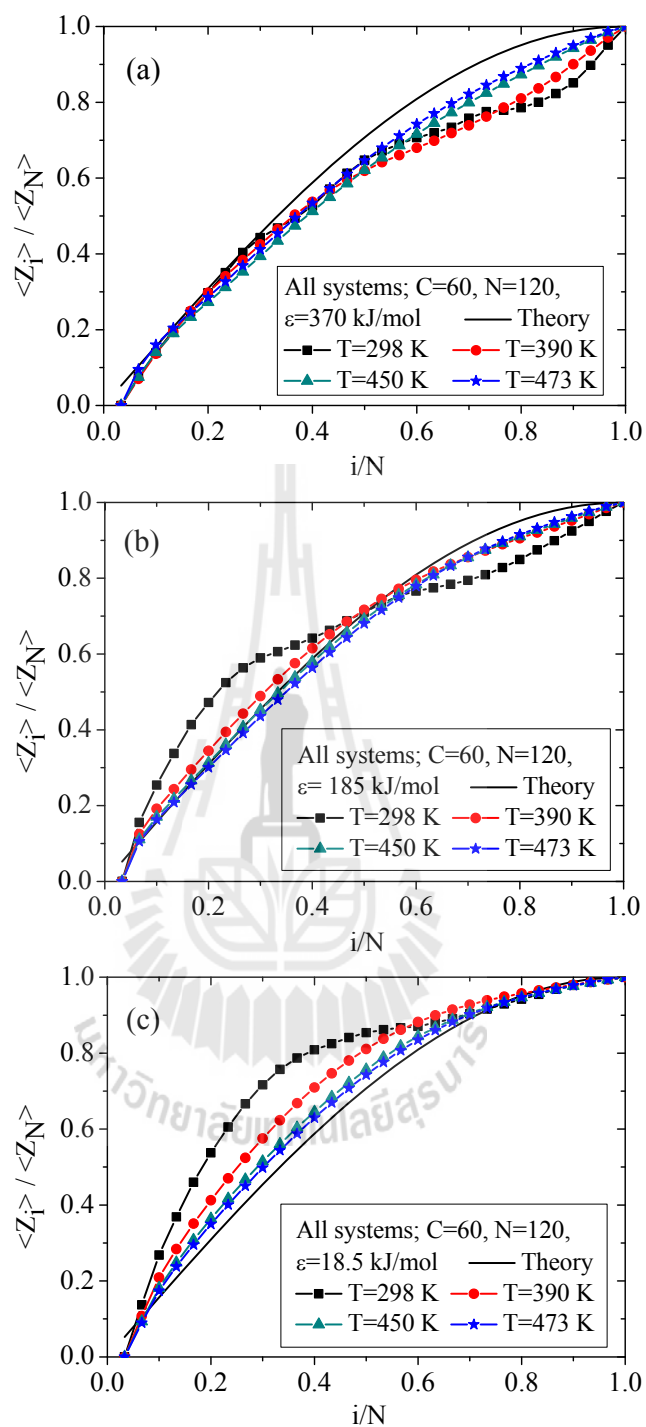


Figure 7.6 The normalized mean height $z(s)$ as a function of the normalized bead coordinate s of C_{60} PE brush with different temp.; (a) $\epsilon = 370$ kJ/mol, (b) $\epsilon = 185$ kJ/mol and (c) $\epsilon = 18.5$ kJ/mol.

solid wall. The chains are contracted at the outer region for the case of the neutral wall system. For the repulsive wall case, the polymer chains are upward at the vicinity of the substrate surface without any back folding to the other region which is displayed in Figure 7.6(c). This leads to the stretching of polymer chains at the inner region and is attributed from the segregation of chains near the wall when the temperature is decreased.

7.4.2.3 End bead distributions

Figure 7.7 shows the end beads distribution of PE grafted on the substrate with different temperature and wall interaction. End beads can be seen in everywhere in polymer brush. All curves have systematic deviation from the SCF theory which predicts that there is no end bead at the substrate surface ($z = 0$). The distribution near the wall is dependent on the nature of wall interaction. For all cases, the maximum peak of end beads density shifts away from the grafting surface with lower density when the temperature is increased. The rather concave curve is found at the inner region with an extension of polymer chains along the z direction when the temperature is increased. This forces the end beads to extent a larger distance and it agrees well with the density profile data. The effect of wall interaction is also related to an extension of PE chains ordering as: attractive > neutral > repulsive wall.

7.4.2.4 Orientation of bond

Figure 7.8 shows the orientation of bond vector of PE brush at different temperature. All PE chains at lower temperature system are more compressed into the inner layer than at higher temperature. The significant changes

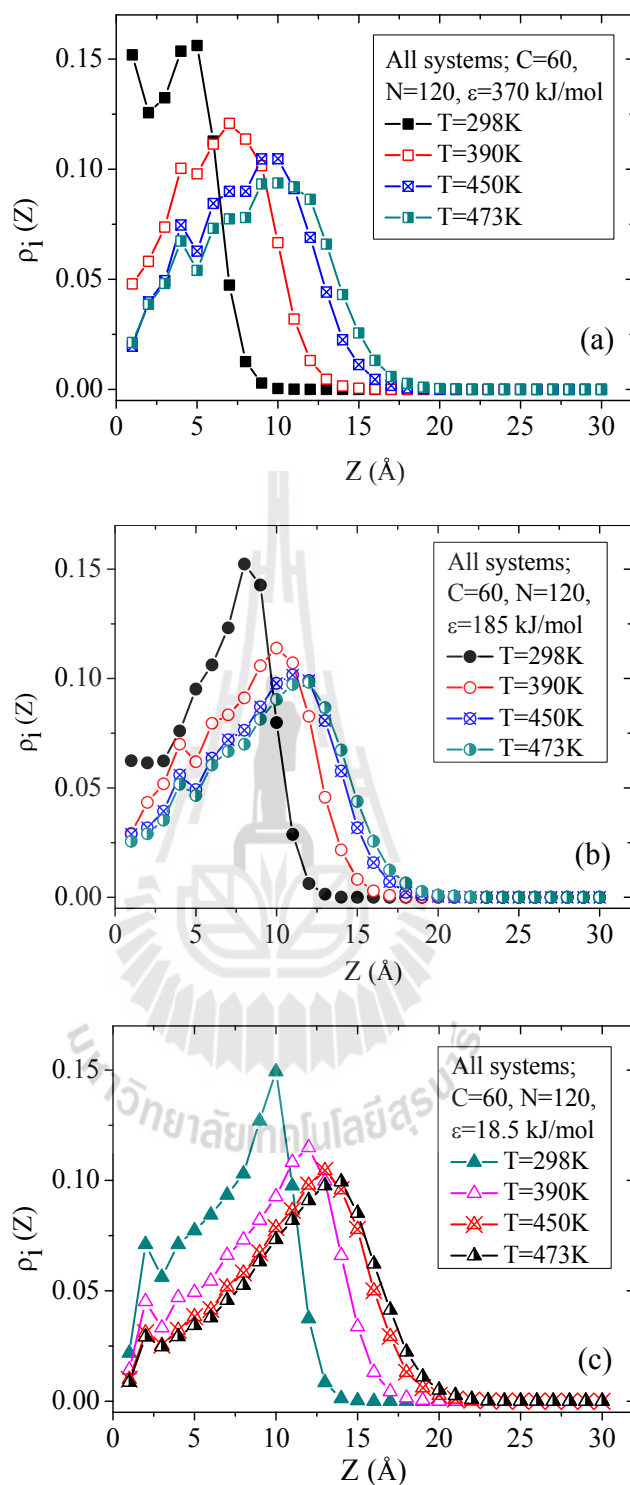


Figure 7.7 Distribution of free ends of C_{60} PE brush with different temp;

(a) $\epsilon = 370$ kJ/mol, (b) $\epsilon = 185$ kJ/mol and (c) $\epsilon = 1.85$ kJ/mol.

are found mostly at the vicinity of the polymer/wall interface at lower temperature. Due to an attractive interaction between PE chains and the grafting wall (in Figure 7.8(a)), the chains are less stretched compared to the case of the neutral and repulsive wall which the chains are more stretched, respectively.

7.4.3 Bidisperse polyethylene grafted on interacting wall

7.4.3.1 Local melt density

For bidispersity system, all interacting wall cases were studied to determine an overall surface densities at $\sigma = 1.85 \text{ nm}^{-2}$ ($N=160$ and $120 < C < 200$). Figure 7.9(a) presents the variation of the density profile with distance from the solid surface of the long (N_L) and short (N_S) PE chains in bidisperse PE brushes. There are also three different interactions between polymer chains and the grafting wall, $\varepsilon = 370$, 185 and 18.5 kJ/mol which are denoted to an attractive, neutral and repulsive wall, respectively.

For all density profiles, they are similar characteristic and also exhibit two main zones corresponding to two boundaries of the brushes; (1) surface/polymer interface at the bottom region and (2) polymer/vacuum interfaces at the upper region. There are the coexist region composed of long and short chains in everywhere. The long chains are more stretched in the outer layer when the density is increased in the middle region. On the other hand, the short chains at inner layer and the long chains at the lower layer are almost equally stretched.

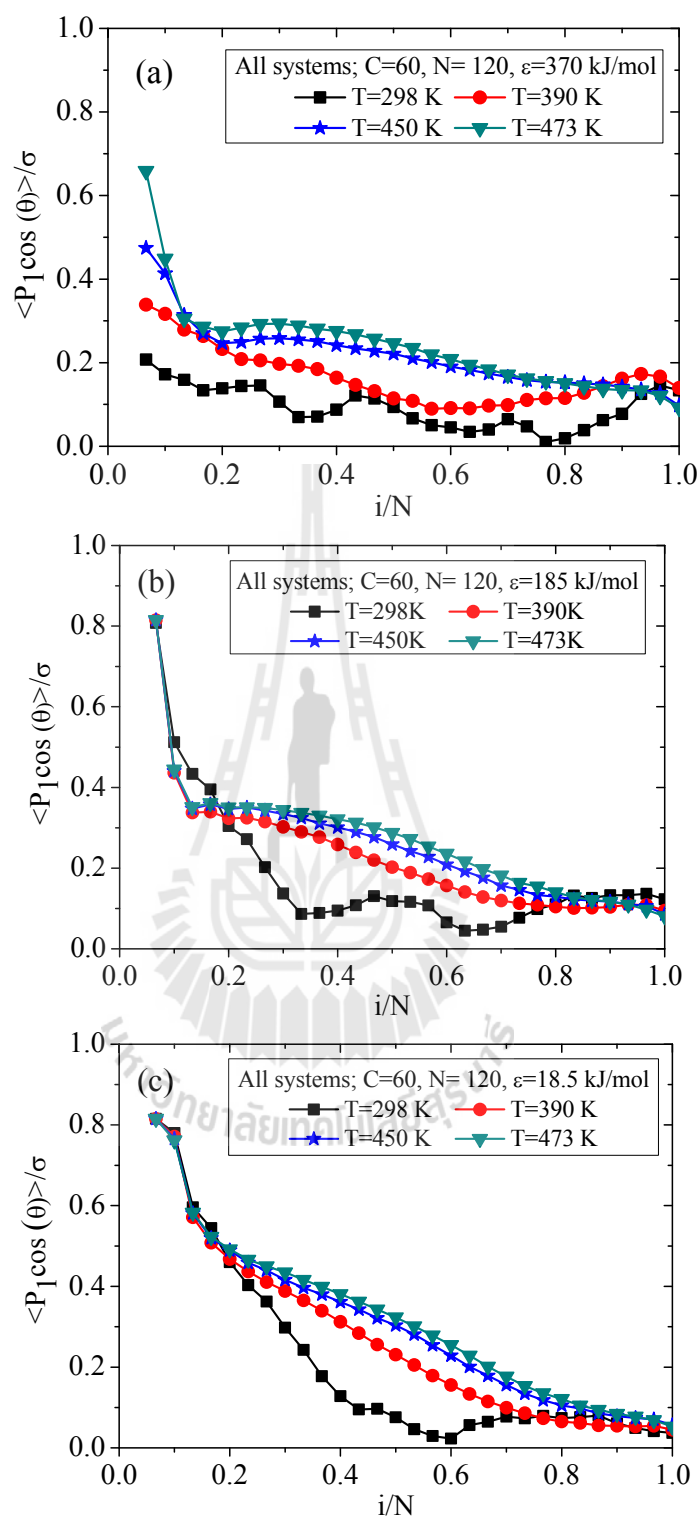


Figure 7.8 The chord-order parameter as a function of distance from the grafting substrate of C_{60} PE brush with different temp; (a) $\epsilon = 370$ kJ/mol, (b) $\epsilon = 185$ kJ/mol and (c) $\epsilon = 18.5$ kJ/mol.

However, the density is strongly depended on the interaction between the wall and PE chains. Hence, the brush density at the first layer is higher than that in the bulk region. Also, the densities of PE grafted on the wall also have interesting results in that there is no bulk region in the PE brush. For an attractive wall case, the depletion layer is larger than that of other systems which is attributed to an adsorption of polymer chains onto the surface at the vicinity of solid substrate. In contrast, the depletion zone for the repulsive wall case is lower than in other systems. This is attributed to the repulsive force of grafting surface to polymer chains.

In addition, when the PE molecular weight is increased (Figure 7.9(b)), the density profiles of the long and short chains are coincided in everywhere along the grafting surface. The overall densities are almost similar with the low molecular weight system as shown in Figure 7.9(a). Both long and short chains are much more stretched compared with lower molecular weight brushes. Besides, chain stretching is less depended on the interaction between the wall and PE chains.

7.4.3.2 Conformational properties

The conformational properties of polymer chains grafted on interacting substrate can be characterized by grouping atoms along the chain according to their scaled coordinated, i/N . Therefore, those atoms are considered to be equivalent and are plotted against the reduced mean height $\zeta(s)$ which is defined by $\langle z(i)/z(l) \rangle$. It should give a universal curve for the fixed grafting density according to SCF theories (Milner *et al.*, 1989).

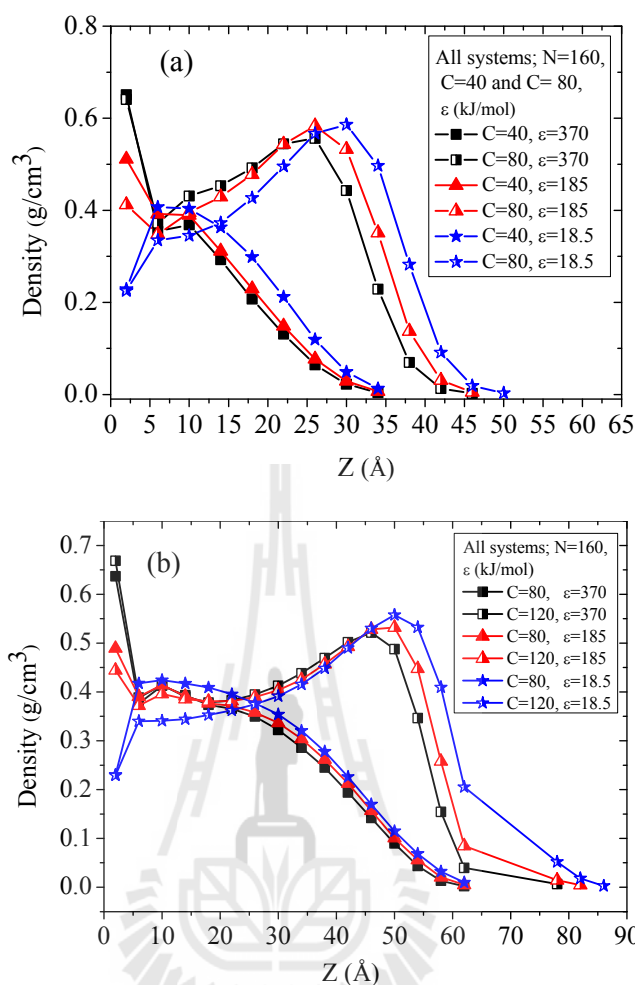


Figure 7.9 Density profile as a function of the distance from the grafting surface of bidisperse PE brush which are grafted with different ϵ ; (a) $N_S=C_{40}$ and $N_L=C_{80}$, (b) $N_S=C_{80}$ and $N_L=C_{120}$.

The $\zeta(s)$ as a function of normalized bead coordinate along the chain contour is presented in Figure 7.10(a). It is very remarkable because all curves do not superimpose as theory prediction. The long chains are upward in the upper layer while the short chains downward without any back folding which indicates the stretching of long chains in the outer region and the compression of short chains in the inner region close to the wall.

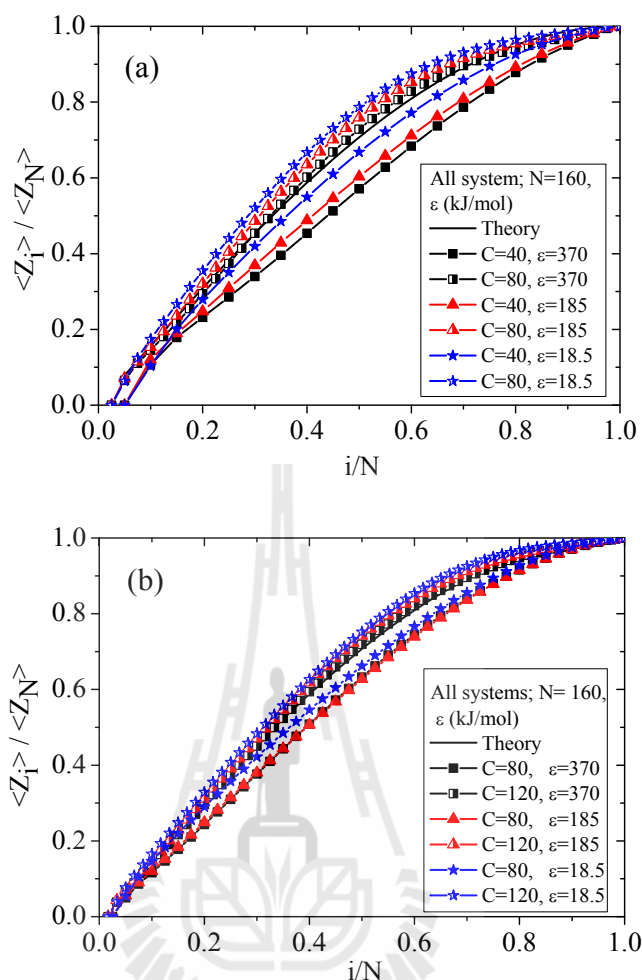


Figure 7.10 The normalized mean height $z(s)$ as a function of the normalized bead coordinate s of bidisperse PE brush which are grafted with different ϵ ; (a) $N_s=C_{40}$ and $N_L=C_{80}$, (b) $N_s=C_{80}$ and $N_L=C_{120}$. The solid line is the Milner *et al.* theory.

Furthermore, the effect of an interaction between polymer chains and the substrate are investigated for conformational properties of PE brushes. Polymer chains are more stretched on the repulsive wall system and more contracted on an attractive and neutral surface, respectively. However, the curve can be superimposed in case of the higher molecular weight, which are displayed in Figure

7.10(b). An extension of long and short chains is observed with similar trends to low molecular weight grafted system.

7.4.3.3 End bead distributions

The end beads distribution of PE grafted on interacting substrate for bimodal molecular weight is illustrated in Figure 7.11(a). The end beads of both short and long chains can be located anywhere in the brush. All curves have a systematic deviation from the SCF theory which predicts that there are no end beads at the substrate surface. It is also noticed that long chains are always more stretched than the short ones. Not only the segregation of the short and long chains is observed but also the penetration of the short chains into outer layer is found. This is represented by the crossover region for both short and long PE chains lengths.

For the long chains, the maximum peak of end beads distribution is shifted away from the grafting surface and exhibits a rather concave in the inner region. This is attributed to an extension of polymer chains in the z direction and the end beads are pushed to the outer layer, which appears to have larger effect on tail stretching and it is in good agreement with the density profiles.

The distribution is strongly depended on the nature of interaction between the polymer chains and the wall. For example, both long and short chains are stretched more when they are grafted on the repulsive wall due to the repulsive force from the substrate to PE chains while it exhibits the less stretched chains. It is clearly confident that an interaction of the wall for the case of an attractive wall on polymer chains becomes more influence for polymer brush size. The attractive wall provides

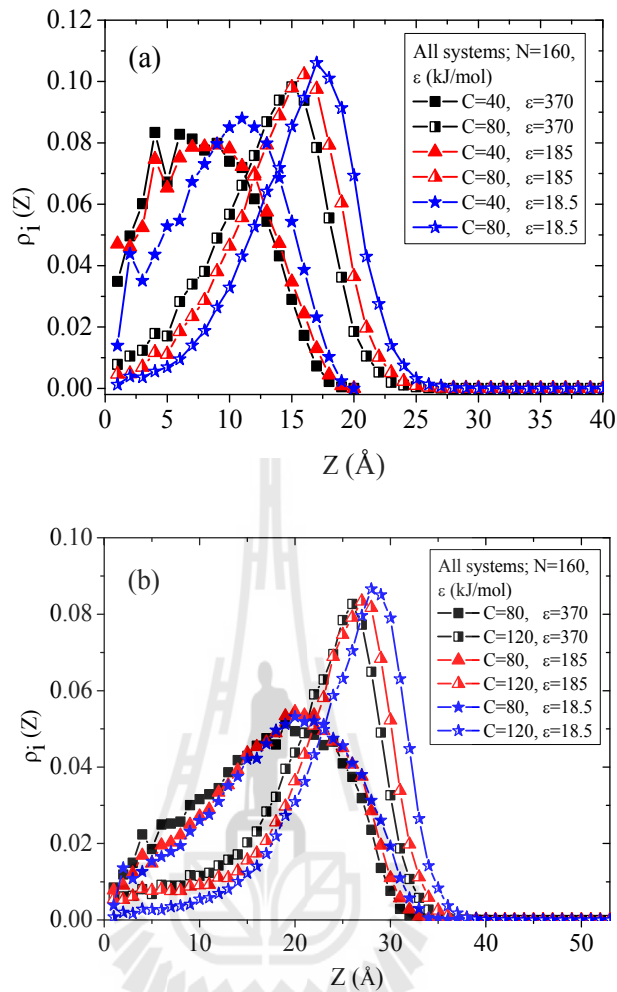


Figure 7.11 Distribution of free ends of bidisperse PE brush which are grafted with different ϵ ; (a) $N_S=C_{40}$ and $N_L=C_{80}$, (b) $N_S=C_{80}$ and $N_L=C_{120}$.

the larger amount of end beads distribution than those in the neutral and repulsive wall system, respectively.

In addition, the end bead distribution at higher molecular weight system is presented in Figure 7.11(b). The PE chain distribution is decreased and shifted to the outer region caused by chain stretching, while the low molecular weight system (Figure 7.11(a)) shows a contraction at the vicinity of the grafting surface. PE

chains when they are grafted on the attractive wall are more extended than those in the neutral and the repulsive wall, respectively.

7.4.3.4 Bond orientation

Data for the stretching parameter in bidisperse PE grafted on interacting surface are demonstrated in Figure 7.12(a). The orientation of bonds is illustrated as a function of the normalized bead coordinate along the chain contour. Long chains in the outer region are more extended than those short chains at the same region. However, at the inner layer, the short chains are more stretched than those in the outer layer. This is in good agreement with SCF theory and previous numerical results. Next, the effect of wall interaction with PE chains on the bond orientation is examined. In the case of an attractive wall, polymer chains in the inner layer are less stretched than those in the neutral and the repulsive walls, respectively. This is attributed to an attractive interaction between polymer chains and the grafting surface. However, there is no different result at the area far away from the grafting surface. This is attributed to the influence of an interaction between PE chains and the solid substrate on properties of PE brush. The chord vector of PE brush with high molecular weight is also displayed in Figure 7.12(b). The orientations for all chain length are closed to each other and are less distinguishable among the attractive, neutral and repulsive wall. This is attributed to less effect of interacting surface on PE chains at the high molecular weight system.

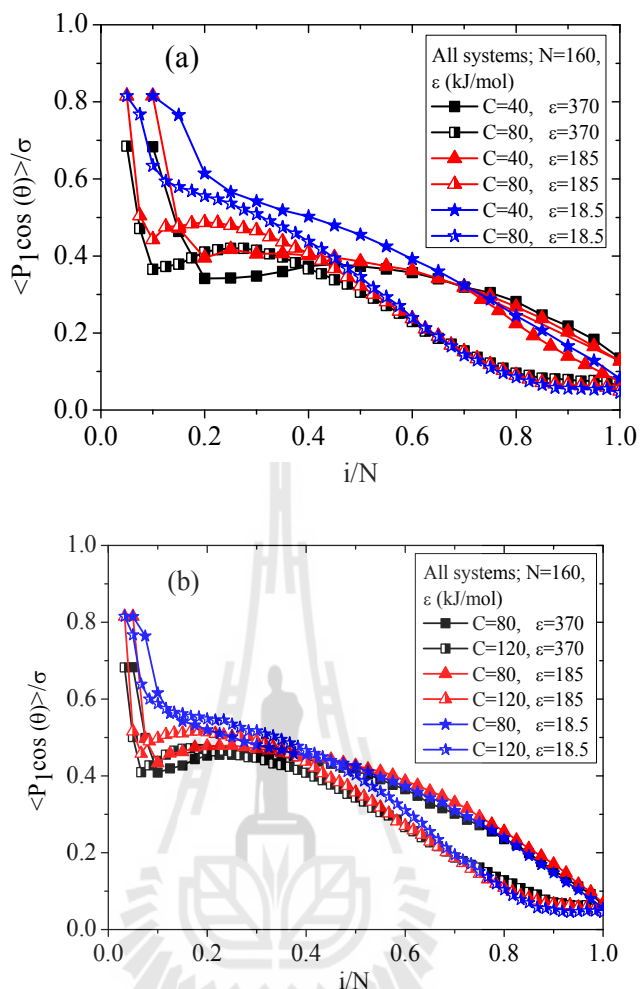


Figure 7.12 The chord-order parameter as a function of distance from the grafting substrate of bidisperse PE brush which are grafted with different ϵ ; (a) $N_S=C_{40}$ and $N_L=C_{80}$, (b) $N_S=C_{80}$ and $N_L=C_{120}$.

7.5 Conclusions

Density profiles, conformation properties, distribution of end beads and bond orientation of polymer brush on interacting surface were investigated by MC simulation. For monodisperse PE brush, PE chains were more stretched in the outer layer with increasing grafting density and chain length. Increasing temperature leads to more chain stretching at the outer region with decreased density. Decreasing

temperature contributes an order structure formation of PE chains with high density at the vicinity of solid wall. The long chains at the outer layer were more stretched while the shorter chains in the inner layer were compressed. The two main boundaries of PE brushes system were illustrated there; surface/polymer interface in the inner layer and polymer/vacuum interfaces in the outer edge. The results are in good agreement with prior numerical and theoretical results as confirmed by density profile $\rho(z)$, normalized mean height $\langle z_i/z_l \rangle$, end bead distribution $\rho_{E,i}(z)$ and bond orientation $\langle \cos(\theta_i) \rangle$. The distribution of PE chains depends on the nature of an interaction between the PE chains and the solid grafting wall. Both long and short chains have larger values for chains stretching than other systems, ordering as: repulsive > neutral > attractive wall case. For high molecular weight PE brush, there was slightly effect for an interaction between polymer chains and the solid wall on properties of PE brush.

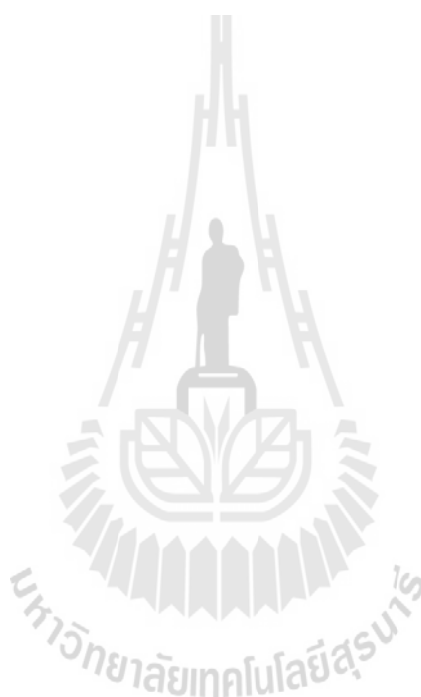
7.6 References

- Ball, R.C., Marko, J.F., Milner, S.T. and Witten, T.A. (1991). Polymers grafted to a convex surface. **Macromolecules** 24: 693-703.
- Chakrabarti, A., Nelson, P. and Toral, R. (1992). Structure of polymer chains end-grafted on an interacting surface. **Physical Review A** 46: 4930-4934.
- Chakrabarti, A. and Toral, R. (1990). Density profile of terminally anchored polymer chains: a Monte Carlo study. **Macromolecules** 23: 2016-2021.
- Chen, H. and Chakrabarti, A. (1995). Effects of grafting geometry and solvent quality on the structure of bimodal polymer brushes. **Physical Review E** 52: 3915-3922.

- Dan, N. and Tirrell, M. (1993). Effect of bimodal molecular weight distribution on the polymer brush. **Macromolecules** 26: 6467-6473.
- Daoulas, K.C., Terzis, A.F. and Mavrantzas, V.G. (2002). Detailed atomistic Monte Carlo simulation of grafted polymer melts. I. Thermodynamic and conformational properties. **The Journal of Chemical Physics** 116: 11028.
- de Gennes, P.G. (1980). Conformations of Polymers Attached to an Interface. **Macromolecules** 13: 1069-1075.
- de Vos, W.M. and Leermakers, F.A.M. (2009). Modeling the structure of a polydisperse polymer brush. **Polymer** 50: 305-316.
- Descas, R., Sommer, J.-U. and Blumen, A. (2006). Concentration and saturation effects of tethered polymer chains on adsorbing surfaces. **The Journal of Chemical Physics** 125: 214702.
- He, S.-z., Merlitz, H., Chen, L., Sommer, J.-U. and Wu, C.-X. (2010). Polyelectrolyte Brushes: MD Simulation and SCF Theory. **Macromolecules** 43: 7845-7851.
- Milner, S.T. (1991). Polymer brushes. **Science** 251: 905-914.
- Milner, S.T., Witten, T.A. and Cates, M.E. (1988). Theory of the grafted polymer brush. **Macromolecules** 21: 2610-2619.
- Milner, S.T., Witten, T.A. and Cates, M.E. (1989). Effects of polydispersity in the end-grafted polymer brush. **Macromolecules** 22: 853-861.
- Skvortsov, A.M., Pavlushkov, I.V., Gorbunov, A.A., Zhulina, Y.B., Borisov, O.V. and Pryamitsyn, V.A. (1988). Structure of densely grafted polymeric monolayers. **Polymer Science U.S.S.R.** 30: 1706-1715.
- Terzis, A.F. (2002). Bidisperse melt polymer brush studied by self-consistent field model. **Polymer** 43: 2435-2444.

Toral, R. and Chakrabarti, A. (1993). Monte Carlo study of polymer chains end-grafted onto a spherical interface. **Physical Review E** 47: 4240-4246.

Zhulina, E.B., Borisov, O.V., Pryamitsyn, V.A. and Birshtein, T.M. (1991). Coil-globule type transitions in polymers. 1. Collapse of layers of grafted polymer chains. **Macromolecules** 24: 140-149.



CHAPTER VIII

THE STUDY OF POLY(ETHYLENE-*CO*-*ATACTIC* PROPYLENE) COPOLYMER NANOFIBER BY LATTICE MONTE CARLO SIMULATION

8.1 Abstract

Poly(ethylene-*co-atactic* propylene) copolymer nanofiber was studied using lattice Monte Carlo simulation. The simulation was performed with the coarse-grained model of Poly(ethylene-*co-atactic* propylene) chains with a density in the range of 0.753-0.760 g/cm³ at 473 K. The properties of nanofiber were characterized at different PE:PP monomer ratio. When the ethylene fraction was increased, the total density of nanofibers was increased in the region near the fiber axis and dramatically decreased in the middle region toward the free surface along the radial direction. The interfacial width of radial density profile was also increased with high ethylene content. The end bead segregation became more abundant in the region closer to the vacuum side of this copolymer nanofiber. The bond at the surface preferred to orient in parallel direction to the surface. All bonds favored parallel and perpendicular orientation to the surface which were depended on the ethylene content in copolymer. Similarly, the largest and smallest molecular axis were oriented parallel and perpendicular to the fiber axis, respectively, and changed toward random orientation when the ethylene content was decreased, especially at PE content lower than 0.5. The

orientation of molecule on L_1 axis was also increased while the orientation on the L_3 axis was decreased. Moreover, the molecular size in X component became smaller along the radial direction and decreased near the surface, similar to the total component, while the R_g in $Y-Z$ component was unchanged. The molecular shape, both asphericity and acylindricity were increased along the radial direction and decreased at the fiber surface. There was a slightly change in the eigenvalues of copolymer radius of gyration of fiber near the surface and most of which were occurred close to the vacuum side. These values increased with ethylene content along the radial direction.

8.2 Introduction

The most versatile vinyl polymers and simplest structure are polyethylene (PE) and polypropylene (PP) which can be used both as plastic and fiber. They are the most popular plastic in the world. It can be made us grocery bags, shampoo bottles, children's toys, bullet proof vest, and even dishwasher-safe food container. Their fiber form has been used to make indoor-outdoor carpeting. Besides the homopolymer form of PE and PP, copolymer of ethylene and propylene random copolymers has also been studied in a wide range of application (Hongjun *et al.*, 1999; Seki *et al.*, 1999) by controlling copolymer compositions. Their structure is similar to *i*PP, but the regular repeating of propylene units is randomly disrupted by the presence of ethylene. EP copolymers have become an important class of thermoplastic elastomers with excellent physical properties. Two classes of EP elastic copolymer are available commercially: ethylene-based copolymer with ethylene being the major component and propylene-based copolymer with propylene being the major component.

In fact, the EP copolymers with ethylene content lower than 60 %w/w are essentially amorphous (Bassi *et al.*, 1970). The advantages of non-crystalline of EP copolymer are improved transparency, relative softness, lower sealing temperature, and moderate low-temperature impact strength due to the lowered glass-transition temperature. Moreover, it is commonly used for toughening of other polymers due to excellent properties, such as resistance to phosphate ester hydraulic fluids, heat and oxidation, good resistance to steam and hot water, standard lining material for steam hoses of EP copolymer but its drawback is easily attacked by any petroleum products.

There have been several studies on the relationships among structure, morphology and properties for ethylene-based copolymers (Mathot *et al.*, 1996; Guerra *et al.*, 1999). It has been known that the physical properties of semi-crystalline polymers depend strongly on their crystalline morphology, which in turn is greatly affected by the crystallization condition during processing (Di Lorenzo and Silvestre, 1999). The ethylene crystals can be formed in the ethylene-based copolymer and propylene crystals are formed in the propylene-based crystals, which are closely associated with the characteristics of the constituting crystals, such as melting point and their corresponding structure changed upon deformation. The crystallization of ethylene-based copolymers suggest the categorized morphology can be classified into two types (Minick *et al.*, 1995): (1) fringed-micellar crystalline morphology without the presence of spherulites when density less than 0.89 g/cm^3 , and (2) both fringed-micellar and lamellar crystalline morphologies in the presence of spherulites when density in the range $0.89\text{-}0.91 \text{ g/cm}^3$.

A significant change in the melting point with decreasing ethylene content (or increasing propylene content) is caused by the reduction of the crystal size from the

ethylene sequence, whereas the corresponding structural behavior during static and dynamic conditions can also be altered. Hence, at research and industrial level, it is intriguing to control and master the crystallization behavior of a polymer, in order to design materials with desirable properties.

The copolymers with 6-18 %w/w ethylene content are inherently elastic with an elongation at break ratio larger than 1000% (Pegoraro *et al.*, 2000). In spite of the relatively low crystallinity (5-15%), such materials can be readily formed into pellets which lead to highly desirable property for transportation/handling use and subsequent processing/mixing operations in the production of elastic fibers. Moreover, a recent study (de Ballesteros *et al.*, 1996) indicates that an insertion of propylene moiety led to a pseudo hexagonal crystalline structure at high-propylene content and disorder in the crystalline phase of ethylene sequence gradually increase. The presence of ethylene units reduces the melting point and crystallinity by introducing irregularities into the main polymeric chain. This is caused by a reduction in the number of PP crystallization nuclei claiming that PE is able to delay nucleation and subsequent crystallization in PP resulted in consequence of crystallization from a miscible melt (Long *et al.*, 1995; Blom *et al.*, 1998). It has been indicated that decreasing the crystallization rate of EP copolymer may be caused by two reasons. First, the PP nucleation is reduced due to PP chains in PE which can be viewed as PP in solution. The other reason, the viscous PE slow down the diffusion of PP chains during crystallization (Li *et al.*, 1997).

The formation of soft materials, elastic fibers of a composition based largely on propylene has long been the goal of the several major industrial laboratories. Those fibers can be made by the existing equipment for the production of inelastic fibers

with only minor modifications to accommodate and enhance the elasticity, which represent a significant breakthrough in the use of propylene-based polymers. In addition, the EP copolymer with dominant propylene moiety and PP has been studied (D'Orazio and Cecchin, 2001; Mighri *et al.*, 2001) for the development of the technological opportunity of these fibers. It has been found the PP chains in EP copolymer can adopt a left-handed or right-handed helix in the solid phase which can be organized into three different polymorphs: α -monoclinic, β -hexagonal and γ -orthorhombic crystal forms, depending on the conditions (Brückner *et al.*, 1991; Caldas *et al.*, 1994; Lotz *et al.*, 1996).

Polymeric materials in nano scale were considerably interesting in past decade owing to their distinctive and fascinating properties in various applications. Confined macromolecules at nanometer scale exhibited a fascinating and unexpected dynamic behavior and provide many unique properties due to the size reduction to the point where critical length scales of physical phenomena become comparable to or larger than the size of the structure. Various experimental techniques have been applied to study polymer surfaces and interfaces. Individual polymeric nanofibers were challenging to characterize experimentally due to their small size. Various simulation techniques have been applied to investigate the confinement of polymeric systems in one or two dimensions. The simulations utilized variety approaches such as the system in discretized lattice (Madden, 1987) or continuous (Müller and MacDowell, 2000) space, adoption of coarse-grained (Doruker and Mattice, 1998) or atomistically detailed (Mansfield and Theodorou, 1991) models, and focus on either static (Theodorou, 1988) or dynamic aspects of the surface. Molecular Dynamics simulation have been also utilized to investigate the effect of nanofiber size to size-

dependent properties of PE nanofibers (Curgul *et al.*, 2007). The results show that the mass density at the center of all fibers was constant and comparable to that of the bulk polymer. The surface layer thickness for all fibers slightly increased with fiber size. The chains at the surface were more confined compared to the chains at the center of the nanofiber.

The structural and dynamic properties of PE nanofiber have been studied. It was found that, the density profiles were hyperbolic tangent with end beads being more abundant than middle beads at the surface. There were orientational preferences at the surface on the scale of individual bonds and the whole chains. It was not observed any significant differences in the local and global equilibrium properties when fibers were different thickness.

In this chapter, the effect of ethylene/propylene monomer ratio in Poly(ethylene-*co-atactic* propylene) copolymer nanofiber was investigated by coarse-grained polymer model. The density profile and density of free ends were analyzed. In addition, conformational, structural and thermodynamic properties of all simulation are studied in this work.

8.3 Model and method

8.3.1 System description

Poly(ethylene-*co*-propylene) chains were modeled with different beads ratio of ethylene and propane for each chain, which were represented by an ethylene units $(-CH-CH-)_n$ and propylene unit $-CH_2CH(CH_3)-$, respectively. The simulation was performed with independent parent chains of 50 polymer beads in periodic boundary condition. This periodic cell produced a density in the range of 0.753-0.760

g/cm^3 with 11.85-18.12% of bead occupancy on 2nd lattice depended on ethylene/propylene ratio. The temperature was set at 473 K for all simulation. The system density was determined by the geometry of the high-coordination lattice and the associated mass of a $-\text{CH}_2\text{CH}(\text{CH}_3)-$ and $(-\text{CH}-\text{CH}-)_n$ unit with each bead placed on this lattice. Simulations were reported for six compositions as expressed in Table 8.1. MC simulation was performed by the method described in Chapter II.

8.3.2 System construction

8.3.2.1 Bulk system

Random configurations of poly(ethylene-*co-atactic* propylene) chains were generated by mapping ethylene or propylene beads on 2nd lattice with an application of periodic boundary conditions in all three directions. In an initial step, the self-avoiding random walk with excluded volume condition was employed and followed by an introducing of an intra- and intermolecular interactions. After that, the initial structure was relaxed by minimizing the potential energy of the system by dynamical Monte Carlo technique.

8.3.2.2 Nanofiber formation

The periodic box was extended in x axis direction about 3 times to the bulk system because it had to ensure that that new box size was large enough for the parent chains and their images not to interact with each other. First, thin film was obtained and was then equilibrated. After that, an initial structure of nanofibers can be obtained by extending the y axis of the latest conformation of thin film about 3 times to prevent any interaction between the parent chains and their images with other

Table 8.1 Box size, chain number, bead occupancy and density of poly(ethylene-*co*-*atactic* propylene) nanofiber.

Ethylene fraction		Bead Occupancy (%)	Box size			Number of chains
weight ratio	(bead)		X	Y	Z	
0.00	0	11.85	30	30	30	64
0.20	14	13.14	29	29	29	64
0.40	25	14.36	28	28	28	63
0.60	35	15.67	27	27	28	64
0.80	43	16.88	27	27	26	64
1.00	50	18.12	26	26	26	63

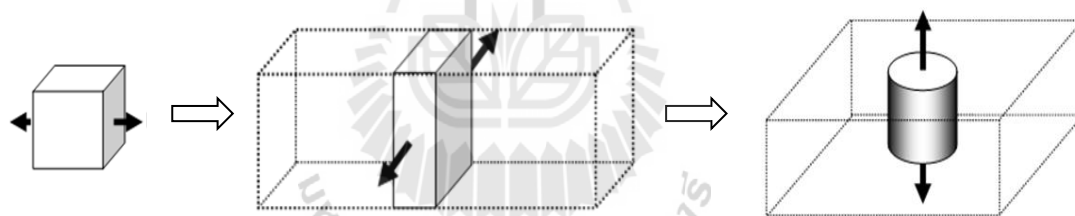


Figure 8.1 Schematic of methodology for generating a new cohesive polymer structure from bulk to nanofiber; bulk (3D) \rightarrow nano-thickened thin film (2D) \rightarrow nanofiber (1D)

chains. Then the nanofiber system was simulated similar to the previous step. Finally, the equilibrated nanofibers were obtained. Step for structural generation can be described by Figure 8.1.

8.4 Results and discussion

8.4.1 Density profile

8.4.1.1 Radial density profile

To calculate the density profile, the fiber is divided into cylindrical bins. Start from the center of fiber with 0.2 nm of thickness. The number of beads that fall into each bin were counted and normalized by its shell volume. So, the radial density profile can be obtained (Vao-soongnern *et al.*, 2000). Figure 8.2(a) shows the density profile of nanofiber with different ethylene content as a function of a displacement from the fiber axis. The total density of nanofibers is increased in region near the vicinity of fiber axis with increasing of ethylene content. Then, total density of high ethylene copolymer system is dramatically decreased at the middle region and the area far from fiber axis *i.e.* near the free surface. These results are attributed from the effect of propylene unit in copolymer chains. The density of fiber is higher with high ethylene content at the surface region. However, it is observed that there is a slightly different of the radial density profiles of fiber. The interfacial region of the radial density profile decays slower for low ethylene content system more than in high ethylene content system. This difference in radial density profile of the fibers is attributed to the difference in the curvature of their surfaces.

8.4.1.2 Bead distribution and segregation of chain ends

Figure 8.2(b) gives the density profile of the middle carbon atoms across the fibers. The profile is in qualitative agreement with the density profile for all beads. The density profile of middle beads of nanofibers is increased in region near the vicinity of the fiber axis. With increasing of ethylene content, middle bead density

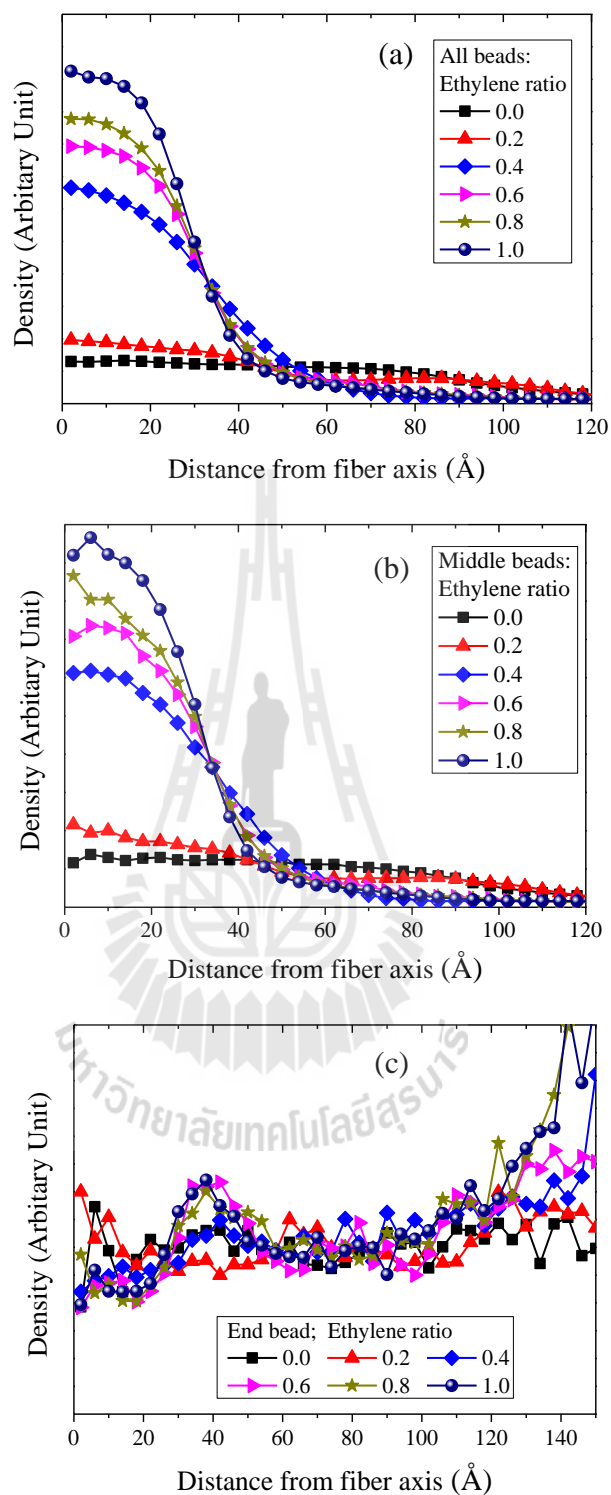


Figure 8.2 The density profile as a function of radial displacement of the center of mass for poly(ethylene-co-atactic propylene) nanofiber at different ratio of ethylene monomer; (a) all bead, (b) middle- and (c) end-beads.

is dramatically decreased at the middle region. Similarly, it shows higher density of middle beads at the area far from the fiber axis with low ethylene content. A small increase in middle bead density close to the fiber axis is indicative of some oscillatory behavior, which was also observed in MD simulation of a short alkane melt free surface (Harris, 1992) and PE thin film (Doruker and Mattice, 1998). The end beads density profile of nanofibers are displayed in Figure 8.2(c). Similar tendency of end beads density are observed at the vicinity of the surface. The density of end beads fluctuates but trend to increase as ethylene monomer increased, especially at the free surface region.

Figure 8.3 gives the bead density profiles which were normalized by the total bead density. It can be observed the segregation of end beads at the surface clearly. According to the results of free standing thin film simulation (Cifra, 1992; Doruker and Mattice, 1998), this segregation is also typical in the sense that the end beads become more abundant closer to the vacuum with increasing ethylene fraction in copolymer nanofibers. The behavior of the end beads distribution is determined mainly by entropic effects, contrary to the enrichment of centers of mass in the interface layer which is dependent on the energetic situation.

All systems exhibit quite similar behavior for both middle beads and end beads with varying monomer composition. The segregation at the surface depends on the number of ethylene monomer in PE-PP copolymer fiber. The middle bead segregation (Figure 8.3(a)) is found near the fiber axis whereas end beads segregation (Figure 8.3(b)) is observed at the surface region. The fluctuation of end beads at the surface area may be results from the effect of monomer at the end of chain. The increasing of bead which adopts propylene monomer shows narrower

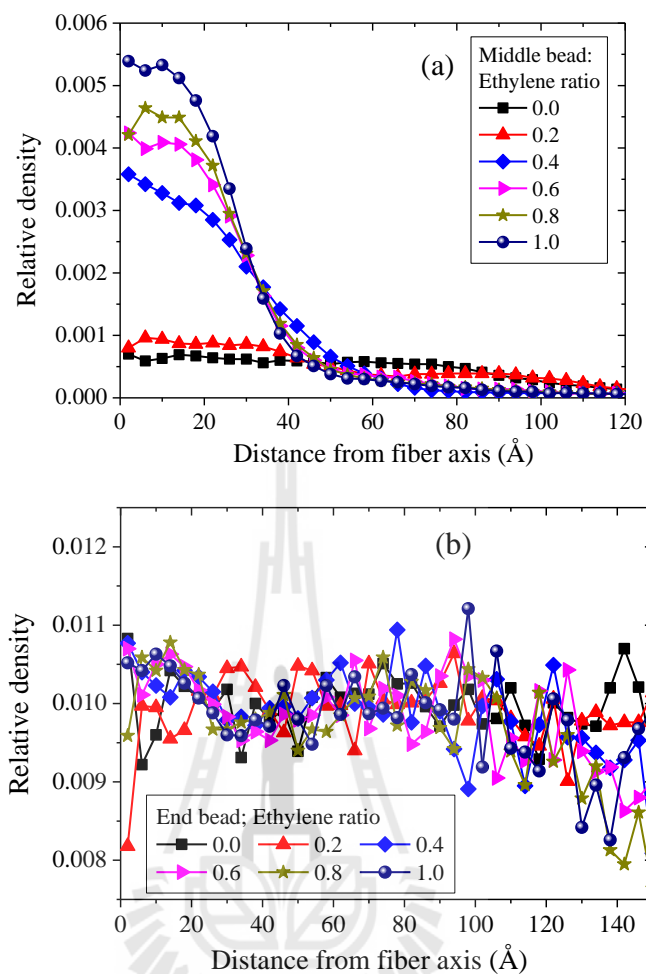


Figure 8.3 The relative density as a function of radial displacement of the center of mass for Poly(ethylene-*co-atactic* propylene) nanofiber at different ratio of ethylene monomer; (a) middle bead and (b) end bead.

fluctuation than in high ethylene monomer composition, which may be due to PE can diffuse faster than PP.

8.4.2 Bond orientation

The chord order parameter is defines as:

$$S_b = \frac{1}{2} \langle 3(\cos^2\theta) - 1 \rangle \quad (8.1)$$

where θ is the angle formed between a $2nd$ bond and the fiber axis. $\langle \quad \rangle$ indicates an ensemble average within the cylindrical bin. The value of S_b are -0.5, 0.0 or 1.0, respectively, correspond to perfectly perpendicular, random, and parallel orientation with respect to the fiber axis.

Local orientational tendencies of chords (from carbon atom i to carbon atom $i + 2$) across the fiber are inspected. Figure 8.4 displays the order parameter of the chords which are plotted as a function of a normal displacement from the fiber axis for all, middle and end beads of copolymer fiber. All three curves show a similar trend of the bond orientation along fiber axis.

Refer to the fiber axis, there is very slightly preference for the bond orientation at vicinity of fiber axis as indicated by $S = 0.15$ which is closed to the random orientation. In the middle region, a little peak is observed for the fiber with high ethylene amount which indicates that some bonds prefer to orient in little parallel direction. Toward the surface, all bonds seem to prefer both parallel and perpendicular orientation to the surface which depended on ethylene content in copolymer. At high ethylene fraction, the orientation of bond at the surface shows a tendency of parallel orientation direction. These two opposite effects of middle- and end-bond orientation are averaged in the orientation of all bonds.

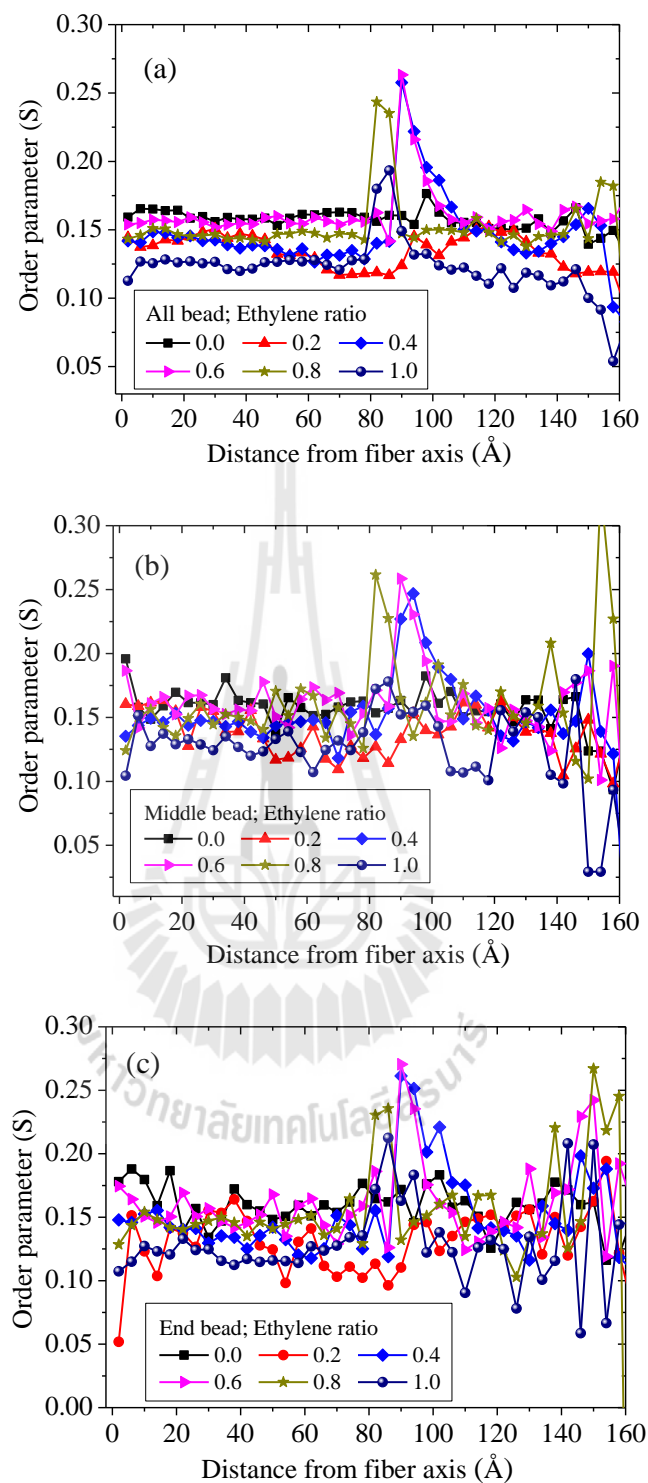


Figure 8.4 The orientation of chords as a function of radial displacement of the center of mass for poly(ethylene-*co-atactic* propylene) nanofiber at different ratio of ethylene monomer; (a) all bead, (b) middle bead and (c) end bead.

8.4.3 Chain properties

8.4.3.1 Molecular orientation

Figure 8.5 shows the orientation of the largest and smallest eigenvectors of the whole chains (L_1 and L_3 , respectively). The definition of the order parameter and the reference axis (fiber axis) are the same as the chord orientation. The first (largest) axis tends to orient parallel to the fiber axis with increasing ethylene monomer while it seems to orient more randomly when the ethylene fraction is lower than 0.5. For the third (smallest) axis, it orients perpendicular to the fiber axis when increased ethylene ratio and orient toward randomly at low ethylene content. The magnitude of both axis can be slightly changed at the surface from the bulk region at the fiber axis and depend on the monomer content in copolymer fiber. The orientation of the L_1 axis increases while the orientation of the L_3 axis decreases with increasing ethylene fraction. These results are similar to those in thin film and melts near a hard wall. The orientation parallel to the surface also appears in the mean-field theories of liquid alkane surfaces as well as in MC simulation of lattice models. It should also be mentioned that similar orientation effects in the interface have been observed for simulation of polymer surfaces and for the interface region of polymer blends.

8.4.3.2 Molecular size

The radius of gyration of the molecules as a function of the radial displacement of its center of mass from the fiber axis are investigated. Figure 8.6 gives the change of the square root mean squared radius of gyration of the X component (Figure 8.6(a)) the root of the average of the Y and Z components (Figure 8.6(b)) and the square root of 1/3 of the total mean-squared radius of gyration of the molecules

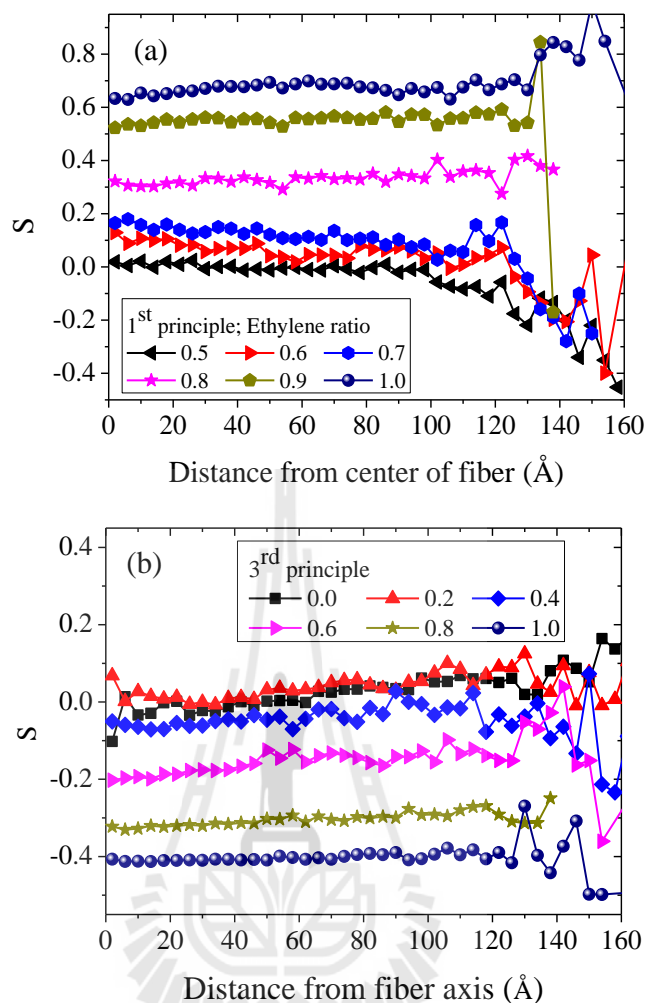


Figure 8.5 The orientation of (a) the largest and (b) smallest principal moment to axis after equilibration as a function of radial displacement of the center of mass for poly(ethylene-*co-atactic* propylene) nanofiber at different ratio of ethylene monomer.

(Figure 8.6(c)), respectively. It can be seen that the molecular size in X component become smaller along fiber axis with increasing ethylene ratio. It is also observed that R_g is decreasing as the chains approach the surface from the bulk side. Similarly, the total component decreases, while Y - Z the R_g remains relatively unaffected. These

results are simply a manifestation of the flattening of chains into pancake like objects as their centers of mass are forced to lie near an impenetrable surface.

8.4.3.3 Chain shape

The chain shapes are investigated by the acylindricity and the asphericity values, which are defined as follow

$$\text{Acylindricity}; c = L_2^2 - L_3^2 \quad (8.2)$$

$$\text{Asphericity}; b = L_1^2 - \frac{1}{2}(L_2^2 + L_3^2) \quad (8.3)$$

These values were divided by the squared radius of gyration to determine the extent of deviation from cylindrical and spherical shape in the range of 0 to 1.

The principal moment of chains are presented in Figure 8.7. The chain shape slightly changes as a function of the displacement from the fiber axis. The asphericity increases with higher ethylene content along the fiber axis and decrease at the surface. The acylindricity is also slightly increased with ethylene monomer increased and trend to decrease at the surface.

8.4.3.4 Principal moment of radius of gyration

The principal moments of the fiber structure is defined by diagonalizing the radius of gyration tensor. The principal axis always lies parallel to the x' axis in coordinate of $2nd$ lattice. The shape and orientation of the chains are defined more clearly by the principal components $L_1 < L_2 < L_3$ of the radius of gyration tensor for individual configurations taken along the principal axes system.

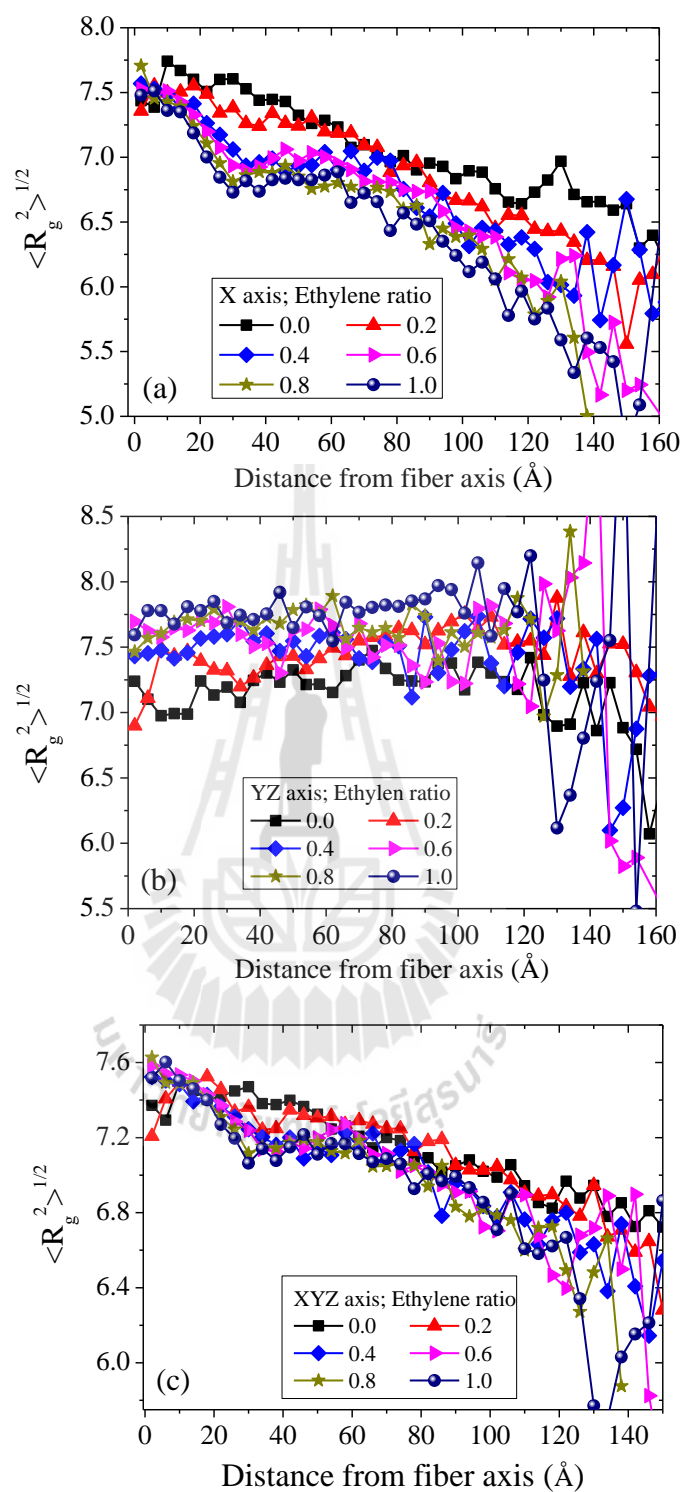


Figure 8.6 The change in R_g components to the center of mass for poly(ethylene-*co*-*atactic* propylene) nanofiber at different ratio of ethylene monomer; (a) in X axis, (b) in YZ axis and (c) in XYZ axis.

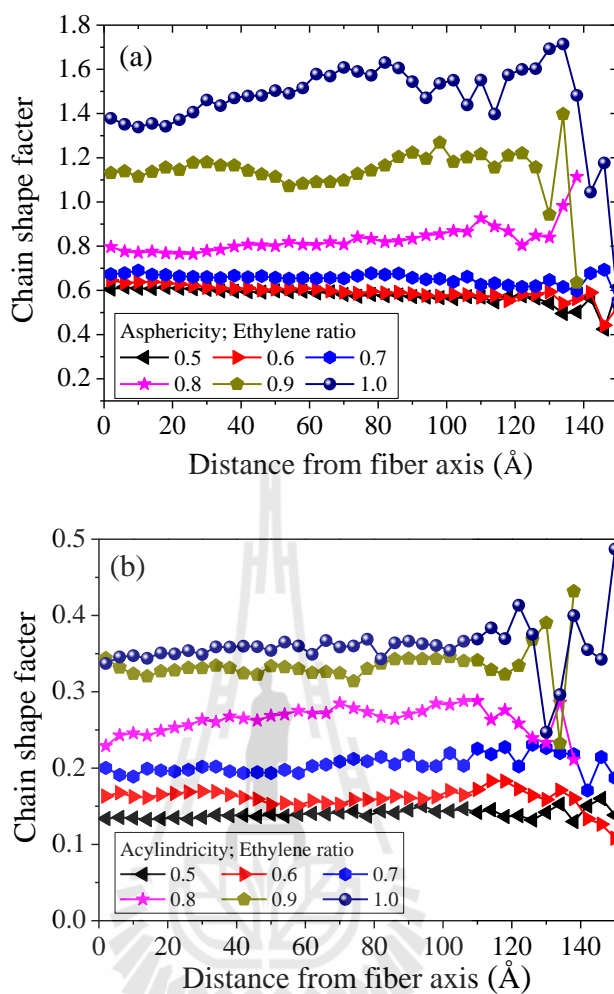


Figure 8.7 The change in molecular shape as a function of distance from the fiber axis for poly(ethylene-*co-atactic* propylene) nanofiber at different ratio of ethylene monomer; (a) asphericity and (b) acylindricity.

Figure 8.8 shows the eigenvalues of the chains normalized by their square radius of gyration as a function of radial displacement of the center of mass of the chain from the fiber axis. There is a slightly change at the vicinity of the surface with increasing ethylene content and the most of which occurs close to the vacuum side. For ethylene ratio < 0.5 , it is slightly decreased with decreasing ethylene content and it can be seen the dramatically increased at high ethylene content (> 0.6).

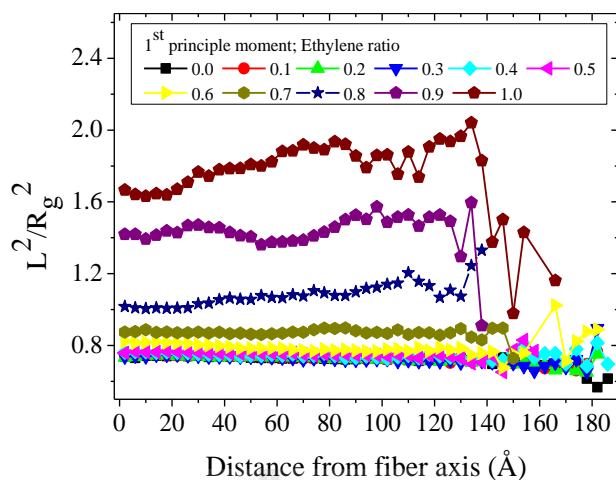


Figure 8.8 The principal moment of chains (normalized by R_g^2) as a function of radial displacement of the center of mass for poly(ethylene-*co-atactic* propylene) nanofiber at different ratio of ethylene monomer.

8.5 Conclusions

The properties of poly(ethylene-*co-atactic* propylene) nanofiber were examined with different ethylene content. Increasing ethylene ratio, the total density of nanofibers was increased near the fiber axis and dramatically decreased at the middle region toward the fiber surface along the axis. The interfacial width of density profile in decreased too. The end beads segregation become more abundant closer to the vacuum of copolymer nanofibers. The orientation of bond at the surface was parallel orientation. Similarly, the largest and smallest axis oriented parallel and perpendicular to the fiber axis, respectively, and changed to randomly orientation with decreasing ethylene fraction, especially at PE < 0.5. The orientation of molecule on L_1 axis is also increased while the orientation on the L_3 axis is decreased. Moreover, the molecular size in X component become smaller along the fiber axis and it is decreased near the surface from the bulk side, similar to the total component, while the R_g in Y -

Z component is unchanged. The molecular shape, both asphericity and acylindricity increased along fiber axis and decreased at the fiber surface. There was a slightly changed in the eigenvalues of copolymer fiber near the surface and the most of which occurs close to the vacuum side.

8.6 References

- Bassi, I.W., Corradini, P., Fagherazzi, G. and Valvassori, A. (1970). Crystallization of high ethylene EPDM terpolymers in the stretched state. **European Polymer Journal** 6: 709-718.
- Blom, H.P., Teh, J.W., Bremner, T. and Rudin, A. (1998). Isothermal and non-isothermal crystallization of PP: effect of annealing and of the addition of HDPE. **Polymer** 39: 4011-4022.
- Brückner, S., Meille, S.V., Petraccone, V. and Pirozzi, B. (1991). Polymorphism in isotactic polypropylene. **Progress in Polymer Science** 16: 361-404.
- Caldas, V., Brown, G.R., Nohr, R.S., MacDonald, J.G. and Raboin, L.E. (1994). The structure of the mesomorphic phase of quenched isotactic polypropylene. **Polymer** 35: 899-907.
- Cifra, P. (1992). Different surface profiles in surface demixing of polymer blends. **The Journal of Chemical Physics** 96: 9157-9160.
- Curgul, S., Van Vliet, K.J. and Rutledge, G.C. (2007). Molecular Dynamics Simulation of Size-Dependent Structural and Thermal Properties of Polymer Nanofibers. **Macromolecules** 40: 8483-8489.

- D'Orazio, L. and Cecchin, G. (2001). Isotactic polypropylene/ethylene-co-propylene blends: effects of composition on rheology, morphology and properties of injection moulded samples. **Polymer** 42: 2675-2684.
- de Ballesteros, O.R., Auriemma, F., Guerra, G. and Corradini, P. (1996). Molecular organization in the pseudo-hexagonal crystalline phase of ethylene-propylene copolymers. **Macromolecules** 29: 7141-7148.
- Di Lorenzo, M.L. and Silvestre, C. (1999). Non-isothermal crystallization of polymers. **Progress in Polymer Science** 24: 917-950.
- Doruker, P. and Mattice, W.L. (1998). Segregation of Chain Ends Is a Weak Contributor to Increased Mobility at Free Polymer Surfaces. **The Journal of Physical Chemistry B** 103: 178-183.
- Doruker, P. and Mattice, W.L. (1998). Simulation of Polyethylene Thin Films on a High Coordination Lattice. **Macromolecules** 31: 1418-1426.
- Guerra, G., De Ballesteros, O.R., Venditto, V., Galimberti, M., Sartori, F. and Pucciariello, R. (1999). Pseudo-hexagonal crystallinity and thermal and tensile properties of ethene-propene copolymers. **Journal of Polymer Science Part B: Polymer Physics** 37: 1095-1103.
- Harris, J.G. (1992). Liquid-vapor interfaces of alkane oligomers: structure and thermodynamics from molecular dynamics simulations of chemically realistic models. **The Journal of Physical Chemistry** 96: 5077-5086.
- Hongjun, C., Xiaolie, L., Dezhu, M., Jianmin, W. and Hongsheng, T. (1999). Structure and properties of impact copolymer polypropylene. I. Chain structure. **Journal of Applied Polymer Science** 71: 93-101.

- Li, L., Chen, L., Bruin, P. and Winnik, M.A. (1997). Morphology evolution and location of ethylene-propylene copolymer in annealed polyethylene/polypropylene blends. **Journal of Polymer Science Part B: Polymer Physics** 35: 979-991.
- Long, Y., Shanks, R.A. and Stachurski, Z.H. (1995). Kinetics of polymer crystallisation. **Progress in Polymer Science** 20: 651-701.
- Lotz, B., Wittmann, J.C. and Lovinger, A.J. (1996). Structure and morphology of poly(propylenes): a molecular analysis. **Polymer** 37: 4979-4992.
- Madden, W.G. (1987). Monte Carlo studies of the melt--vacuum interface of a lattice polymer. **The Journal of Chemical Physics** 87: 1405-1422.
- Mansfield, K.F. and Theodorou, D.N. (1991). Molecular dynamics simulation of a glassy polymer surface. **Macromolecules** 24: 6283-6294.
- Mathot, V.B.F., Scherrenberg, R.L., Pijpers, M.F.J. and Bras, W. (1996). Dynamic DSC, SAXS and WAXS on homogeneous ethylene-propylene and ethylene-octene copolymers with high comonomer contents. **Journal of thermal analysis** 46: 681-718.
- Mighri, F., Huneault, M.A., Aji, A., Ko, G.H. and Watanabe, F. (2001). Rheology of EPR/PP blends. **Journal of Applied Polymer Science** 82: 2113-2127.
- Minick, J., Moet, A., Hiltner, A., Baer, E. and Chum, S.P. (1995). Crystallization of very low density copolymers of ethylene with α -olefins. **Journal of Applied Polymer Science** 58: 1371-1384.
- Müller, M. and MacDowell, L.G. (2000). Interface and Surface Properties of Short Polymers in Solution: Monte Carlo Simulations and Self-Consistent Field Theory. **Macromolecules** 33: 3902-3923.

- Pegoraro, M., Severini, F., Di Landro, L., Braglia, R. and Kolarik, J. (2000). Structure and morphology of a novel ethylene-propylene copolymer and its blends with poly(propylene). **Macromolecular Materials and Engineering** 280-281: 14-19.
- Seki, M., Nakano, H., Yamauchi, S., Suzuki, J. and Matsushita, Y. (1999). Miscibility of Isotactic Polypropylene/Ethylene–Propylene Random Copolymer Binary Blends. **Macromolecules** 32: 3227-3234.
- Theodorou, D.N. (1988). Lattice models for bulk polymers at interfaces. **Macromolecules** 21: 1391-1400.
- Vao-soongnern, V., Doruker, P. and Mattice, W.L. (2000). Simulation of an amorphous polyethylene nanofiber on a high coordination lattice. **Macromolecular Theory and Simulations** 9: 1-13.



CHAPTER IX

CONCLUSION

The study of copolymer was the main subject of this dissertation. Both natural and synthetic copolymers were investigated to understand at the molecular level and some works were tried to improve properties of these copolymer. For an example of natural copolymer, silk as a model of alternating copolymer of glycine and alanine is known as high quality and performance fiber with outstanding properties and used as excellent materials. This made silk the attractive material for both in textile and in non-textile applications. Even though, silk lacks of some tough competition from the synthetic fibers, such as thermal stability *etc.* So, surface modification methods were utilized to improve natural silk properties, including graft copolymerization and electrospinning method.

Graft copolymerization of silk fiber was studied with various methacrylic monomers. The silk fibers were grafted by using both conventional and microwave irradiation method. The yield and grafting efficiency were increased when monomer content was increased. Silk grafted with methacrylates and dimethacrylates had graft yields higher than methacrylamide (MAA). MAA-grafted and dimethacrylates-grafted were hydrophilic and softer hand while HEMA-grafted was stiff fibers. The structural pattern of grafted silk fibroin confirmed an addition and was not affected by the vinyl monomers-grafted. Thermal stability of grafted silk was increased when grafted with dimethacrylate monomers. There was a deposit of some polymers on the grafted silk

surface indicating there was a specific interaction between silk and polymer.

Silk fiber is a fixed pattern of alternating amino (Gly-Ala) sequence and the molecular structure of silk cannot be changed. One of an interesting approach is to enhance the property of silk is to increase the surface to volume ratio of silk fiber. The electrospinning was one of such technique and was applied to make silk fibroin nanofiber. It was found that the concentration of silk fibroin solution, needle diameter and an electric field were effect on the regenerated electrospinnability of silk fibroin nanofiber. The rheological behavior of regenerated silk fibroin solution changed from Newtonian to non-Newtonian fluid and turned to gelation at high concentration. Moreover, the viscosity of silk solution also increased with increased concentration. Silk fibroin at low concentration had an insufficient molecular entanglement and cannot form fibers. They were less beaded on the fiber surface and slightly became smoother when the concentration of silk fibroin solution was increased. An averaged fiber diameter was affected by an electric field, ratio of an applied voltage to the distance between the tip and collector. At high applied voltage, small fibers were electrospun with an increase in the distance between tip and collector. For co-solvent system, the beaded-fibers became smoother fiber when an applied voltage was increased and when Ionic Liquids (AmimCl) concentration was decreased. Fiber characteristics were was slightly changed to connected-fiber when AmimCl concentration was increased.

Since the main sequence of copolypeptide in silk fibroin were Ala and Gly residues and presented as alternating poly(Ala-Gly). Hence, to represent the conceptual model of silk copolypeptide with other copolymer pattern, poly(ethylene-*co*-propylene) was used to mimic the silk system to investigate a complicated of

copolymer pattern apart from an alternating copolymer when it form nanofiber. Moreover, PE and PP were first simulated to investigate static and dynamic properties of PP/PP blend with different tacticity and PP melts as a model of stereochemical copolymer, PE brush with interacting wall as a conceptual model for grafted silk, and poly(ethylene-*co-atactic* propylene) nanofiber as the conceptual model to mimic silk behavior in addition to an alternating copolymer.

For PP/PP blend with different tacticity, the diffusion rate of PP was ordered as $iPP > aPP > sPP$. For PP blend with 50:50 wt% binary mixtures, immiscibility was observed when sPP was introduced into the mixtures. The diffusion rate of iPP and aPP became lower after mixing, while sPP diffused faster in the mixtures significantly. Intramolecular contribution did not provide the correlation to the diffusion rate of PP pure melts. The mobility of chains was depended on both intramolecular and intermolecular interaction. The effect of intramolecular interaction was a greater effect than intermolecular contribution in the case of iPP and aPP chains in binary PP/PP mixtures. In contrast, intermolecular contribution affects polymer dynamics greater than intramolecular interaction in sPP chain.

To understand the fundamental physics of copolymer behavior, copolymer with the same monomer unit but different side chain configuration i.e. stereochemical isomer was also studied. aPP melts were also studied and found that aPP chain with alternate m diads sequence had a tendency to diffuse faster than other sequences. At an intermediate stereochemical composition, the chains with long consecutive diads with the same sequence diffuse slower than the mixed stereochemical sequence. The effect of intramolecular interaction was greater than that of intermolecular interaction at the stereochemical composition containing m diads close to $P_m = 0.0$ (all r or

syndiotactic chain). For P_m close to 1.0, the intermolecular interaction affects the diffusion greater than the intramolecular effects.

PE brush grafted on interacting surface which was employed as a conceptual model for grafted silk were in good agreement with prior numerical and theoretical of polymer brush. For monodisperse PE brush, the PE chains were more stretched in the outer layer with increasing both grafting density and chain length. An increasing temperature can lead to a more stretching of chain at the outer region which the density in the bulk region was decreased. For bimodal PE brushes, the long chains at the outer layer were more stretched while the shorter chains were compressed in the inner layer of the bidisperse PE brushes. PE chains stretching were also found to depend on the nature of interaction between PE chains and the grafting wall. There is a larger chain stretching for both long and short chains when PE chains were grafted on the repulsive surface more than other interactive wall systems. The influence of an interacting wall on the properties of PE brush can be ordered as: repulsive > neutral > attractive system. However, there was a similar effect of an interaction between polymer chains and the solid substrate on the properties of PE brush at high molecular weight system.

Poly(ethylene-*co-atactic* propylene) copolymer nanofiber was studied as an additional model for silk nanofiber. The results indicated that the properties of nanofiber were depended on the ethylene/propylene ratio. When the ethylene fraction was increased, the total density of nanofibers was also increased near the fiber axis and decreased at the middle region toward the free surface. The interfacial region of radial density profile was increased at high ethylene content. The end beads segregation became more abundant closer to the vacuum side of copolymer

nanofibers. The bond at the surface preferred to orient in parallel rather than perpendicular direction. All bonds favored both parallel and perpendicular orientation to the surface which was depended on the ethylene content in this copolymer. Similarly, the largest and smallest axis of an equivalent ellipsoid representing molecular shape were oriented parallel and perpendicular to the fiber axis, respectively, and changed to randomly orientation when ethylene content was decreased, especially at lower than 0.5. The orientation of molecule L_1 axis was also increased while the orientation of L_3 axis was decreased. Moreover, the molecular size in X and total component became smaller along fiber axis and decreased near the surface, while the R_g component in Y - Z was unchanged. The molecular shape, both asphericity and acylindricity were increased toward the fiber axis and decreased at the surface. There was a slight change in the eigenvalues of the fiber near the surface and mostly occurred close to the vacuum side. It was increased with increased ethylene monomer.

CURRICULUM VITAE

Name Miss Tanissara Pinijmontree

Date of Birth 30 September 1981

Place of Birth Udon Thani

Education **2008, Chiang Mai University**, Master of Science,
Majored in Industrial Chemistry (Ceramic).

2005, Khon Kaen University, Diploma Program,
Majored in Teaching Profession.

2004, Khon Kaen University, Bachelor of Science,
Majored in Chemistry.

Grants and Fellowships

- **1997-2004:** The Project for the Promotion of Science and Mathematics Talented Teachers (PSMT), The institute for the Promotion of Teaching Science and Technology (IPST)
- **2008-2011:** Strategic Scholarships Fellowships Frontier Research Networks, Office of the Higher Education Commission
- **August-October 2011:** Invitation Program for East Asian Young Researchers (JSPS Program)